Atmos. Chem. Phys., 7, 5815–5860, 2007
www.atmos-chem-phys.net/7/5815/2007/

Atmospheric Chemistry and Physics

A new tropospheric and stratospheric Chemistry and Transport Model MOCAGE-Climat for multi-year studies: evaluation of the present-day climatology and sensitivity to surface processes

H. Teyssèdre[1], M. Michou[1], H. L. Clark[1], B. Josse[1], F. Karcher[1], D. Olivié[1], V.-H. Peuch[1], D. Saint-Martin[1], D. Cariolle[2], J.-L. Attié[3], P. Nédélec[3], P. Ricaud[3], V. Thouret[3], R. J. van der A[4], A. Volz-Thomas[5], and F. Chéroux[1]

[1]GAME/CNRM (Météo-France, CNRS) Centre National de Recherches Météorologiques, Toulouse, France
[2]Centre Européen de Recherches et de Formation Avancée en Calcul Scientifique (CERFACS), Toulouse, France
[3]Laboratoire d'Aérologie (Université Toulouse III, CNRS), Toulouse, France
[4]KNMI (Royal Netherlands Meteorological Institute), De Bilt, The Netherlands
[5]Institute of Chemistry and Dynamics of the Geosphere, Juelich, Germany

Received: 26 June 2007 – Published in Atmos. Chem. Phys. Discuss.: 2 August 2007
Revised: 31 October 2007 – Accepted: 6 November 2007 – Published: 26 November 2007

Abstract. We present the configuration of the Météo-France Chemistry and Transport Model (CTM) MOCAGE-Climat that will be dedicated to the study of chemistry and climate interactions. MOCAGE-Climat is a state-of-the-art CTM that simulates the global distribution of ozone and its precursors (82 chemical species) both in the troposphere and the stratosphere, up to the mid-mesosphere (∼70 km). Surface processes (emissions, dry deposition), convection, and scavenging are explicitly described in the model that has been driven by the ECMWF operational analyses of the period 2000–2005, on T21 and T42 horizontal grids and 60 hybrid vertical levels, with and without a procedure that reduces calculations in the boundary layer, and with on-line or climatological deposition velocities. Model outputs have been compared to available observations, both from satellites (TOMS, HALOE, SMR, SCIAMACHY, MOPITT) and in-situ instrument measurements (ozone sondes, MOZAIC and aircraft campaigns) at climatological timescales. The distribution of long-lived species is in fair agreement with observations in the stratosphere putting aside the shortcomings associated with the large-scale circulation. The variability of the ozone column, both spatially and temporarily, is satisfactory. However, because the Brewer-Dobson circulation is too fast, too much ozone is accumulated in the lower to mid-stratosphere at the end of winter. Ozone in the UTLS region does not show any systematic bias. In the troposphere better agreement with ozone sonde measurements is obtained at mid and high latitudes than in the tropics and differences with observations are the lowest in summer. Simulations using a simplified boundary layer lead to larger ozone differences between the model and the observations up to the mid-troposphere. NO_x in the lowest troposphere is in general overestimated, especially in the winter months over the Northern Hemisphere, which may result from a positive bias in OH. Dry deposition fluxes of O_3 and nitrogen species are within the range of values reported by recent inter-comparison model exercises. The use of climatological deposition velocities versus deposition velocities calculated on-line had greatest impact on HNO_3 and NO_2 in the troposphere.

Correspondence to: H. Teyssèdre
(hubert.teyssedre@meteo.fr)

1 Introduction

The modelling of chemistry and climate interactions has become increasingly complex over the last twenty years. A first approach was to use climatologies of the trace gases that have a radiative impact upon climate, such as carbon dioxide (CO_2), methane (CH_4) or ozone (O_3). Then, simplified chemistry of stratospheric O_3 was introduced in models, like the linear scheme developed by Cariolle and Déqué (1986), or described in McLinden et al. (2000). Large scale perturbations of the atmosphere, e.g., the Antarctic ozone hole or the evolution of the halogen loading of the atmosphere, were thus taken into account. The Cariolle and Déqué (1986) scheme has been introduced in many models such as the ARPEGE-Climat General Circulation Model (GCM) (Déqué et al., 1994; Cariolle et al., 1990) or the European Center for Medium-Range Weather Forecasts (ECMWF) IFS model (Oikonomou and O'Neill, 2006). A more sophisticated approach deals with the chemistry of a few tens of chemical species of the stratosphere (Lefèvre et al., 1994; Chipperfield et al., 1994). The strato-

spheric composition can then be simulated at seasonal or longer time-scales. For example, the REPROBUS Lefèvre et al. (1994) scheme has been coupled to the ARPEGE-Climat GCM (WMO, 1998). For a comprehensive description of the atmospheric chemistry, including the modelling of the chemistry of the troposphere, much shorter time-scales have to be considered to represent processes such as scavenging or dry deposition at the surface. The chemistry of short-lived chemical species, with a lifetime of several hours like many Volatile Organic Compounds (VOCs), needs to be accounted for, but this substantially increases modelling costs.

Very few models nowadays consider the chemistry of the entire atmosphere up to the mesosphere with a detailed description of the complex chemical reactions in the troposphere, though it has become more and more evident that it is crucial to take into account both the stratosphere and the troposphere to better simulate the coupling between these two layers. For example, the description of one of these models and its direct evaluation with in-situ and satellite data appears in Jöckel et al. (2006).

MOCAGE is the multiscale 3-D Chemistry and Transport Model (CTM) of Météo-France that is an evolution of the Lefèvre et al. (1994) stratospheric model. It represents processes from the regional to the planetary scale, and extending from the surface up to the middle stratosphere. The model comprises several levels of two-way nested domains, the parent global grid providing fully-consistent boundary conditions to the inner grids. This set-up enables the model to be used for a wide range of scientific applications, from the study of global-scale distributions of species (Josse et al., 2004), to "chemical weather" forecasting, down to the regional scale (Dufour et al., 2004; Drobinski et al., 2007), and chemical data assimilation (Cathala et al., 2003; Geer et al., 2006; Pradier et al., 2006; Clark et al., 2007). MOCAGE has been evaluated against several observational campaigns such as ESCOMPTE (Etude sur Site pour COntraindre les Modèles de Pollution atmosphérique et de Transport d'Emissions, Dufour et al. (2004)), and ICARTT/ITOP (International Consortium for Atmospheric Research on Transport and Transformation /Intercontinental Transport of Ozone and Precursors, Bousserez et al. (2007)). In addition, it is part of a number of international projects, and it has been run in operational mode (24 h/7 d) since the summer of 2005 on the Météo-France supercomputers for air quality simulations on the French Prévair national platform (http://www.prevair.org, Honoré et al. (2007)).

In this article, we present MOCAGE-Climat that is the version of MOCAGE developed for the study of climate and chemistry interactions. Therefore, this version of the model covers the whole troposphere and the whole stratosphere. The objective of our work here is to evaluate efficiently how the MOCAGE-Climat CTM represents the climatological chemical state of the atmosphere when driven by ECMWF meteorological forcing commonly used for this kind of exercise. This objective is achieved by analysing comprehensive comparisons with observations. Such a thorough review is required before undertaking the coupling of MOCAGE-Climat with the ARPEGE-Climat GCM. This coupling will enable us to consider the feedback of the chemistry on radiation and dynamics within the Coupled Chemistry-Climate Model (CCM). The Météo-France CCM will then become one of the participants of international projects such as the World Climate Research Programme (WCRP) Stratospheric Processes And their Role in Climate (SPARC) Chemistry-Climate Model Validation Activity (CCMVal) (http://www.pa.op.dlr.de/CCMVal/), that has involved an increasing number of CCMs in recent years. We also show in this paper the results of a number of sensitivity studies. The aim here is twofold, on the one hand improve our knowledge of the impact of the lower troposphere on the rest of the atmosphere, and on the other hand evaluate if and how CPU time could be reduced in order to perform longer simulations.

We present MOCAGE-Climat in Sect. 2. In Sect. 3, we evaluate the model against observed climatologies, both in the stratosphere and the troposphere, focusing on quantities that are important for the simulation of ozone. We first present long-lived species, as they are an indication of the robustness of the transport, and then we describe the reservoir and short-lived species. These comparisons enable us to identify strengths and weaknesses in the chemistry. The final evaluation section deals with ozone, that is affected by all the compounds first presented, and that is the trace gas most observed in the atmosphere. Finally, results from a sensitivity study to surface processes appear in Sect. 4 and conclusions in Sect. 5.

2 Model description

2.1 General features

The horizontal and vertical resolutions of MOCAGE-Climat are specific to the study of global processes, with a special focus on studies pertaining to the stratosphere and Upper Troposphere Lower Stratosphere (UTLS) regions. In the horizontal, Gaussian grids are used as they are closer to the original Numerical Weather Prediction (NWP) calculations. In the vertical, the coverage of the model has been extended, 60 vertical levels cover the troposphere, the whole stratosphere and the lower mesosphere, up to 0.07 hPa (approximately 70 km). The number of vertical levels and their distribution are identical to those of the ECMWF analyses used in this paper (see Sect. 3.1). This vertical distribution agrees with the recommendations of Strahan and Polansky (2006) for a realistic representation of the middle atmosphere.

The model has been run in an off-line mode, driven by a variety of meteorological inputs, including data from NWP models, such as the analyses or forecasts of the ECMWF system. Wind, temperature, humidity, and pressure, available every 3 or 6 h, are then linearly interpolated to yield hourly

values, which is the time step for advection. Shorter time steps are used for physical processes and chemistry. Large-scale transport of chemical constituents or tracers is ensured by a semi-Lagrangian advection scheme (Williamson and Rasch, 1989) which is not supposed to conserve mass, as soon as the grid is irregular. MOCAGE that has σ-pressure levels is in such case. We therefore apply a global uniform correction, since the whole mass of tracer has to remain constant considering advection processes only. This is relevant as our 3D wind field is conservative and as volumic mixing ratios have the property to be conservative. However, although this conservation appears necessary, Chipperfield (2006) indicated that many CTMs seem to give reasonable simulations without concern over mass conservation in advection schemes or the balance of winds. Turbulent diffusion follows Louis (1979), while the convection scheme (mass-flux type) adopted after a number of studies is that of Bechtold et al. (2001). For further details on the transport in MOCAGE and its evaluation, see Josse et al. (2004).

Wet removal by precipitation is included. In convective clouds, it is parameterized according to Mari et al. (2000); convective transport and scavenging are therefore computed simultaneously. In large-scale precipitation clouds, removal follows the first-order scheme of Giorgi and Chamedeis (1986). Below clouds, the recommendations of Liu et al. (2001) (again a first-order scheme) are used. Wet removal has been evaluated with simulations of ^{210}Pb, a highly soluble tracer, by comparing model outputs with both climatologies and fine temporal resolution observations.

At the crossroads between dynamics, physics and chemistry, we use the mixing ratios of the ECMWF analyses up to the 380 K isentropic level for the representation of water vapour. Above this level, H_2O is calculated by the chemical scheme of MOCAGE-Climat (see below) and advected by its semi-lagrangian transport scheme. Prescribing the water vapour field between the surface and the 380 K level allows MOCAGE-Climat to benefit from the ECMWF analyses and from their modelling of the physical processes in the troposphere and the UTLS region. At middle and high latitudes the 380 K surface may be partly in the stratosphere, depending on the meteorological situation. The numerical diffusion of H_2O into the stratosphere is thus reduced and the stratospheric profile is still satisfactory since the ECMWF analyses include a simple parameterization of water vapour production by methane oxidation (Oikonomou and O'Neill, 2006).

Radiation is taken into account both indirectly via the external meteorological forcing provided to the CTM and directly via photolysis rates. These photolysis rates have been computed off-line from the solar radiation with the Tropospheric Ultraviolet-Visible model version 4.0 (see Madronich and Flocke, 1998). The impact of clouds on the photolysis rates is calculated on-line, increasing (weakening) photolysis rates above (below) clouds according to Brasseur et al. (1998).

Table 1. Transported trace gases of the RELACS chemical scheme (* species that are not included in the REPROBUS chemical scheme).

	Species	Name/Group
1	N_2O	nitrous oxide
2	CH_4	methane
3	H_2O	water vapour
4	HNO_3	nitric acid
5	N_2O_5	dinitrogen pentoxide
6	CO	carbon monoxide
7	OClO	chlorine dioxide
8	HCl	hydrochloric acid
9	$ClONO_2$	chlorine nitrate
10	HOCl	hypochlorous acid
11	Cl_2	diatomic chlorine
12	H_2O_2	hydrogen peroxide
13	$ClNO_2$	chlorine nitrite
14	HBr	hydrogen bromide
15	$BrONO_2$	bromide nitrate
16	HNO_4	peroxynitric acid
17	Cl_2O_2	dichlorine peroxide
18	HOBr	hypobromous acid
19	BrCl	bromochlorine
20	HCHO	formaldehyde
21	MO2	methyl peroxy radical (CH_3O_2)
22	OP1	methyl hydrogen peroxide (CH_3O_2H)
23	CFC11	chlorofluorocarbon-11
24	CFC12	chlorofluorocarbon-12
25	CFC113	chlorofluorocarbon-113
26	CCl_4	chlorofluorocarbon-10
27	CH_3CCl_3	methyl chloroform
28	CH_3Cl	methyl chloride
29	HCFC22	hydrochlorofluorocarbon-22
30	CH_3Br	methyl bromide
31	H1211	halon-1211
32	H1301	halon-1301

The chemistry scheme of MOCAGE-Climat, so-called RELACS, comprises both tropospheric and stratospheric species. It is a combination of the RELACS scheme described in Crassier et al. (2000), which is a simplified version of the tropospheric RACM scheme (Stockwell et al., 1997), and of the REPROBUS scheme (Lefèvre et al., 1994) relevant to the stratosphere that includes the heterogeneous stratospheric chemistry described in Carslaw et al. (1995). A total of 82 chemical species (see Tables 1 and 2) are considered throughout 242 thermal reactions. 65 of these species are transported while the remaining 17 are assumed at instantaneous chemical equilibrium, as described in Brasseur and Solomon (1986). This scheme is a compromise between a detailed representation of the tropospheric-stratospheric chemistry and the CPU time that strongly constrains multi-year CTM simulations. As for the chemistry of the strato-

Table 1. Continued.

	Species	Name/Group
33	H_2SO_4	sulfuric acid
34	PSC	polar stratospheric cloud tracer
35	HONO*	nitrous acid
36	SO_2^*	sulfur dioxide
37	ETH*	ethane
38	ALKANEbis*	alkanes, alcohols, esters, and alkynes
39	ALKENEbis*	ethene, terminal alkenes, internal alkenes, butadiene and other anthropogenic dienes
40	ISOTOT*	isoprene, α-pinene, d-limonene, and other terpenes
41	AROMATIC*	toluene, xylene, cresol, and other aromatics
42	ALD*	acetaldehyde and higher aldehydes
43	KET*	ketones
44	MACR*	glyoxal, methyglyoxal, and other alpha-carbonyl aldehydes, unsaturated dicarbonyls, metacrolein and other unsaturated monoaldehydes, unsaturated dihydroxy dicarbonyl, hydroxy ketone
45	ONIT*	organic nitrate
46	PAN*	peroxyacetal nitrate and higher saturated PANs, unsaturated PANs
47	OP2*	higher organic peroxides, peroxyacetic acid and higher analogs
48	$LINO_3^*$	linear ozone
49	HC8P*	peroxy radicals formed from ALKANEbis
50	OLIP*	peroxy radicals formed from ALKENEbis
51	ISOP*	peroxy radicals formed from ISOTOT
52	PHO*	phenoxy radical and similar radicals
53	TOLP*	peroxy radicals formed from AROMATIC
54	ACO3*	acetyl peroxy and higher saturated acyl peroxy radicals, unsaturated acyl peroxy radicals, peroxy radicals formed from RACM species KET
55	OLNN*	NO_3-alkene adduct
56	XO2*	accounts for additional NO to NO_2 conversion
57	SULF*	sulfate
58	O_x	odd oxygen
59	NO_x	nitrogen oxides
60	ClO_x	chlorine oxides
61	BrO_x	bromine oxides
62	NO_y	total nitrogen family (radicals + reservoirs)
63	Cl_y	total chlorine family (radicals + reservoirs)
64	Br_y	total bromine family (radicals + reservoirs)
65	TRACEUR.FROID*	cold tracer

sphere, the scheme allows the description of the nitrogen, chlorine, and bromine species, from source to radical form, through reservoir species. In the troposphere, both inorganic and organic species are taken into account. The use of RELACS versus RACM was evaluated in Crassier et al. (2000) for clean to polluted conditions and showed that RELACS compared favorably with RACM for ozone and other atmospheric oxidants. Similar conclusions were made when RELACS was included in MOCAGE-Climat. About 30% of the computer time is saved making simulations with RELACS instead of RACM.

A specific procedure can be applied in the boundary layer of MOCAGE-Climat, again for the sake of saving computer time. The computing of the chemical tendencies within the boundary layer represents about 90% of the time dedicated to chemistry, due to the large number of chemical species with a short lifetime (less than 1 min). We then deal with the chemical evolutions in the boundary layer considering it as one layer only. The boundary layer is simply defined as the 10 levels closest to the surface. Firstly, we calculate at time t the average mixing ratios of each chemical species and necessary meteorological parameters. These vertical averages are weighted by the air density profile. Then the chemistry scheme simulates the new averages at $t+\Delta t$, and we deduce mean evolutions between t and $t+\Delta t$, noted here τ for a specific compound. τ is then applied to the original full vertical profile, yielding to the entire profile at $t+\Delta t$. Simulations at all levels of the boundary layer are performed every 6 h. With this procedure, an extra 30% of computer time is saved, leading to a final cost of 23 min of CPU-time per day simulated at T42 with 60 layers, on the Fujitsu VPP5000 of Météo-France. We will present in this paper results from simulations both with the full boundary layer chemistry calculations included and approximating the boundary layer as a single bulk layer.

In addition to the RELACS chemical scheme, MOCAGE-Climat can consider a parameterization of the linear ozone chemistry as first presented in Cariolle and Déqué (1986) and recently revised by Cariolle and Teyssèdre (2007). This parameterization is essentially valid for the middle-atmosphere, with "linear ozone" mainly driven by dynamics in the UTLS, and with increasing photo-chemical influence as the altitude increases.

2.2 Surface exchanges

The set of emissions that we used for our simulations is multi-fold. Most of the emissions from anthropogenic sources are those of the model inter-comparison exercise, so-called "2030 Photocomp experiment" (referenced hereafter as 2030PE, see Dentener et al. (2006)). The baseline emission scenario is considered as representative of the year 2000 and consists of International Institute for Applied Systems Analysis (IIASA) emissions and EDGAR v3.2 biomass burning emissions normalized with the results presented in van der Werf et al. (2003). For further information on these emission datasets see Dentener et al. (2004). With regard to emissions from biogenic sources, the 2030PE only made recommendations on the total emissions which are emitted annually. We adopted these recommendations and thus complemented the set of anthropogenic emissions as follows: NO_x emitted by soils, CH_4 by oceans, and CO from vegetation and oceans are those of a personal communication from L. Emmons and J.-F. Lamarque (NCAR, 2004). CH_4 from wetlands are taken from Matthews and Fung (1987) (monthly data for the reference year 1985), and emissions from termites are described in Fung et al. (1991). SO_2 from volcanoes are presented in Andres and Kasgnoc (1998). Biogenic emissions of hydrocarbons from vegetation include isoprene, monoterpenes, and other VOC emissions; monthly distributions are taken from Guenther et al. (1995).

Table 2. Trace gases at chemical equilibrium for RELACS.

	Species	Name/Group
1	$O(^3P)$	atomic oxygen
2	$O(^1D)$	atomic oxygen
3	O_3	ozone
4	N	atomic nitrogen
5	NO	nitrogen monoxide
6	NO_2	nitrogen dioxide
7	NO_3	nitrogen trioxide
8	ClO	chlorine monoxide
9	Cl	atomic chlorine
10	BrO	bromine monoxide
11	Br	atomic bromine
12	H	atomic hydrogen
13	OH	hydroxyl radical
14	HO_2	hydroperoxyl radical
15	CH_3	methyl radical
16	CH_3O	methyl-oxygen
17	ADDT*	product from aromatic-OH combination

N_2O data, not provided for the 2030PE, are available from the Global Emissions Inventory Activity (GEIA) web site; we used the dataset described in Bouwman et al. (1995) that we grouped into broad IPCC (1995) categories (reference year 1990). It can be noted that our annual total emissions of N_2O (IPCC, 1995) are higher than those of other models (Michou and Peuch, 2002). Finally for the emissions of chlorofluorocarbons, spatial distributions of CFC−11 and CFC−12 are the ones of the GEIA v1 datasets, and for the other compounds listed in Table 3 they are those of Olivier et al. (1996); we adopted the annual totals of WMO (2002) for the year 2000.

The splitting of the original VOCs into the VOCs of the RELACS chemical scheme, both from anthropogenic and biogenic sources, has been made according to the recommendations of the IPCC Third Assessment Report (TAR) and to Crassier et al. (2000). The annual global totals are presented in Table 4.

The version of MOCAGE-Climat used in this paper does not include NO_x emissions from lightning (total estimated to 7 Tg(N) yr^{-1}). Implementation in MOCAGE of a parameterization of these emissions is on-going and the first results have been reported in Bousserez et al. (2007).

All the emission datasets have an original horizontal resolution of $1^\circ \times 1^\circ$ and, depending on the source, vary according to the month or remain constant throughout the year. Table 3 details this temporal resolution, as well as the total amounts

Table 3. Surface emissions considered in MOCAGE-Climat, A. for annual data, M. for monthly data (see references in the text).

Species	Source	Total
N_2O Tg(N) yr^{-1}	Oceans	3.0 A.
	Continental soils	9.5 A.
	Anthropogenic	2.2 A.
	All sources	14.7
NO_x Tg(N) yr^{-1}	Industrial	10.2 A.
	Traffic	16.1 A.
	Domestic	1.5 A.
	Continental soils	5.0 M.
	Bioma. burning	8.5 M.
	All sources	41.3
CH_4 Tg(CH_4) yr^{-1}	Industrial	83.6 A.
	Land use	216.2 A.
	Termites	24.9 A.
	Wetlands	159.7 M.
	Oceans	14.9 M.
	Bioma. burning	21.3 M.
	All sources	520.6
CO Tg(CO) yr^{-1}	Industrial	37.5 A.
	Traffic	194.3 A.
	Domestic	238.0 A.
	Oceans+Vegetation	100.6 M.
	Bioma. burning	444.1 M.
	All sources	1013.4
COVNM anth. Tg yr^{-1}	Industrial	39.3 A.
	Traffic	47.7 A.
	Domestic	28.8 A.
	Bioma. burning	31.2 M.
	All sources	147.0
COV bio. Tg(C) yr^{-1}		
	Isoprene	501.6 M.
	Monoterpenes	114.4 M.
	Other VOC	259.6 M.
SO_2 Tg(S) yr^{-1}	Industrial	43.8 A.
	Traffic	5.6 A.
	Domestic	4.8 A.
	Bioma. burning	1.2 M.
	Volcanoes	14.6 A.
	All sources	70.0
CFC−11 Gg yr^{-1}	all	86 A.
CFC−12 Gg yr^{-1}	all	122 A.
CFC−113 Gg yr^{-1}	all	23 A.
CH_3CCl_3 Gg yr^{-1}	all	5 A.

emitted. We used the same emissions for the six years of our simulations (2000–2005, see Sect. 3.1). Emissions are distributed in the eight lowest levels of the model (that correspond on average to a layer of 600 m), in order to avoid too strong vertical gradients, as proposed in Josse et al. (2004).

Table 4. Surface emissions of the VOCs of RELACS that are emitted.

Species	Tg(C) yr^{-1}
ALKANEbis	281.8
ALKENEbis	23.6
ALD	3.9
AROMATIC	21.1
ETH	5.9
HCHO	0.4
ISOTOT	616.0
KET	21.8

In addition to dealing with surface emissions, the surface module of MOCAGE-Climat enables the simulation of the dry deposition sink of gaseous species and aerosols (Nho-Kim et al., 2004). To compute realistic time-dependent fluxes at the surface, a 2-D interface (Michou and Peuch, 2002) between MOCAGE and outputs of NWP models has been developed. The dry deposition velocity of about a hundred compounds including O_3, SO_2, nitrogen-containing compounds, as well as long-lived and short-lived intermediate organic compounds, was parameterized on the basis of Wesely (1989), considering the "big-leaf" resistance approach. The module calculates dry deposition velocities from three resistances in series, aerodynamic, laminar, and surface. In the case of the work reported here these resistances are computed using the surface meteorological fields of the 6 hourly analyses of the ECMWF NWP model. The original surface resistance scheme was modified with the introduction of a specific parameterization for the stomatal resistance depending upon environmental factors; it is based on Noilhan and Mahfouf (1996), and follows the Jarvis-type meteorological approach that attempts to modify a minimum stomatal resistance defined a priori through external factors, such as moisture and radiation availability. This parameterization of the stomatal resistance has been first validated in Michou and Peuch (2002) and further analyzed in the context of Mediterranean regions in Michou et al. (2004), as the coupling with meteorological analyses allows the study of specific events.

We present in Sect. 4 results of a sensitivity study to the deposition velocity.

3 Model results and evaluation

3.1 Description of the simulations performed

The MOCAGE-Climat model was run using the analyses of the NWP model of ECMWF (IFS). The model was integrated for six years using the same vertical resolution as IFS, 60 layers from the surface up to 0.07 hPa, from 1 January 2000 to 31 December 2005, at two truncations T21 and T42. For

each horizontal resolution, we performed simulations with and without the simplified treatment of the boundary layer (see Sect. 2.1); four simulations have been performed, noted in the rest of the paper by T21, T21BL1, T42 and T42BL1. In general, unless otherwise specified, we analyse climatological model monthly means calculated over the 2000–2005 period.

The initial conditions of the stratospheric species have been derived from a zonal climatology built from a 6-year simulation performed using the ARPEGE-Climat GCM coupled to the REPROBUS CTM (WMO, 1998). This climatology represented conditions of the mid-90s and was adapted for the year 2000 according to the values reported in WMO (2002). The climatological state provided to the model allows us to reduce the spin-up in the stratosphere. For the tropospheric species, a mean global value is used in the lowest levels of the model that correspond approximately to the boundary layer; this crude initial state is rapidly lost, within a few days.

Another 6-year simulation was performed with the "cheapest" configuration of MOCAGE-Climat (i.e., T21BL1) in order to analyze the model stability over a longer time period, initializing 1 January 2000 with the conditions of 31 December 2005 obtained from the first 6-year sequence, and driving the CTM again with the 2000–2005 ECMWF analyses (experiment T21BL1bis). Finally, a 6-year simulation was performed as a sensitivity test to the dry deposition velocity; forcings were identical to the T21 forcings, except for the deposition velocities that were climatological (simulation T21DvClim, see Sect. 4 for details and results).

A summary of the six simulations appears in Table 5. Model outputs retained to appear in the various figures correspond to results whose resolution is the closest to the observations (e.g., T21 for stratospheric zonal comparisons, T42 for tropospheric CO), unless explained otherwise in the text. Statistics compiled from all simulations appear in paragraph 3.8.

Prior to these experiments, specific simulations had been completed to evaluate the transport processes in MOCAGE-Climat. Considering idealized tracers only, a total of 20 years were simulated using repeatedly the ECMWF operational analyses of 2000 and 2001. These simulations were performed according to the Stratospheric-Climate Links with Emphasis on the Upper Troposphere and Lower Stratosphere (SCOUT-O3) specifications; for instance, the use of a continuous and linearly increasing source in the tropical troposphere allowed us to access to age of air, and thus to transport accuracy; we present a summary of the results obtained in Sect. 3.2.

Before looking further into the results, it is important to make sure that the model is conservative, that it does not produce or destroy mass during the simulations, especially for climate purposes when simulations should run over decades. One way to assess the numerical stability is to look at the evolution of the global mean of the ozone column (zonal and latitudinal average), as ozone is directly or indirectly linked to all other chemical species. Drifts of individual species could in the end compensate and result in no drift of the ozone column, but analyzing the evolution of this parameter provides a first estimation of the robustness of the model. The model reaches equilibrium around 290 Dobson units (DU) for the T21 simulation, 292 for T21BL1, 308 for T42, and 309 for T42BL1; these figures are consistent with the generally accepted value of 300 DU (see the figure provided in supplementary material: http://www.atmos-chem-phys.net/7/5815/2007/acp-7-5815-2007-supplement.pdf).

Table 5. Summary of the 6-year simulations completed with MOCAGE-Climat (see text for details).

Name	Characteristics
T21	full version of MOCAGE-Climat at T21
T21BL1	same as T21 but with a simplified boundary layer
T21BL1bis	same as T21BL1 with a different initial state
T21DvClim	same as T21 but with climatological deposition velocities
T42	full version of MOCAGE-Climat at T42
T42BL1	same as T42 but with a simplified boundary layer

A bias smaller than 2 DU exists between the T21 and the T21BL1 simulations while the T42 simulations lead to ozone columns higher by 17–18 DU than the T21 case. This increase, in parallel with an increase in horizontal resolution, could be related to stronger meridional circulation, and to less numerical diffusion that would counteract the rapidity of the circulation (see Sect. 3.2). The same behaviour has been found when using the linear ozone chemistry within MOCAGE-Climat. This tends to confirm the hypothesis of dynamical causes for higher ozone columns when the horizontal resolution increases. Using climatological deposition velocities in experiment T21DvClim, the resulting ozone is quasi-identical to that obtained with the T21 simulation which included a detailed calculation of these velocities.

According to this simple test, the numerical stability of the various simulations completed with MOCAGE-Climat appears satisfactory as there is no drift in the total ozone column even after a 12-year integration of the model.

3.2 Age of air (AOA)

Transport in the stratosphere involves a meridional circulation, the so-called Brewer-Dobson circulation (Brewer, 1949), mixing across mid-latitudes, and vertical diffusion. Mixing across latitudes is highly inhomogeneous with transport barriers in the subtropics, and at the edge of winter time polar vortices. Air parcels coming from the troposphere enter the stratosphere at tropical latitudes.

Once in the stratosphere, they are elevated by the Brewer-Dobson circulation, meridionally transported towards the

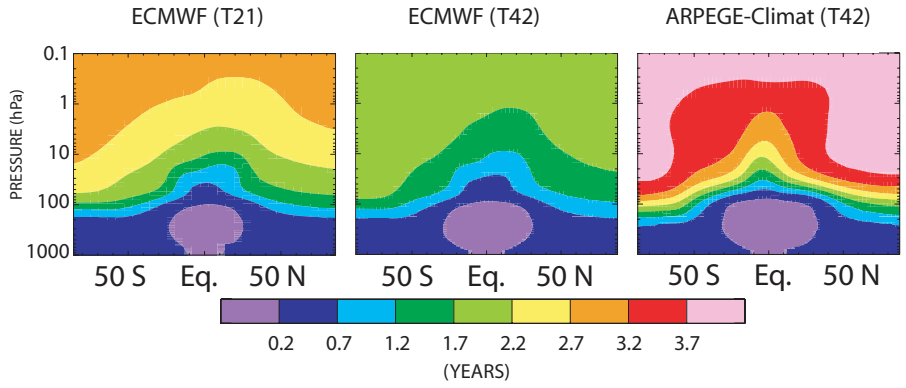

Fig. 1. Latitude-pressure cross sections of the resulting age of air (years) when MOCAGE-Climat is driven by the ECMWF operational analyses, at T21 (left) and T42 resolutions (middle), and by outputs from the ARPEGE-Climat GCM at T42 resolution (right). Fields are those of the last year of the simulation.

winter pole and descend at mid- and high latitudes. The longer a parcel stays in this stratospheric circulation, the higher is the probability that it can be chemically or photochemically affected. Therefore, the correct representation of this circulation in a CTM is of primary importance as it determines the accurate simulation of long-lived chemical components originating from the troposphere (the stratospheric source species). One way to assess the quality of this transport is to follow air parcels from the troposphere to the lower polar stratosphere. As there is an infinity of pathways corresponding to the so-called "age spectrum", an alternative way is to determine the mean age of air (AOA) that is the first moment of the age spectrum. A simple tropospheric tracer continually emitted with a linear growth in time can be used to diagnose the model mean age of air (Hall and Waugh, 1997).

MOCAGE-Climat simulations were performed at T21 and T42 resolutions (see Fig. 1). The zonal distribution shows the AOA to have minimum values in the tropical lower stratosphere, illustrating the rapid motion of air through the tropopause. AOA is maximum in the upper stratosphere with a smoother latitudinal gradient as altitude increases. Simulations of MOCAGE-Climat show much younger AOA than deduced from observations of SF_6 (Harnisch et al., 1996; Boering et al., 1996): at 20 km of altitude, AOA derived from measurements ranges from 1 year in the tropics up to 4.5–6 years at polar latitudes. The simulated AOA differs depending on the horizontal resolution, from 0.5 to 2.3 years for the T21 simulation, and from 0.3 to 1.8 years for the T42 simulation, indicating that the transport is significantly too fast in the stratosphere of MOCAGE-Climat when driven by the ECMWF operational analyses. This was noted by Bregman et al. (2006) for their CTM TM5 using the ECMWF operational analyses of 1999 and 2000. They obtained much older AOA however, and this appears to be mainly related to the fact that their CTM is Eulerian while MOCAGE-Climat has a semi-lagrangian transport scheme (Chipperfield, 2006).

We might expect the age of air to increase with increasing horizontal resolution as has been observed in several Eulerian CTMs (Norton, 2000). In our case, with increasing horizontal resolution, the age of air has slightly decreased which is in agreement with the results of Scheele et al. (2005) and of Chipperfield (2006). It is also consistent with the results presented later in the paper. We repeated the same AOA experiment driving MOCAGE-Climat with the meteorological outputs of the ARPEGE-Climat GCM; the resulting AOA ranges from 0.7 to 3.5 years, agreeing better with observations, but still too young. We chose however to drive our simulations with the ECMWF meteorological analyses rather than the ARPEGE-Climat outputs as these analyses are the closest to the real atmospheric fields and are therefore the best to use for an evaluation of the CTM against observations. Outputs from ARPEGE-Climat will be used for long-term simulations.

3.3 Observations used for the evaluation

The main characteristics of the observational datasets used are presented in Appendix. They consist in satellite and in-situ observations for which derived climatologies have been evaluated and described in the literature (see Table 6 for a summary). Unless otherwise specified, the satellite instruments from which information on atmospheric trace gas constituents is retrieved fly in near-polar, sun synchronous, low earth orbits; for low and mid latitudes, this results in observations at a constant local time. Global satellite climatologies are already available for several chemical species in the stratosphere, and the last decade has seen the implementation of satellite measurements of tropospheric constituents.

Table 6. Main characteristics of the observational datasets.

Species	Horiz. resol.	Vert. extens.	Temp. resol.	Period of obs.	Reference
O_3 column	1° lat×1.25° lon Uncertainty: 1%	tot.	month	1978–2005	Bodeker et al. (2005)
O_3	∼10 km, 2.8° ×2.8° Uncertainty: 2%	UTLS and tropo.	1 min, season	2000–2004	Marenco et al. (1998)
NO_2 column	0.25°×0.25° Uncertainty: 1–3.5 10^{15} molec cm^{-2}	tot. and tropo.	month	2003–	http://www.temis.nl
NO_y	∼10 km, 2.8°×2.8° Uncertainty: 10%	UTLS and tropo.	1 min, season	2002–2004	Volz-Thomas et al. (2005)
Strato. CH_4, H_2O	5° lat Uncertainty: lower strato. CH_4 11–19%, H_2O 14–24% – upper strato. CH_4 6–27%, H_2O up to 30%	316–0.1 hPa	month. clim.	1991–2002	Grooss and Russel (2005)
Strato. NO_x, HCl, O_3	5° lat Uncertainty: lower strato. NO_x 14–21%, HCl 14–24%, O_3 9–25% – upper strato. NO_x up to 30%, HCl 12–15%, O_3 9–20%	316-0.1 hPa	month. clim.	1991-2002	Grooss and Russel (2005)
Strato. HNO_3	4° lat Uncertainty: 0.1–3 ppbv	100–0.32 hPa	month. clim.	1991–1993	Randel et al. (1998)
Strato. N_2O	4° lat Uncertainty: up to 22%	100–0.32 hPa	month. clim.	1991–1993	Randel et al. (1998)
Strato. ClO	4° lat Uncertainty: 15–25%	100–0.32 hPa	month. clim.	1991–1997	Randel et al. (1998)
Strato. N_2O	10° lat Uncertainty : up to 35 ppbv	100–1 hPa	month	2001–2005	Urban et al. (2005)
Tropo. CO	1°×1° Uncertainty: 10%	surf.-150 hPa	month	2000–	Emmons et al. (2004)
CO	∼10 km, 2.8°×2.8° Uncertainty: 2%	UTLS and tropo.	1 min, season	2002–2004	Nédélec et al. (2003)
Tropo. OH	8° lat×10° lon Uncertainty: winter north tropics. 15–20% – south trop. 10–15% – south extra tropics. 25%	1000–200 hPa	month. clim.	1978–1996	Spivakovsky et al. (2000)
Tropo. O_3	∼40 stations Uncertainty: ±5% (strato.)	surf.-10 hPa	month. clim.	1980–1993	Logan (1999a,b)
Tropo. HNO_3	camp. regions Uncertainty: 15–60%	Surf.-200 hPa	clim.	variable	Emmons et al. (2000)

3.4 Long-lived species

Chemical species that have a rather long lifetime, typically more than one year, are often sources of stratospheric radicals and reservoirs. The chemistry of these source species is rather simple and mostly restricted to photo-dissociation or thermal reaction with OH or $O(^1D)$, the latter being mainly present in the middle atmosphere. Therefore, long-lived species are well-mixed within the troposphere and their concentrations start to decrease once they enter the stratosphere. As a consequence, they can be relatively good markers of transport processes, particularly in the UTLS region, as used for instance by El Amraoui et al. (2007). They are also of primary importance for validating photo-dissociation rates as they determine the nitrogen, chlorine or bromine contents of the atmosphere of the model.

3.4.1 Methane (CH_4) and water vapour (H_2O)

CH_4 is an atmospheric gas emitted at the surface that has a major radiative impact on the atmosphere. It interacts with the whole atmospheric chemistry through reacting with OH, and therefore with several chemical cycles such as those involving halogens (Brasseur and Solomon, 1986). In 2000,

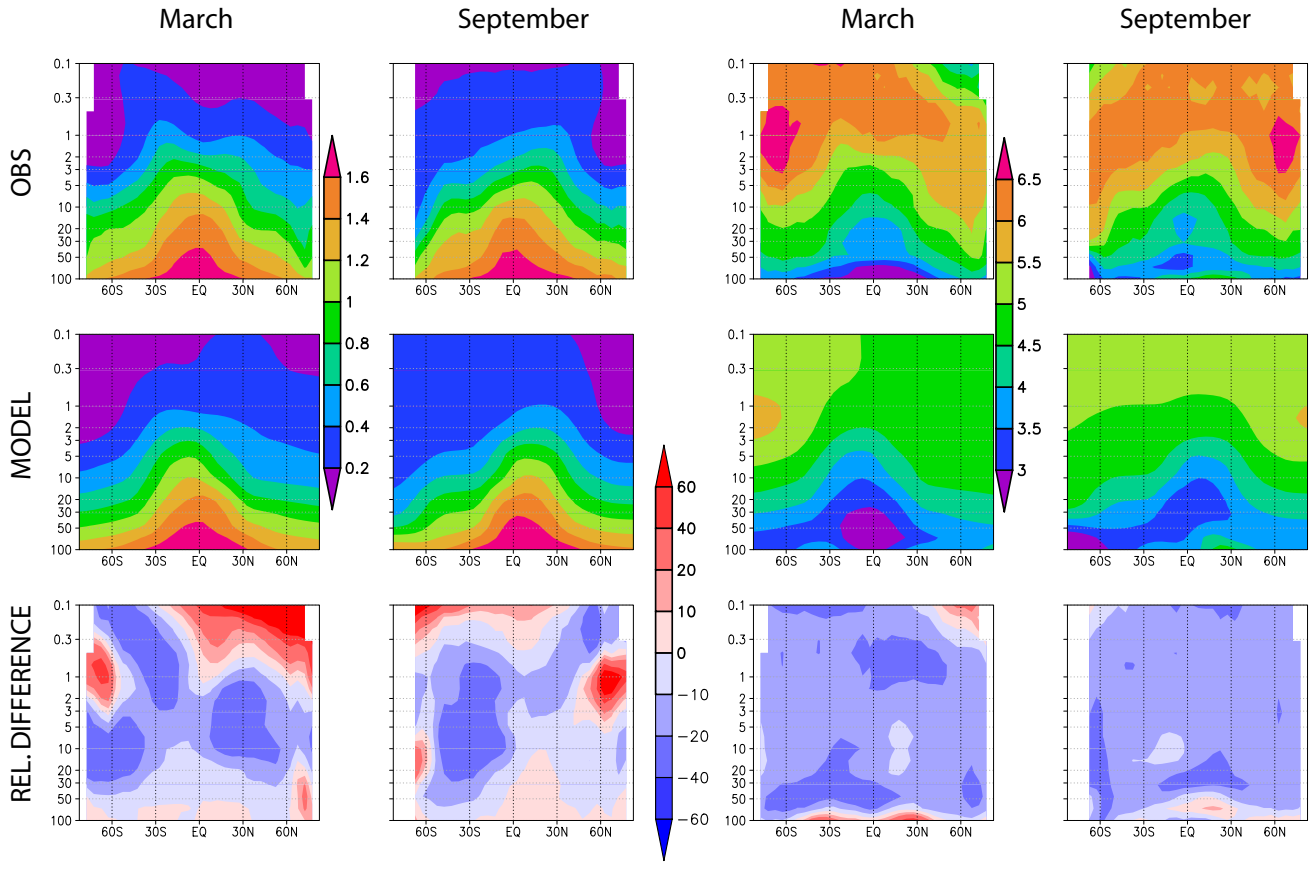

Fig. 2. MOCAGE-Climat T21 zonal monthly mixing ratios against the Grooss and Russel (2005) climatology, and relative differences (100×((Model−Obs)/Obs)), between 100 and 0.1 hPa, in March (left panels) and September (right panels): first two columns CH_4 (ppmv), and last two columns H_2O (ppmv).

the average mixing ratio at the surface ranged from 1708 to 1784 ppbv (WMO, 2002). The mean global growth for the period 1983–2000 is estimated as 8.5 ppbv yr^{-1}; however, in the past few years, this rate has displayed striking fluctuations, with for instance a negative rate in 2000 (Simpson et al., 2002). The reason for these changes in behaviour is still unclear and shows that extrapolations for the future are difficult. The strengths of many of the sources are still uncertain due to the difficulty in assessing the global emission rates of the biospheric sources which are highly variable in space and time (e.g., emissions from wetlands that represent approximately 160 $Tg(CH_4)$ yr^{-1}). Due to its long lifetime, around 8.4 years (Houghton et al., 2001), methane is a good dynamical tracer and may be used to verify the simulations of meridional transport and diabatic descent in the polar vortices. The ability to correctly simulate CH_4 (and H_2O) is a useful benchmark for numerical models of the middle atmosphere (Randel et al., 1998). In the stratosphere, the overall structure and variability of CH_4 is strongly coupled with H_2O: as a first approach, it can be considered that the destruction of one molecule of CH_4 yields to the production of two molecules of H_2O.

Comparisons between outputs of the MOCAGE-Climat T21 simulation and the zonal climatology of Grooss and Russel (2005) are shown in Fig. 2, between 100 and 0.1 hPa, for the months of March and September. Even though the T21 AOA is too young (see paragraph 3.2), the overall model CH_4 distribution resembles the observed one: CH_4 decreases with height and latitude. However, the diabatic descent in the southern polar vortex in September does not seem as marked in the simulations (although observations exist up to 65 S only), and the distinctive 'rabbit-ears' shape in the observations in March is not clearly simulated. Nevertheless, the seasonal shift of the maximum towards the winter hemisphere appears similarly in the model and in the observations. For H_2O, the shape of the zonal distribution is qualitatively well simulated, with low equatorial mixing ratios above the tropical tropopause and generally a positive gradient towards higher altitudes and latitudes. Moreover, the dehydration is very similar in the simulations and in the observations. More quantitatively, CH_4 mixing ratios from the model appear generally too low, 5 to 30% (±-0.05 to -0.25 ppmv), and in parallel H_2O mixing ratios are underestimated throughout the stratosphere, with relative differences between simula-

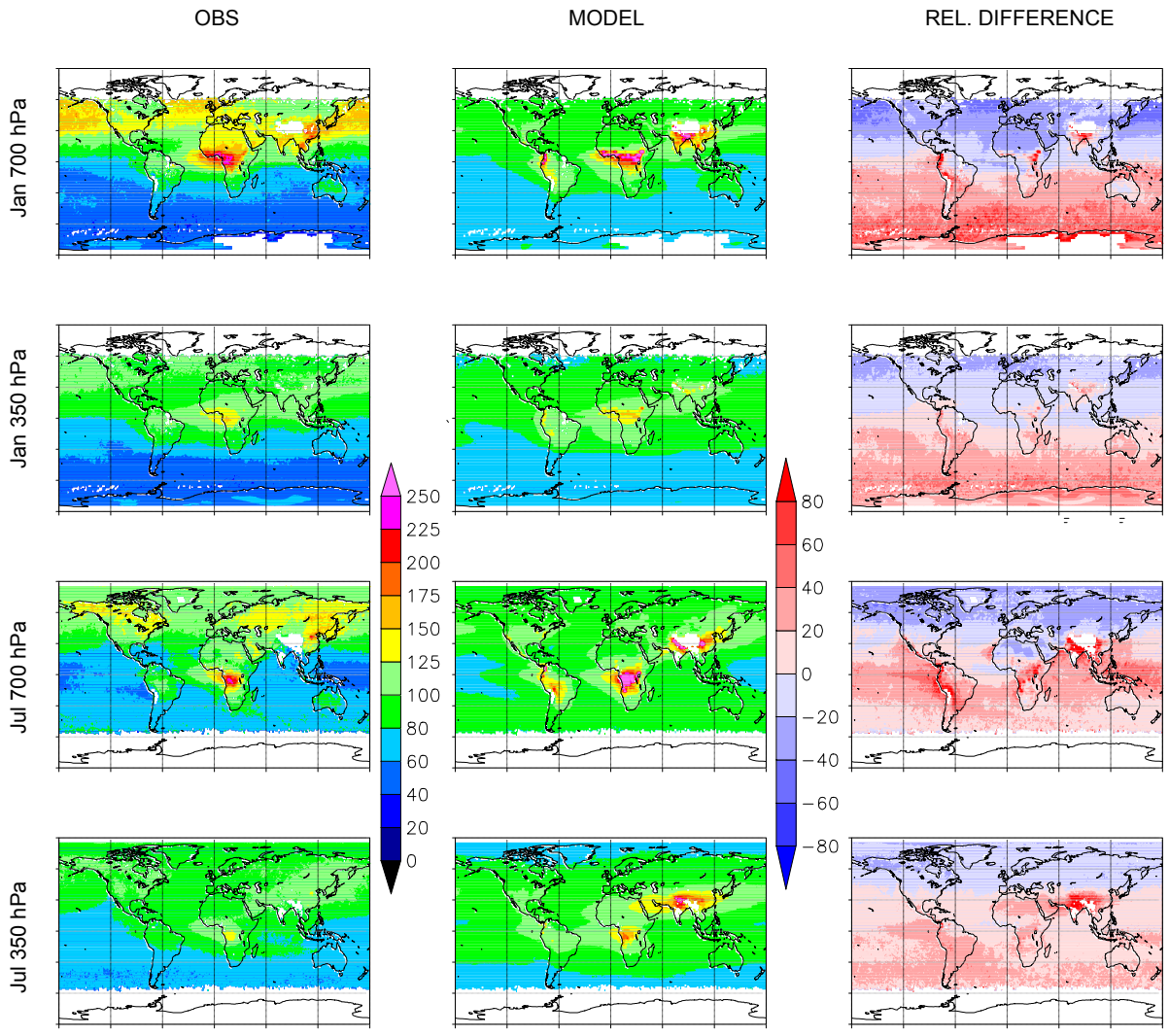

Fig. 3. MOCAGE-Climat CO mixing ratios (ppbv) from the T42 simulation versus MOPITT mixing ratios (see text), and relative differences (100×((Model−Obs)/Obs)), in January (2 upper rows) and July (2 bottom rows), at 700 and 350 hPa. The time versus latitude diagrams are also shown.

tions and observations varying from −10 to −25% over large parts of the stratosphere (±−0.9 to −1.3 ppmv). These differences can have several causes including the chemical destruction of CH_4 (consequently production of H_2O), the underestimation of the mixing ratios at the entry level, or the deficiencies of the meridional transport. Further light on this is provided by the analysis of the T42 simulation and of an additional simulation with MOCAGE-Climat driven by the ARPEGE-Climat GCM.

As expected in agreement with increasing age of air (ECMWF T42 AOA < ECMWF T21 AOA < Arpege-Climat T42 AOA, see paragraph 3.2), there is much more CH_4 in the entire stratosphere in the ECMWF T42 simulation than in the T21 simulation, the T42 simulation overestimating observations. T21 CH_4 outputs are in turn larger than those of the ARPEGE-Climat simulations. For H_2O, mixing ratios are lower in T42 than in T21. They are similar in T21 and in ARPEGE-Climat, but the shape of the distribution from the ARPEGE-Climat simulation, being more centered around the equatorial latitudes, is more realistic (see the figures provided as supplementary material: http://www.atmos-chem-phys.net/7/5815/2007/acp-7-5815-2007-supplement.pdf). The underestimation of the T21 CH_4 could explain the negative deviation of H_2O, however this explanation does not hold for the T42 outputs. The entry levels of CH_4 are overestimated in March and September. Therefore, there seems to be some deficiency in the oxidation chain of CH_4 as one would expect to obtain T21 CH_4 mixing ratios that are too large since the circulation is too fast. As for H_2O, both that the circulation is too fast

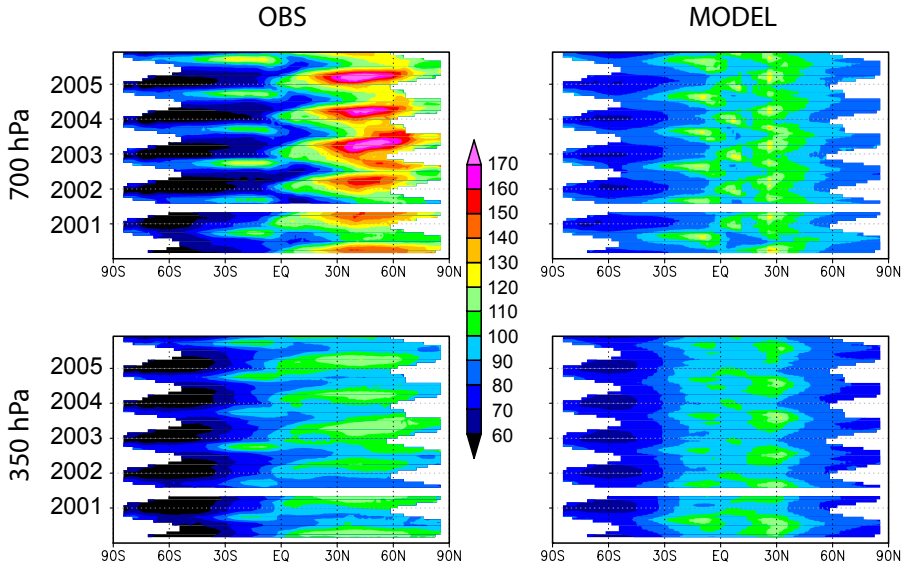

Fig. 3. Continued.

and that the entry-level mixing ratios are too low are plausible explanations of its deficient simulation. Indeed, if the circulation is too fast, there is insufficient time for moistening through methane oxidation. This problem is even greater in the T42 simulation, hence the lower H_2O mixing ratios in this case. The rate of methane oxidation could also possibly be too slow. All this requires further investigation.

3.4.2 Carbon monoxide (CO)

Carbon monoxide is a precursor to tropospheric ozone, it influences the abundance of OH and hence the tropospheric oxidation capacity and methane, and it is a source of carbon dioxide. It thus affects two of the most important greenhouse gases. Because of its relatively long lifetime in the troposphere (∼1 month) it provides a view of transport processes in the model in this layer. Tropospheric CO is directly emitted at the Earth's surface and is also chemically produced by the oxidation of hydrocarbons in the troposphere. Both direct and indirect sources include a mixture of contributions from natural (e.g., oceans or vegetation) and anthropogenic activities (e.g., biomass burning). Of all the tropospheric primary pollutants, CO is among the best observed in the troposphere on a global scale from satellites. It is the only pollutant for which global satellite data includes information on the vertical distributions.

We applied the monthly averaging kernels available with the MOPITT data set (1° grid) to the monthly outputs of the T42 simulation interpolated on the same 1° grid. We therefore obtained transformed model data, comparable to the MOPITT data (Emmons et al., 2004). Figure 3 presents comparisons between the model and the observations as latitude-longitude maps on pressure levels. We focus on January and July which are monthly means of the six years of data as the initial state is lost after about one month. These months are intermediate between April, where there is a springtime maximum of CO in the Northern Hemisphere, and October, with the peak of the Southern Hemisphere biomass burning season linked to biomass burning emissions in South America, southern Africa, the maritime continent, and northern Australia (see Shindell et al., 2006; Edwards et al., 2006). Two pressure levels that contain vertically independent information are shown. The 700 hPa level gives an indication of the agreement in the lowest levels of the troposphere, while the 350 hPa level gives additional insight on the transport processes.

MOCAGE is able to capture some of the characteristics of the global spatial distribution of CO as observed by MOPITT. For instance, at 700 hPa the model successfully reproduces the maxima over Africa north of the Equator in January and south of the Equator in July, while the maximum over South America in July is about 1 to 2 months too early. This temporal shift induces positive biases of more than 40% (around 30 ppbv) that extend over the tropical western Pacific following trade winds. Agreement between model outputs and observations is better in July than in January, and better at 350 than at 700 hPa. The model underestimates the concentration of CO in the Northern Hemisphere in January, and north of 30N in July, with relative differences varying from less than 20% at 350 hPa over most of the globe in July to around 30% over large parts of the Northern Hemisphere at 700 hPa in January. In contrast, the model overestimates the concentration of CO in the Southern Hemisphere, for both seasons and pressure levels, with the largest relative differences (above 40%) essentially at low mixing ratios

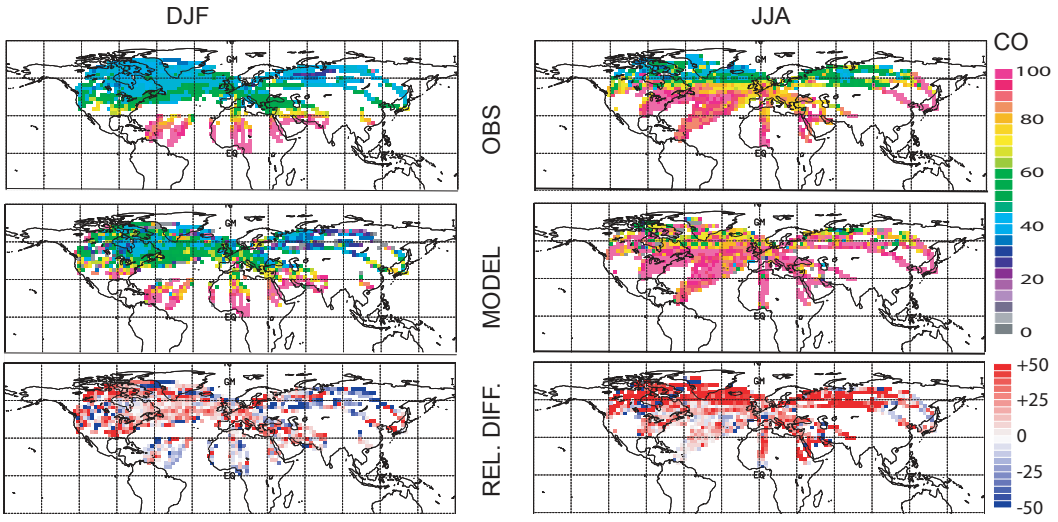

Fig. 4. Distribution of CO mixing ratio (ppbv) in 3-D boxes (2.8°×2.8° along the horizontal, 340–350 K potential temperature layer), as seen by MOZAIC (top panels), simulated by MOCAGE-Climat (T42 experiment, middle panels) and relative differences (bottom panels) (100×(MOCAGE−MOZAIC)/MOZAIC) for winter (DJF, left) and summer (JJA, right) of the 2000/2004 period.

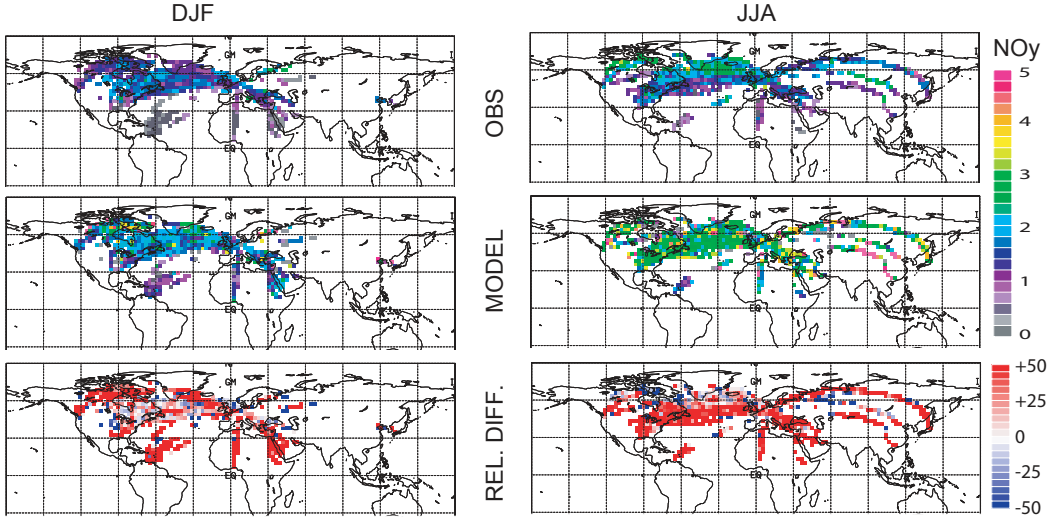

Fig. 4. Continued. As in Fig. 4, for NO_y mixing ratios (ppbv).

(<60 ppbv). The model accumulates CO over northern India and the Himalaya, and this is related to high emissions in the populated regions at the base of the mountains further relayed by the Asian summer monsoon. Li et al. (2006) reported on how the anthropogenic emissions are "trapped" by the Tibetan anticyclone. However, the accumulation by the model is too large compared with observations.

The time versus latitude diagrams (Fig. 3) at 700 hPa clearly show that the variability is lower in the model. Some large structures are correctly reproduced, such as the lower mixing ratios between 70 S and 30 S around the boreal winter time, and the higher mixing ratios between 30 S and the Equator that appear too early, as already mentioned. The duration of this feature is also too long. Between the Equator and 30 N, the seasonality is correctly simulated but with an overestimation of the minima and an underestimation of the maxima. The major discrepancy is north of 30 N, and this also appears in the diagram at 350 hPa.

On-going validation of the MOPITT CO is reported in the literature and gives a context to these results. Emmons et al. (2004) validated MOPITT measurements from the beginning of operations until December 2002 with a variety of aircraft in-situ profiles. Over North America, they report at 700 hPa a positive bias of 7–14% (±7–18%) consistent with that of

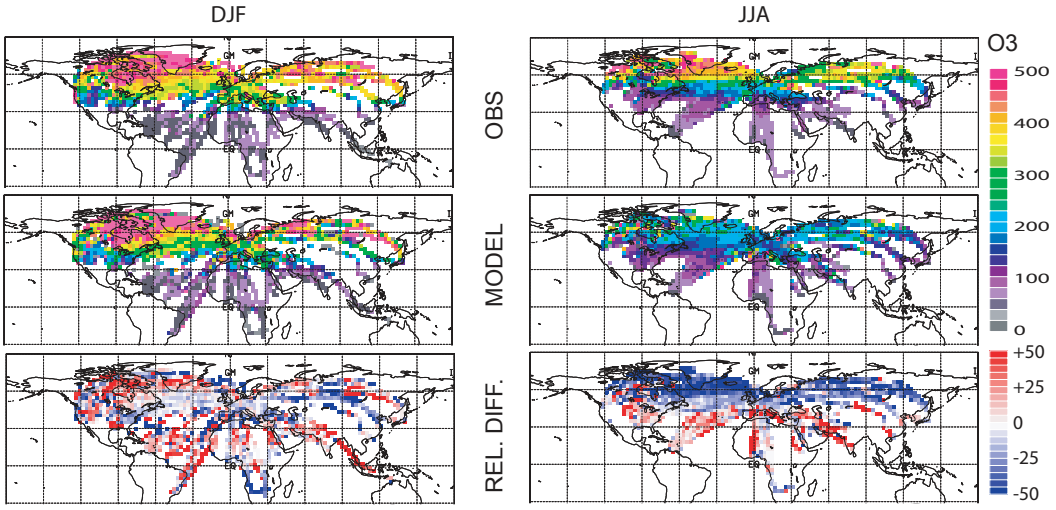

Fig. 4. Continued. As in Fig. 4, for O_3 mixing ratios (ppbv).

Emmons et al. (2007) who validated MOPITT measurements over North America during several aircraft experiments in the summer of 2004. At 350 hPa the bias was estimated as ∼3% (±6–8%). Emmons et al. (2004) indicate that larger biases are seen in clean environments, such as the south Pacific.

Further insight on model simulation of CO is given in Shindell et al. (2006) who analyzed present-day and future carbon monoxide simulations in 26 state-of-the-art atmospheric chemistry models against MOPITT observations and local surface measurements. The models showed large underestimations of Northern Hemisphere extra-tropical CO, while typically performing reasonably well elsewhere. Shindell et al. (2006) attributed the negative bias to a substantial underestimation of CO emissions. The same emissions were used in this study. It is also probable that some of the underestimation is due to the fact that there is no seasonality in the anthropogenic emissions that dominate over these regions. In the Southern Hemisphere, the overestimation of MOCAGE-Climat that we show suggests that emissions of CO south of the Equator, which are mainly from a biomass burning origin, are too strong. It could be also that the transport from the Equator towards the polar regions is too fast, bringing too much CO towards latitudes where its lifetime is longer.

In the UTLS, systematic CO observations are mainly provided by MOZAIC measurements. For our evaluation, we made on-line interpolations during the simulations to obtain model outputs coincident in time and space with the MOZAIC observations. At aircraft cruise level (Fig. 4), MOZAIC shows a strong meridional gradient between the Equator and 70N, modulated by a seasonal cycle; the highest CO mixing ratios are encountered at low latitudes, with values up to 100 ppbv that extend in summer to mid-latitudes. This gradient is related to air sampling, as aircraft fly in the lower stratosphere at mid-latitudes, and in the troposphere at low latitudes. MOCAGE-Climat captures both the latitudinal gradient and the seasonal cycle. However, the model generally overestimates CO in boreal summer while there is no systematic bias in winter.

When looking at frequency distributions of CO with MOZAIC measurements made at all flight levels, over various regions of the globe (see Sect. A6 for their definition, and Fig. 5), MOCAGE-Climat exhibits narrower distributions than MOZAIC, with the T42 simulation closer to observations than the T21 simulation. This is most likely due to the better description of the convection and to a better resolution of the tropopause. In the tropical band, while the model clearly underestimates measurements over South America, the agreement is very good over Africa, particularly for the T42 simulation. At northern mid-latitudes, MOCAGE-Climat underestimates the highest CO mixing ratios, as already seen in the comparisons with the MOPITT observations.

3.4.3 Nitrous oxide (N_2O)

N_2O is considered as one of the three most important anthropogenic greenhouse gases along with CO_2 and CH_4; it is also the major source of stratospheric nitrogen that can affect O_3 (Crutzen, 1970; Randeniya et al., 2002). Its atmospheric burden has increased from 295–299 ppbv in 1978 up to 315–317 ppbv in 2002, as reported by Prinn et al. (2000) and WMO (2002). Surface emissions represent the main source of N_2O, and comprise anthropogenic emissions (cultivated soils, industrial processes, and biomass burning), and natural emissions (continental soils and oceans). Its principal sinks are photo-dissociation and reaction with $O(^1D)$ in the stratosphere. Both reactions produce molecular nitrogen N_2, but can also lead to NO_x production. In this case, the main chan-

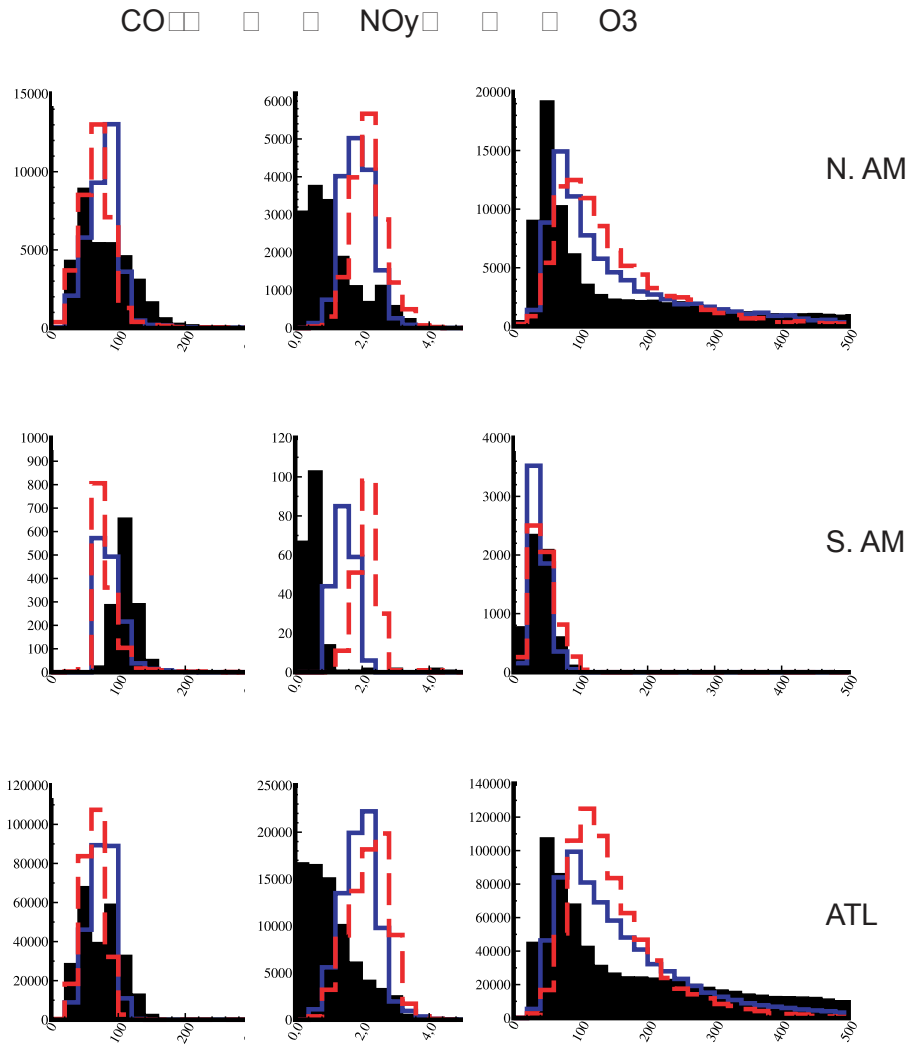

Fig. 5. Left column: histograms of CO classes (20 ppbv bins) measured by MOZAIC (black) and simulated by MOCAGE-Climat at T21 (red) and T42 (blue), for North America (N.AM), South America (S.AM), northern Atlantic (ATL), Europe (EUR), Africa (AFR), and Asia (ASIA) (see Appendix A6 for the definition of the geographical areas). Middle column: same as CO for NO_y classes (0.4 ppbv bins). Right column: same as CO for O_3 classes (20 ppbv bins).

nel is $N_2O + O(^1D) \rightarrow 2 \times NO$ with a relatively fast chemical reaction rate. The lifetime of N_2O has a mean value of 120 years (WMO, 2002), it is therefore rather well mixed within the troposphere. Nevertheless, Ricaud et al. (2007) showed from ODIN N_2O observations that this compound can have spatial variations in the UTLS, especially in the tropics where troposphere to stratosphere exchange sometimes takes place in association with convective events.

Figure 6 presents the UARS climatology of Randel et al. (1998) and model outputs from the T21 simulation for March and September: the modeled N_2O field is consistent with the observations, maximizing in the lower stratosphere and decreasing as the altitude increases. In the lower stratosphere, MOCAGE-Climat simulates a smoother N_2O field as a function of latitude than UARS, with higher mixing ratios than the measurements. In the upper stratosphere (from 10 to 1 hPa), at equatorial and mid-latitudes, the model underestimates the observations, in March and September. This tends to indicate that the destruction of N_2O (photolysis + reaction with $O(^1D)$) may be somehow too strong as we would expect the contrary on the basis of the too quick circulation alone. This hypothesis is confirmed by the outputs of both the ARPEGE-Climat driven simulation and of the T42 simulation (see the figures provided as supplementary material: http://www.atmos-chem-phys.net/7/5815/2007/acp-7-5815-2007-supplement.pdf). Indeed, in the former case, with a relatively realistic AOA (see paragraph 3.2) N_2O mixing ratios are lower than observations by 20% or more throughout the stratosphere. In the T42 case, the model overestimates observations, again throughout the

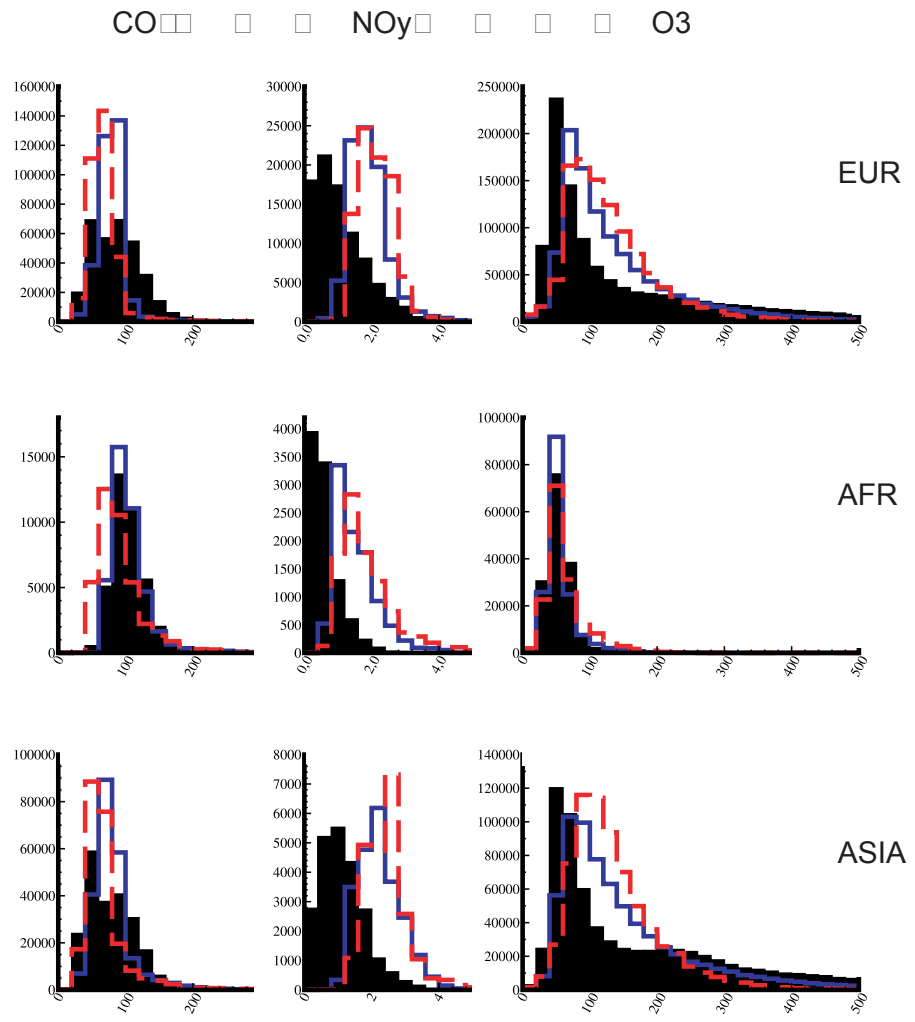

Fig. 5. Continued.

stratosphere by 20% or more which reveals that, though too strong, the destruction of N_2O is not too far off to counteract the fast T42 circulation. Further light is thrown on the deficiencies of the N_2O field by analysing the NO_y field (see paragraph 3.4.4). At high latitudes, differences between the model and the UARS observations have a seasonal cycle; this is also visible in the ODIN/SMR observations. For comparison with these observations, the simulated N_2O fields have been averaged in 10 degree latitude boxes. Figure 7 shows the evolutions between 2001 and 2005 of the zonal averages over three latitude bands with different dynamical characteristics, 80 S–70 S, 10 S–EQ, and 50 N–60 N. In the tropical high stratosphere (10 S–EQ), the underestimation of the model, already mentioned in the comparison with the UARS observations, appears in the time series for all years, though in a limited way for the year 2002. In the tropical high troposphere, that corresponds to the lowest altitudes ODIN can observe, N_2O is rather well mixed both in MOCAGE-Climat and in the satellite observations. However, as mentioned before, some variability appears around the 100 hPa level observed by ODIN with a minimum occurring during the spring of 2004; this minimum is not reproduced by the model. At high southern latitudes (80 S–70 S), the seasonal cycle of larger and smaller mixing ratios at a given altitude is not as marked in the model as in the observations. This is related, in winter to a too weak mesospheric subsidence in the ECMWF analyses, and in summer to the bias of the chemical destruction already mentioned. It results in alternating underestimations and overestimations of the observations. In the 50–60 N latitude band, differences are generally not as important as for the other latitude bands, except for 2003, which reflects that the circulation is better simulated in the Northern Hemisphere.

3.4.4 Total nitrogen oxides (NO_y)

The NO_y family consists of all nitrogen compounds excluding N_2O. NO_y is produced from one branch of the reaction

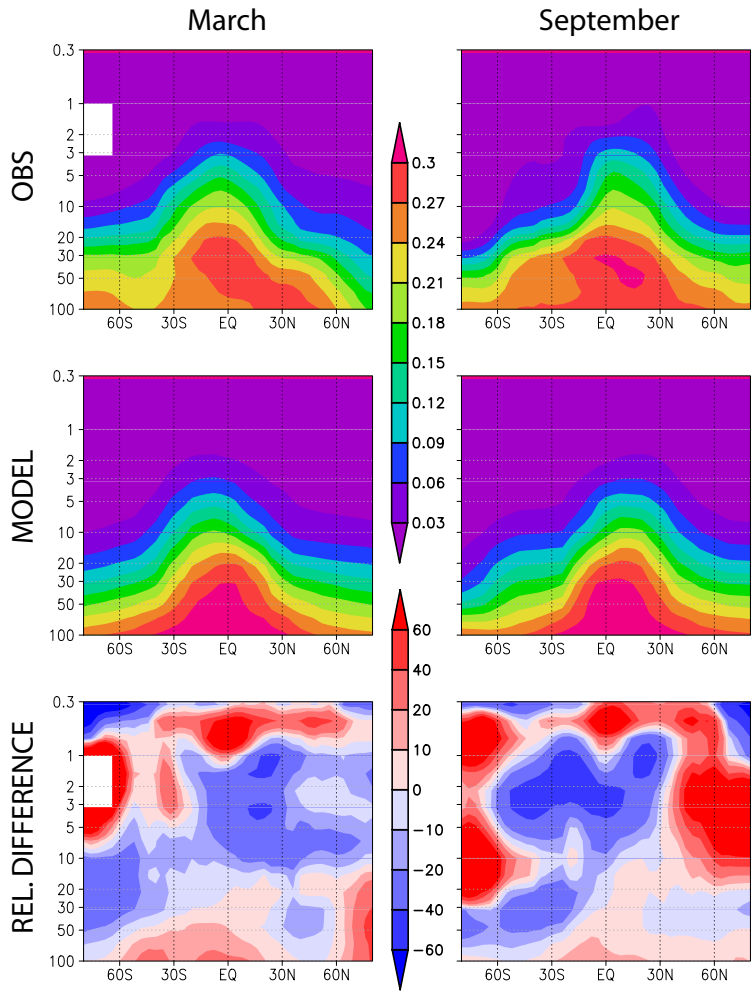

Fig. 6. MOCAGE-Climat T21 zonal monthly mixing ratios of N_2O (ppmv) against the Randel et al. (1998) climatology, and relative differences (100×((Model−Obs)/Obs)), between 100 and 0.3 hPa, in March (left panels) and September (right panels).

of N_2O with $O(^1D)$. $O(^1D)$ itself comes from the photolysis of N_2O or O_3. We have first validated the simulated NO_y in the UTLS with the MOZAIC observations. The comparisons between MOCAGE-Climat T42 outputs and observations in DJF and JJA appear in Fig. 4, while histograms of NO_y classes for several regions of the world are presented in Fig. 5 (observations versus T21 and T42 simulations). The model always presents a positive bias, over all regions of the world. This overestimation is higher in the summer months when the chemistry that controls NO_y is the most effective. It appears clearly in the plotted distributions of Fig. 5: peaks of the distributions of the model are 2 to 4 times higher than peaks of the observations, depending on the region. Furthermore, shapes of the distributions differ: observations have asymmetric distributions with large occurrences of very low mixing ratios (<0.4 ppb), mainly observed in winter, while distributions of the model are quite symmetric and show no occurrence of these low mixing ratios. In the UTLS, various sources can contribute to augmenting the NO_y content, including lightning and aircraft emissions, transport from the troposphere and stratospheric intrusions. In our case, the first two sources are not relevant as we did not take them into account in the present simulations. On the contrary, transport from the troposphere can be incriminated for this positive bias in the UTLS: we will see later in the paragraph on nitrogen oxides (paragraph 3.5.1) that MOCAGE-Climat shows a general overestimation of the NO_2 tropospheric content, in particular in winter. The impact on the UTLS is the positive deviation against the MOZAIC observations that we see here. As for the last hypothesis (intrusions from the stratosphere), we got a sense of the validity of the stratospheric NO_y of the model by comparing it to the sum of HNO_3 and sunset $NO + NO_2$ from the UARS observations, along the recommendations of Park et al. (1999). In March and September (not shown), months presented in our N_2O comparison, the model overestimates observations (by 10 to 20% between 50

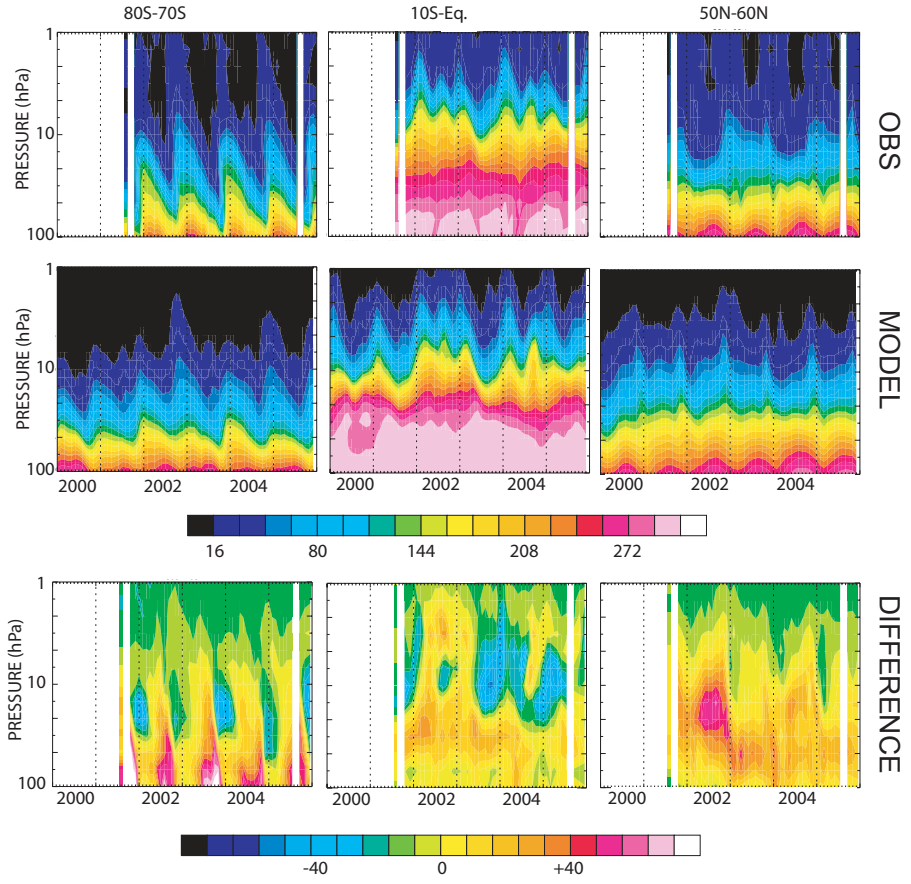

Fig. 7. Time/pressure series for N_2O zonally averaged bands of 10 degrees, 80 S–70 S (left panels), 10 S–EQ (middle panels) and 50 N–60 N (right panels), for ODIN observations (upper line, in white no observations), simulated by MOCAGE-Climat (T21BL1 simulation, middle line) and absolute differences (model – observations) (ppbv) (bottom line).

and 2 hPa) over most latitudes and altitudes, for both months. This positive bias in the stratosphere could well play a role in the positive bias in the UTLS, and it is in agreement with the destruction of N_2O being too large (see paragraph 3.4.3).

3.5 Short-lived species

Long-lifetime species can degrade into chemical species that are rather "aggressive" and therefore, have short lifetimes as they may react with a large number of chemical constituents in the atmosphere.

3.5.1 Nitrogen oxides (NO_x)

Generally, the sum of nitrogen monoxide (NO) and nitrogen dioxide (NO_2) is referred to as "nitrogen oxides" (NO_x). These two components are strongly linked to each other as in the atmosphere they can change from one form to the other very quickly. Hence the NO_x family is more stable than its two components. These species play a key role in the ozone budget, particularly in the lower stratosphere (Brasseur and Solomon, 1986), together with the HO_x and ClO_x families, and so their correct representation is essential to simulate a realistic ozone distribution there. In MOCAGE-Climat, NO_x is a so-called family that gathers NO, NO_2, nitrogen trioxide (NO_3), and atomic nitrogen (N) that is mainly present in the middle atmosphere with mixing ratios lower than a few pptv. The use of NO_3 within the NO_x family allows us to take into account the equilibrium with NO_2 that occurs at night-time. In any case, day or night, the NO_3 mixing ratio is at least one order of magnitude smaller than the one of NO_2. Therefore, the NO_x family defined within MOCAGE-Climat can be considered as consistent with the NO_x of Grooss and Russel (2005).

Figure 8 presents the stratospheric mixing ratios, from 100 to 0.01 hPa, of MOCAGE-Climat and of Grooss and Russel (2005), for January, May, and September. MOCAGE-Climat are monthly averages that include day and night values. Although there is an inconsistency here as the Grooss and Russel (2005) climatology have been compiled from sunset measurements only, we obtained very similar outputs using daytime data of the model. The general features of the NO_x distribution are quite well reproduced by the model, both spa-

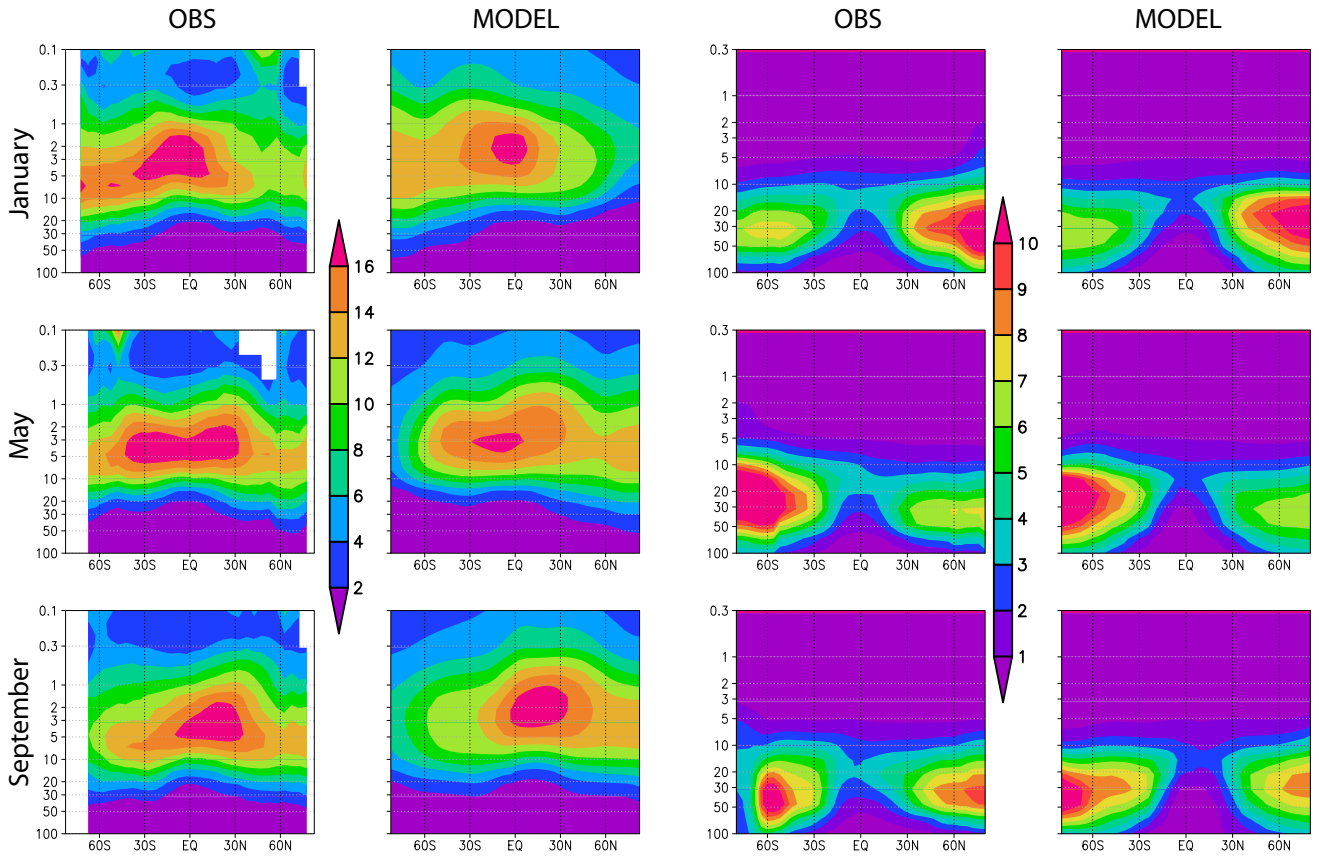

Fig. 8. First two columns: MOCAGE-Climat T21 zonal monthly mixing ratios of NO_x (ppbv) against the Grooss and Russel (2005) climatology, between 100 and 0.1 hPa, in January (upper panels), May (middle panels), and September (lower panels). Last two columns: MOCAGE-Climat T21 zonal monthly mixing ratios of HNO_3 (ppbv) against the Randel et al. (1998) climatology, between 100 and 0.3 hPa, in January (upper panels), May (middle panels), and September (lower panels).

tially and temporally: the vertical gradient conforms with observations, with a rapid increase and then a decrease around a maximum centered at ∼3 hPa. The seasonal cycle appears correctly simulated with higher mixing ratios in the mid-upper stratosphere at all latitudes in the summer season. Furthermore, the "rabbit-ear" shape clearly exists both in model results and in observations in May. Above the stratopause, the model overestimates NO_x in all seasons. This can be explained by several factors: firstly, we can expect a poorer performance of MOCAGE-Climat in the highest levels of the model due to both a combination of a poorer performance of the forcing model and of a less accurate description of the chemistry. We can also note that observations are of a poorer quality in these regions: Grooss and Russel (2005) report a 30% combined systematic and randon uncertainty of NO, that dominates in the upper stratosphere.

Total (sum of stratospheric and tropospheric) NO_2 columns from MOCAGE-Climat at 10.00 am local time for May and September are shown in Fig. 9, together with monthly total columns derived from SCIAMACHY measurements interpolated on the T42 grid. High values are correctly simulated above regions of strong emissions of NO_x from fossil fuel combustion (e.g., over China or Western Europe) or biomass burning. Furthermore, the seasonality of biomass burning appears similar in both simulations and observations, with in May relative maxima in Africa along 10 N and 5 S, and in September strong emissions in southern Africa and Central South America. In September also, smaller columns are correctly simulated in the 15 N–15 S equatorial band. However, values from MOCAGE-Climat are generally higher than those from SCIAMACHY. In May, the model is within ±20% of the observations over most of the Northern Hemisphere and South America. In September, relative differences are higher, overestimation is particularly important in regions of biomass burning emissions. This is coherent with the overestimation we identified for CO. Our bias is similar to the one presented in Bousserez et al. (2007) who compared tropospheric NO_2 columns from MOCAGE with those from SCIAMACHY, over the northern Atlantic from the USA to Europe, in July–August 2004. Above southern oceans, where the total column is almost entirely of stratospheric origin, model mixing ratios show a

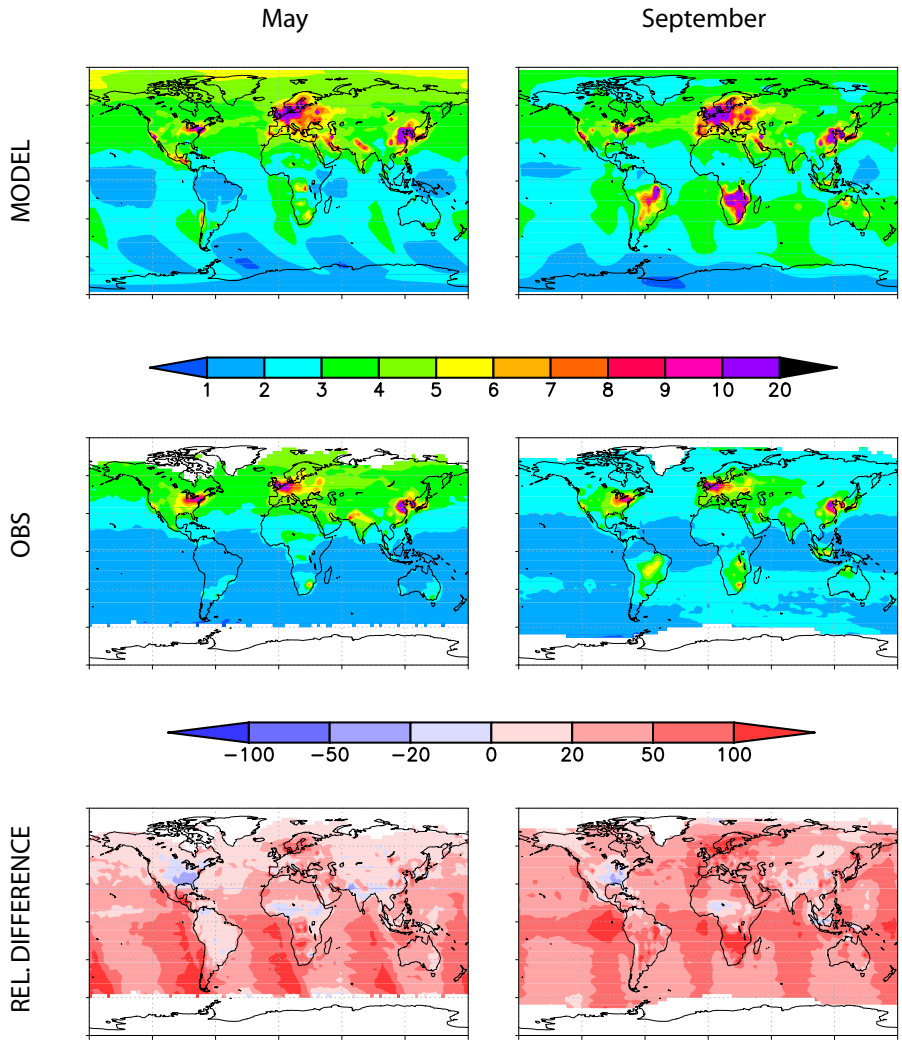

Fig. 9. MOCAGE-Climat T42 total NO_2 columns (10^{15} molec cm^{-2}) versus SCIAMACHY columns at T42 resolution also, and relative differences (100×((Model−Obs)/Obs)), in May (left panels) and September (right panels).

pattern that is linked to the way we estimated off-line the amounts of NO_2 at 10.00 a.m. Indeed, we computed these amounts from the 6-hourly 3-D archive, with a linear interpolation to yield hourly values. As NO_2 exhibits strong discontinuities between day and night, such a linear interpolation even though not fully adequate, still produces valuable results.

MOCAGE-Climat simulations lead to larger NO_2 column biases during the boreal winter than during other seasons. In the winter months, ratios between tropospheric and total columns from MOCAGE-Climat are larger than 0.7 over most of the Northern Hemisphere (north of 30N, not shown). These ratios are much larger than the SCIAMACHY ones; there is no such dissimilarity between the model and the observations during the rest of the year. However, one has to keep in mind that detailed validation of NO_2 satellite products is ongoing, with special attention to tropospheric NO_2 (Piters et al., 2006). It should also be noted that Savage et al. (2004) who compared measurements of NO_2 by GOME to outputs from the TOMCAT global CTM reported measurements to model ratios of 1.4 for North America and 1.9 for Europe (mean values for an entire year). Several hypotheses could explain the overestimation of NO_2 in MOCAGE-Climat (and TOMCAT). Firstly, there is no heterogeneous loss of N_2O_5 on tropospheric aerosols in the model at present. Noije et al. (2006) and references therein indicate that considering such reactions could reduce the tropospheric NO_x concentrations at middle and high latitudes by up to 80% in winter and 20% in summer, and in the tropics and subtropics by 10–30%. Secondly, too high mixing ratios near the surface could be related to the local vertical diffusion scheme of Louis (1979) that we use. Savage et al. (2004) reported that the boundary layer mixing in the model has been improved by replacing the Louis (1979) scheme

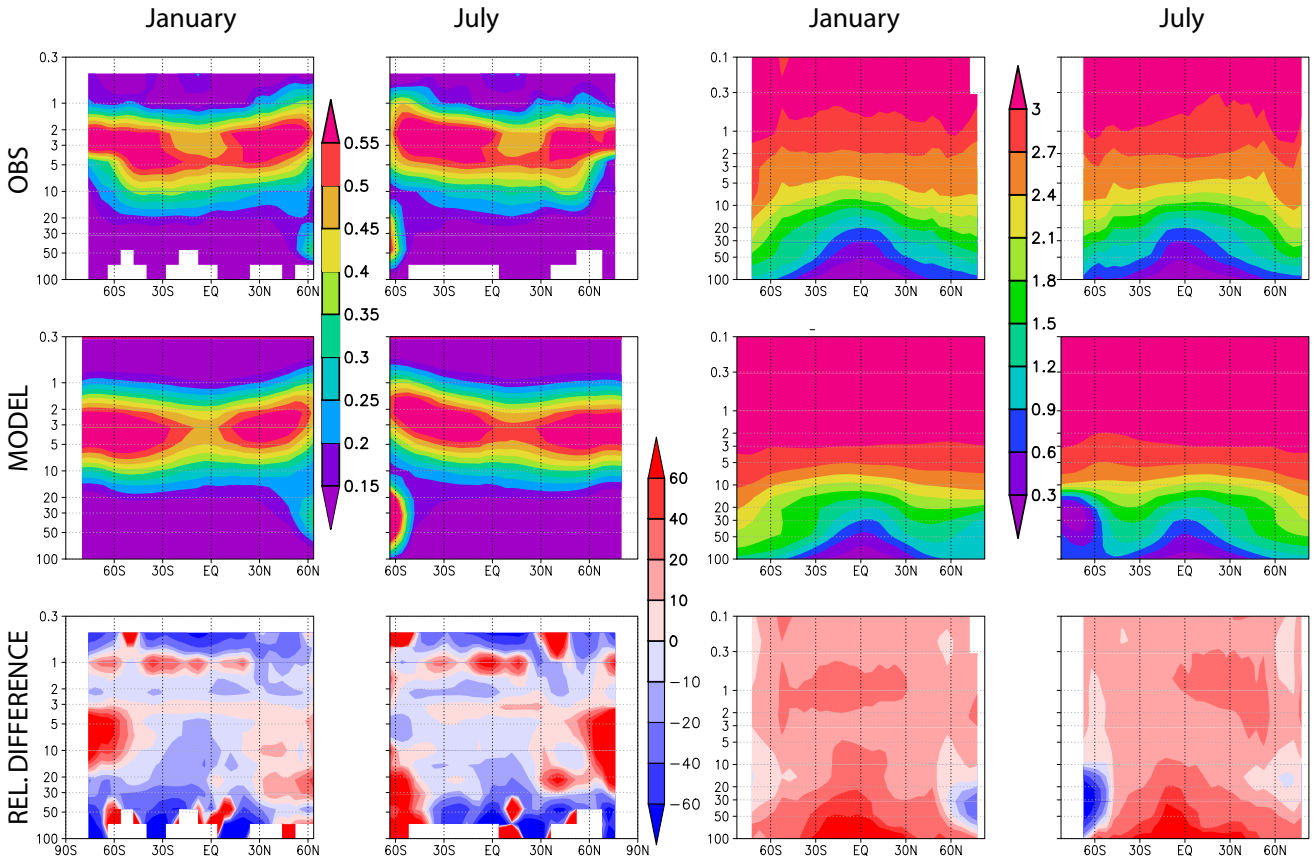

Fig. 10. Left columns: MOCAGE-Climat T21 zonal monthly mixing ratios of ClO (ppbv, day-time values only) against the Randel et al. (1998) climatology, and relative differences (100×((Model−Obs)/Obs)), between 100 and 0.3 hPa, in January (left panels) and July (right panels). Right columns: MOCAGE-Climat T21 zonal monthly mixing ratios of HCl (ppbv) against the Grooss and Russel (2005) climatology, and relative differences (100×((Model−Obs)/Obs)), between 100 and 0.1 hPa, in January (left panels) and July (right panels).

by a non-local vertical diffusion scheme. Finally, the biases of MOCAGE-Climat could be related to how the various species within the NO_x family are handled; indeed, if the repartition of these species is satisfactory for the stratosphere (Lefèvre et al., 1994), the NO_2 mixing ratios modelled here reveal that further investigation on the use of this family concept in the troposphere should be pursued.

3.5.2 Chlorine monoxide (ClO)

As suggested by Farman et al. (1985) and confirmed by various studies reported in WMO (1998) for instance, the amount of chlorine monoxide is of primary importance for the ozone depletion throughout the stratosphere, and especially for the representation of the ozone hole. In the upper part of the stratosphere, the ozone controlling regime is mainly driven by the amount of chlorine, whereas at lower altitudes it is driven by nitrogen oxides, the role of HO_x being very important throughout the atmosphere.

Figure 10 presents the MOCAGE-Climat T21 monthly mixing ratios of ClO (day-time values only), between 100 and 0.3 hPa, in January and July along with the Randel et al. (1998) climatology, and their relative differences. On the whole, the model reproduces the typical structures of the observations, i.e., the two cells with higher values at approximately 3 hPa, and their seasonal shift towards high latitudes of the summer hemisphere, as well as the relative maxima between 50 and 20 hPa at high latitudes of the winter hemisphere. These relative maxima appear somewhat too large and shifted towards higher pressures. Quantitatively, modeled ClO mixing ratios seem rather too low over part of the stratosphere. This might result from a too large transformation of active chlorine into its reservoir form HCl (see Sect. 3.6.2).

3.5.3 Hydroxyl radical (OH)

OH is the primary oxidant in the troposphere and is responsible for the removal of many reduced compounds; in addition, it determines the lifetimes of CH_4, CO, and other pollutants. Errors of 15–25% in the global mean concentration of OH may signify major misunderstandings about the chemistry or

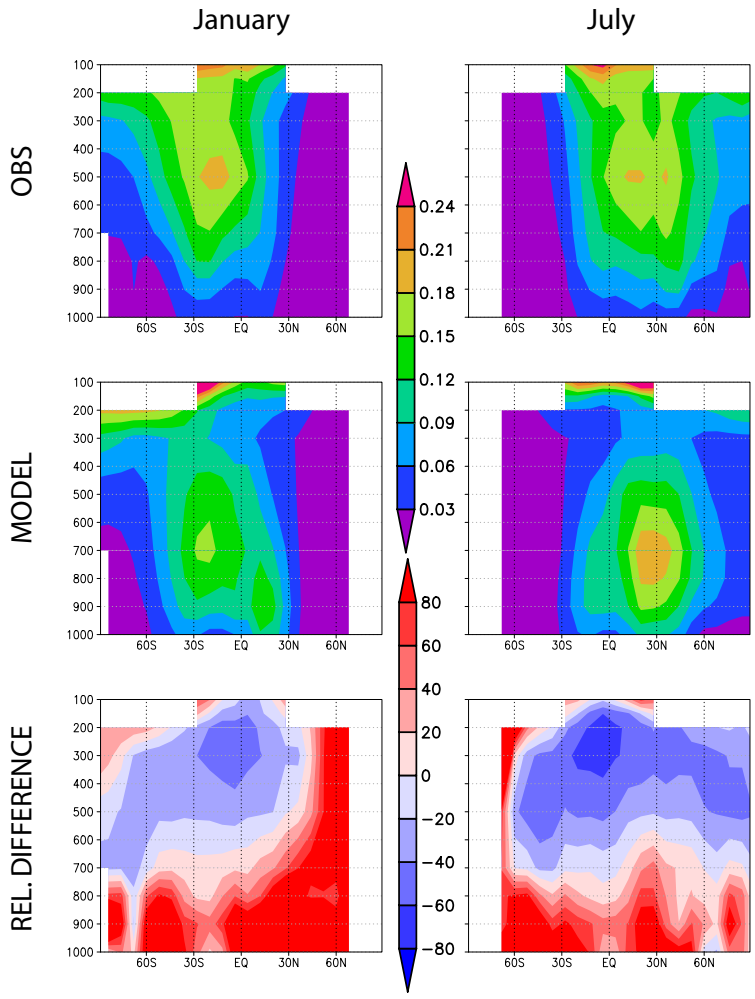

Fig. 11. MOCAGE-Climat T21 zonal OH mixing ratios (pptv) versus Spivakovsky et al. (2000) mixing ratios, between 1000 and 100 hPa, in January (left panels) and July (right panels).

the abundance of precursors of OH in the troposphere (Spivakovsky et al., 2000).

Zonal means of OH from MOCAGE-Climat at T21 resolution and as shown by Spivakovsky et al. (2000), for January and July between 1000 and 100 hPa, are presented in Fig. 11. Both model and the "reference" data set derived from observations reveal the seasonality of the OH mixing ratios, with higher values in the Northern Hemisphere from March to September, that reflects variations in sunlight and water vapour. In general, simulated mixing ratios are larger than Spivakovsky et al. (2000), from the surface up to 800 hPa, and lower from 500 hPa up to the tropopause that is the upper limit of the Spivakovsky et al. (2000) dataset. In the lower troposphere, the overestimation exceeds 80% at most latitudes.

Biases in OH mixing ratios are reported in recent publications: Bousserez et al. (2007) also found that MOCAGE overestimated the observations performed from research aircraft during the ITOP campaign between the surface and 4 km, by a factor of 2, while it underestimated them for altitudes higher than 7 km, with analysed H_2O consistent with the observations. They suggested that the positive OH bias in the lower troposphere may be due to photo-chemical effects of aerosols not included in the MOCAGE used, e.g., aerosol scattering, absorption of ultraviolet radiation and reactive uptake of HO_2, NO_2 and NO_3. Ren (2007) found that their box model over-predicted OH by a factor of 1.7 throughout much of the troposphere in northern mid-latitudes; their analysis suggested the presence of unknown atmospheric constituents or unknown reactions with OH that were suppressing the observed OH at mid-latitudes.

Finding the causes of these discrepancies appears necessary for understanding the global-scale tropospheric oxidation capacity. Spivakovsky et al. (2000) indicated that the available tests did not establish significant errors in their estimates of OH except for a possible underestimate in winter

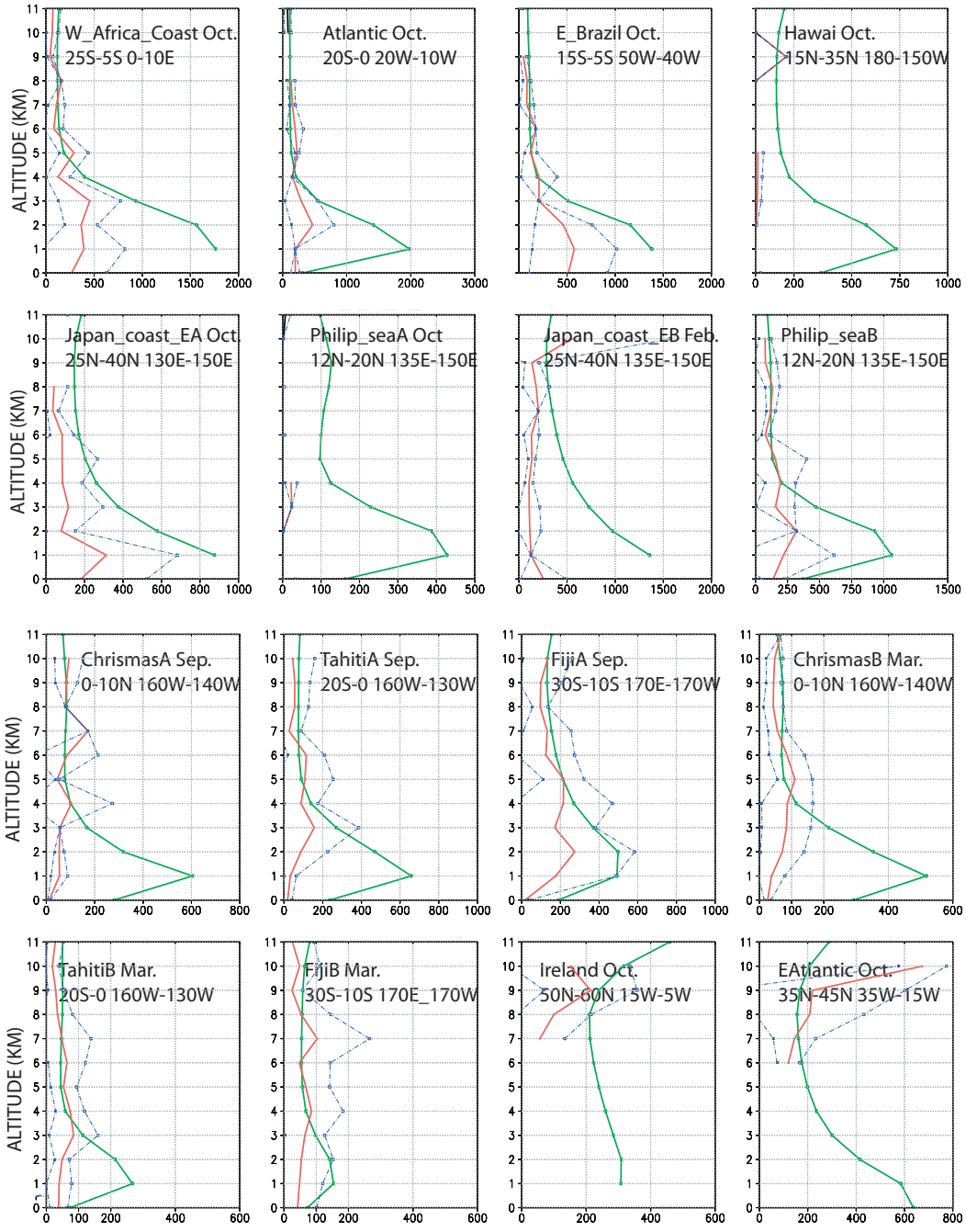

Fig. 12. MOCAGE-Climat T42 mean vertical profiles of HNO_3 mixing ratios (pptv, in green) against aircraft field campaign observations (Emmons et al., 2000). Regions of the world are as presented in Horowitz et al. (2003); vertical is between the surface and 11 km. The observations are shown as mean (red lines), ±2 standard deviations (blue dotted lines).

in the northern and southern tropics by 15–20% and 10–15%, respectively, and an overestimate in southern extratropics by ∼25%. However, the sparsity of observations did not allow for an unambiguous characterization of the distributions.

3.6 Reservoir species

Reservoir species, whose lifetime is longer than that of radical species, store radicals that they eventually release, and by doing so they modulate chemical cycles. For instance, the highly reactive radicals chlorine monoxide and nitrogen dioxide can react together to form chlorine nitrate that has a

much longer lifetime and inhibits ozone destruction by these two radicals.

3.6.1 Nitric acid (HNO_3)

Nitric acid is likely to be the main reservoir of nitrogen species in the troposphere and the lower stratosphere. It is a highly soluble species and therefore, strongly affected by precipitation in the troposphere. It is a sink for nitrogen species in the stratosphere.

Figure 8 presents the zonal monthly HNO_3 mixing ratios for the model and the observations, in January, May and September, from 100 to 0.3 hPa. HNO_3 is evidently very dependent on the season at high latitudes, with an "eye-glasses" shape distribution, and maximum values in the winter hemisphere. The model reproduces quite accurately this distribution, both in terms of its latitudinal and vertical distributions, and its seasonality; however, mixing ratios that are too large at very high latitudes of the Southern Hemisphere in September reveal that the sedimentation of HNO_3, associated with Polar Stratospheric Cloud particles, is too weak in MOCAGE-Climat.

We have evaluated HNO_3 in the troposphere by comparing model outputs to a selection of observations obtained from aircraft campaigns, as compiled by Emmons et al. (2000) and presented in Horowitz et al. (2003). We display in Fig. 12 model outputs corresponding to average profiles over the region and for the months of the campaign. Our agreement with observations in the troposphere above 4 km is quite satisfactory at most locations shown. However, simulations are generally higher than observations in the layer between the surface and 3 km. The HNO_3 concentrations are very sensitive to the parameterization of the wet deposition, and this needs to be further investigated in MOCAGE-Climat. Another possible source of discrepancy could be higher biomass burning emissions in the model compared to the emissions at the time of the observations, and this could explain for instance the profile in the E-Brazil region. Furthermore, this overestimation of HNO_3 is consistent with the overestimation of the NO_2 mixing ratios shown in Sect. 3.5.1 as HNO_3 is predominantly produced by the oxidation of NO_2. One has to mention however that many other current 3-D CTM overestimate HNO_3 concentrations at many locations throughout the troposphere (Horowitz et al., 2003). Hauglustaine et al. (2004) and references therein also outline the difficulty to simulate nitric acid in CTMs.

3.6.2 Hydrochloric acid (HCl)

Hydrochloric acid is the main chlorine reservoir in the middle atmosphere. It is formed by thermal reactions between ClO_x and HO_x and therefore is mainly present in the upper atmosphere where both families exist simultaneously.

Figure 10 presents the zonal monthly HCl mixing ratios for the model and the UARS observations, in January and July, from 100 to 0.1 hPa, together with the relative differences. Most of the time, the values from the model are higher than the observations, at all seasons and all latitudes, except for the low values from the model at high latitudes in the winter hemisphere, particularly in July, that do not appear in the observations. The positive bias in the model is mostly in the range of the uncertainties reported by Grooss and Russel (2005) who indicate that the combined systematic and random uncertainty of single HCl profiles in the lower stratosphere is between 14 and 24%, and between 12 and 15% in the upper stratosphere. In addition, Grooss and Russel (2005) note that HCl mixing ratios increased monotonically over the investigated time period, i.e., from about 2.8 ppbv to 3.35 ppbv at 0.3 hPa between 1992 and 1997; however, much slower mean changes have been observed thereafter (WMO, 2002). The model values might therefore be in better agreement with observations performed during the period of simulations (2000 to 2005). Nevertheless, the spatial characteristics of model outputs and observations are quite similar, with a positive gradient from the low stratosphere to the mesosphere, and with an equatorial low up to around 10 hPa; at lower pressures, zonal mixing ratios do not show any latitudinal gradient.

As already mentioned in Sect. 3.5.2, active chlorine in the model mainly ends up in the reservoir form HCl in the stratosphere whilst it remains more in an active form in the observations. This is not the case at polar latitudes during winter and spring. At seen in Sect. 3.6.1, HNO_3 sedimentation appears too weak, thus heterogeneous reactions occuring on particles formed from HNO_3 deplete HCl too much. As a consequence ClO amounts are too high in polar vortices (see Fig. 10).

3.7 Ozone (O_3)

Ozone is the most abundant trace constituent of the stratosphere that is chemically active. It is produced by a cycle initiated by photolysis of O_2 (Chapman, 1930) which is most efficient in the tropical middle stratosphere. Additional reactions, involving nitrogen oxides, chlorine and bromine species consume ozone; these reactive species can be temporarily removed from catalytic cycles by being stored in reservoir species. It should be mentioned that though ozone mixing ratios in the stratosphere can be greater than 10 ppmv, it is in "chemical equilibrium" with trace species whose mixing ratios can be from one thousand to one million times smaller.

Interest in tropospheric ozone results from its impact both on the radiative forcing (Ramaswamy et al., 2001), on human health (WHO, 2003) and on vegetation. Present and future conditions of air quality are a subject of concern and scientific studies have recently turned to the potential influence of climate change on future levels of ozone (Stevenson et al. (2006) and references therein). There are two sources of tropospheric ozone: transport from the stratosphere, and in situ

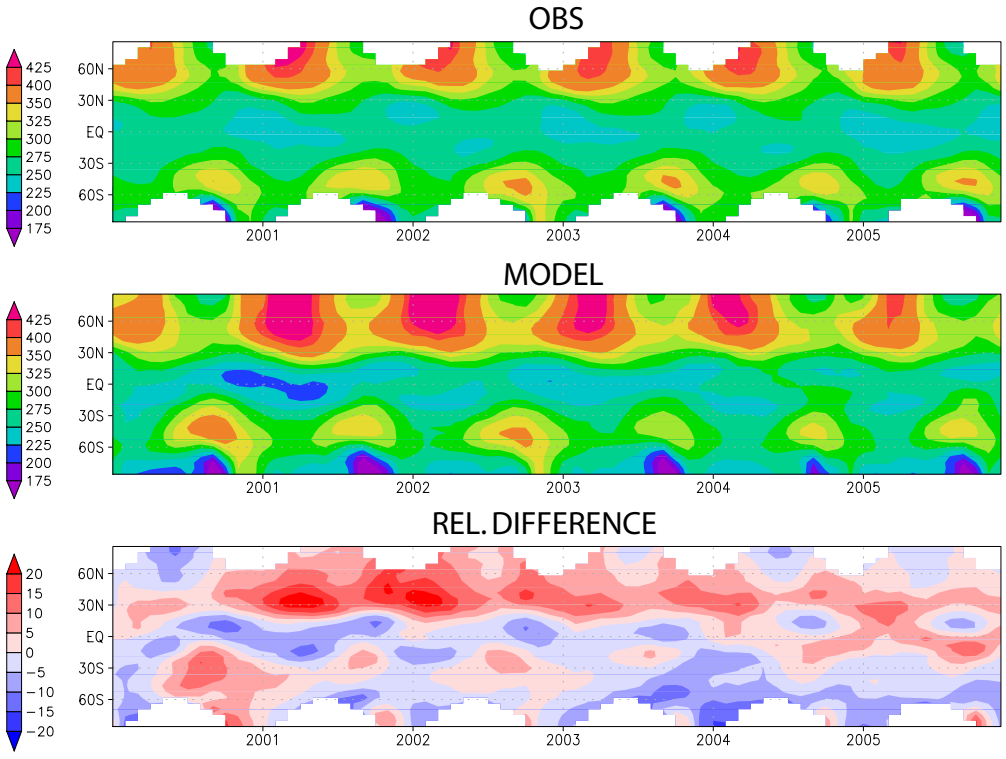

Fig. 13. Evolutions between 2000 and 2005 of the zonal mean total ozone column (DU) on a T21 grid, as in the NIWA climatology (top panel, in white no observations), simulated by MOCAGE-Climat (middle panel), and relative differences (100×(model−obs)/obs).

chemical production. Ozone production takes place when carbon monoxide and hydrocarbons are photo-oxidized in the presence of nitrogen oxides. The main ozone precursors are emitted by human activities, but also have significant natural sources.The ozone budget is closed by two loss processes: dry deposition to the Earth's surface, and chemical destruction (Wild, 2007). Ozone destruction occurs mainly via reactions with water vapour (following photolysis) and with hydroperoxyl (HO_2) and hydroxyl radicals.

3.7.1 Total ozone column

The evolution between 2000 and 2005 of the zonally averaged total ozone column from the model is in fair agreement with the NIWA climatology (see Fig. 13). The well known features of highest ozone values in northern spring, low ozone values in the tropics with a small seasonal cycle, a relative ozone maximum in the mid-latitudes of the Southern Hemisphere in late winter/early spring, and a minimum ozone column above the Antarctic are well represented. However, two positive biases appear: first, there is too much ozone at high and mid-northern latitudes, especially at the end of the boreal winter. This bias is consistent with the ECMWF forcings that drove our simulations; as shown in Sect. 3.2, the Brewer-Dobson circulation is too fast, resulting in too large a decrease in the amount of tropical ozone while accumulating too much ozone in the polar lower stratosphere in winter. As a result, the band of minimum ozone columns in the tropics is too narrow, inducing stronger meridional gradients than observed. This stratospheric circulation becomes even faster when increasing the resolution to T42: maxima of total ozone reach then unrealistic values over the pole (up to 600 DU, not shown).

A second bias appears in the modeled Antarctic ozone hole that is not deep enough in comparison to the NIWA climatology. This seems in contradiction with the (too) large ClO amounts found in the vortex (see Fig. 10). On further analysis of various compounds, we noted that upon return of the sunlight in September, ClO reacted preferably with large amounts of NO_2 rather than deplete ozone. These too large amounts of NO_2 were produced by the photolysis of HNO_3, whose sedimentation during winter appeared insufficient (see Fig. 8). One has to note however that observations at high zenith angles have larger uncertainties (McPeters et al., 1996). Interestingly, the variability in area and depth of the ozone hole is well captured by MOCAGE-Climat. For instance, in September 2002 when the ozone hole split up into two cores, MOCAGE-Climat reproduced the two structures (not shown). This original feature of the ozone hole is mainly driven by atmospheric dynamics.

Figure 14 shows latitude/longitude distributions of the ozone column in January and July. MOCAGE-Climat reproduces total ozone extrema in association with tropospheric

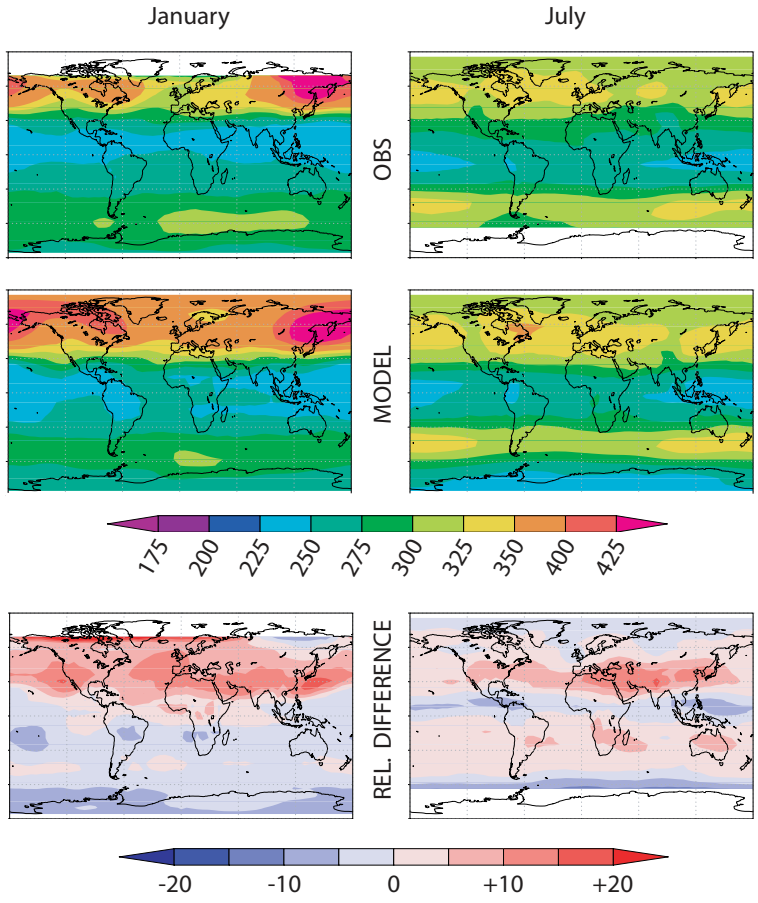

Fig. 14. Total ozone columns (DU) for January (left panels) and July (right panels) on a T21 grid, in the NIWA climatology (top panels, in white no observations), simulated by MOCAGE-Climat (middle panels), and relative differences (100×(model−obs)/obs).

meteorological systems that affect the tropopause height, inducing longitudinal variations in the ozone column. For instance, the two maxima over the Labrador and Aleutian Islands, linked to winter depressions, are well reproduced by the model. However, the northern Atlantic ridge brings too much ozone from the tropics towards northern high latitudes; this could be due to wave breaking in the ECMWF analyzes being too strong, or to too strong horizontal diffusion linked to the T21 resolution. Over the western tropical Pacific, a minimum related to convection activated by warm sea-surface temperatures can be seen in the observations and is well captured by the model. In July, the total ozone distribution in the Northern Hemisphere is mainly driven by photochemistry, and therefore by solar zenith angle, leading to latitudinal bands of total ozone, with weak zonal gradients. Relative differences are smaller than in January and are lower than 10% over most of the globe.

The variability of the daily total ozone columns over a month is presented in Fig. 15 for January, April, July and October. TOMS and MOCAGE-Climat standard deviations show similar patterns. Low standard deviations are found in the tropics, with values typically smaller than 10 DU; the main source of variation is related to convection that can inject tropospheric air which is poor in ozone into the lower stratosphere during sporadic convective events. Higher standard deviations are calculated near synoptic depressions in winter or spring, for instance in April south of Greenland and east of Japan (40 DU for the TOMS). Even larger deviations appear at the edge of the polar vortices: in the Northern Hemisphere they reach 60 DU in January, while in the Southern Hemisphere TOMS deviations linked to the polar vortex are above 75 DU in October. Effectively, if the polar vortex of the Northern Hemisphere is subject to strong planetary wave breaking, inducing high geographical variations of its shape, the differences in total ozone between the inside and the outside of the vortex are almost similar to the differences observed in relation to the moving of a depression. In contrast, in Antarctica the meteorological situation consists of a huge vortex almost centered over the South Pole, surrounded by several depressions. In the vortex, heterogeneous chemistry occurs during austral spring and strongly depletes ozone. Thus, the ozone column is minimum within the vortex while it is maximum over the neighbouring depressions. During the austral spring, distortion of the vortex

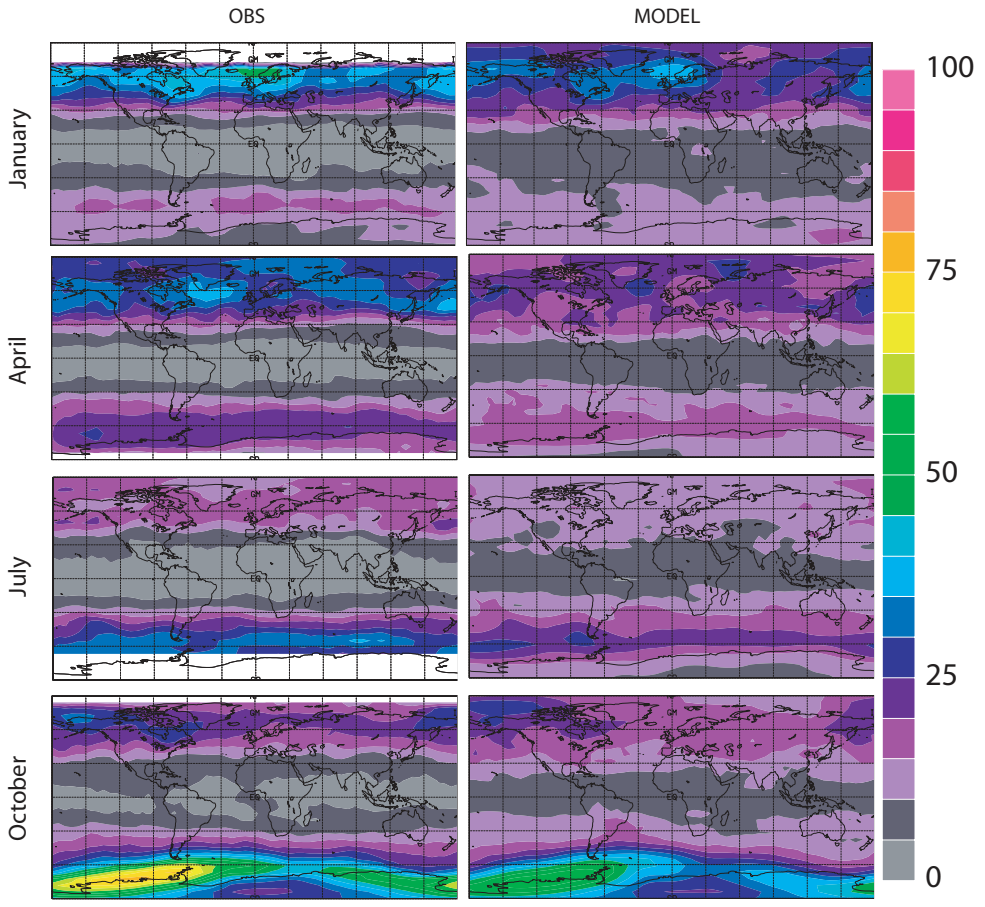

Fig. 15. Standard deviation of the daily total ozone column (DU) for January (first line), April (second line), July (third line), and October (bottom line) on a T21 grid, as observed by TOMS (left panels, in white no observations) and simulated by MOCAGE-Climat (right panels).

due to baroclinic activity can then lead to rapid changes in the ozone amount, and to large standard deviations.

The main patterns of the standard deviation are well reproduced by MOCAGE-Climat, showing that the model is able to capture the principal features of the variability of the total ozone column.

3.7.2 Stratospheric ozone

The total ozone column reflects especially the ozone amount in the lower stratosphere, and thus is not representative of what occurs at higher levels. Therefore, it is worth comparing modeled ozone with available climatologies. Figure 16 shows MOCAGE-Climat T21 zonal monthly mixing ratios of O_3 in April and October against the Grooss and Russel (2005) climatology, between 300 and 0.1 hPa. The vertical distribution is well reproduced by the model, with a clearly marked maximum at tropical latitudes around 10 hPa; this maximum is a little larger in the model (with relative differences smaller than 10%.) The broad envelope of large mixing ratios distorts depending on the season, and the model correctly reproduces these distortions. The minimum at high latitudes of the Southern Hemisphere in October, in the polar vortex below 30 hPa, is more pronounced in the observations. Simulated ozone mixing ratios in the mid-mesosphere (at altitudes above 0.3 hPa) are larger than measurements. This is largely linked to the marked diurnal cycle that exists at these altitudes (see for instance Geer et al. (2006)). To test it in MOCAGE-Climat, we compared day-time values from the model with observations in July. The positive bias at these altitudes was reduced then by ∼0.4 ppmv. Our underestimation of H_2O in the stratosphere (see paragraph 3.4.1) could also contribute to this bias as the destruction of O_3 is mostly driven by HO_x in the mesosphere. Furthermore, it should be noted also that the peculiarities of the mesospheric chemistry which involves species under ion form (see Brasseur and Solomon (1986)) are not considered in MOCAGE-Climat. The homogeneous gas-phase chemistry of the model may therefore not be representative for the mesosphere, though it appears to provide reasonable upper boundary conditions.

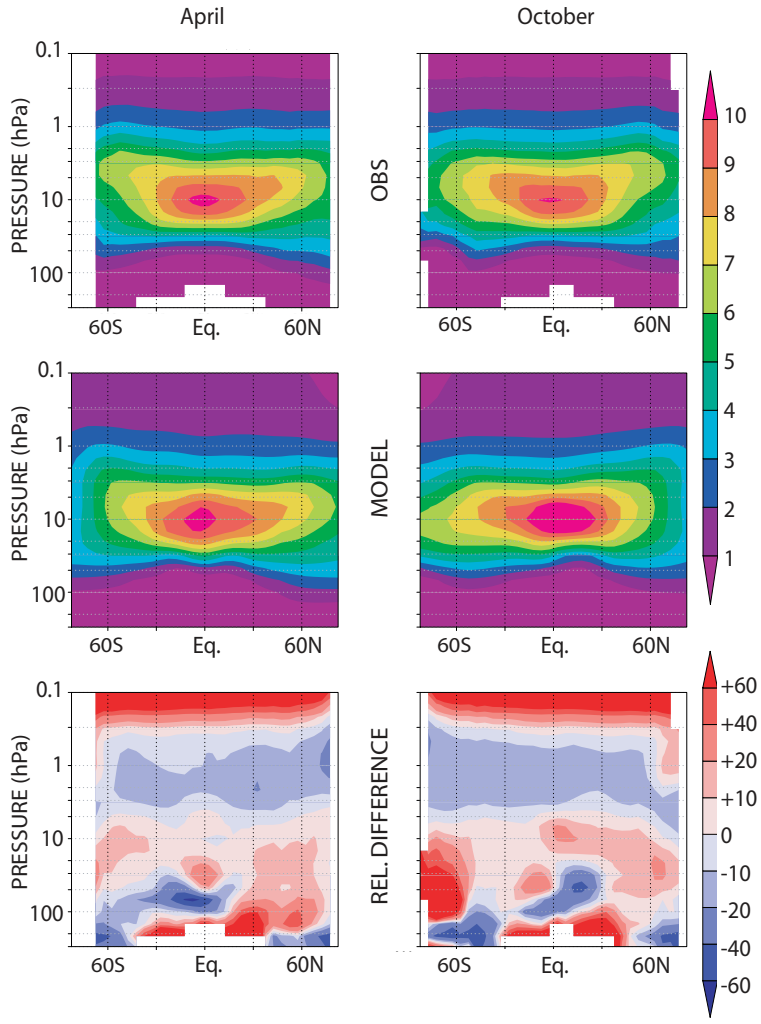

Fig. 16. MOCAGE-Climat T21 zonal monthly mixing ratios of O_3 (ppmv) against the Grooss and Russel (2005) climatology, and relative differences (100×((Model−Obs)/Obs)), between 300 and 0.1 hPa, in April (left panels) and October (right panels).

3.7.3 Ozone in the UTLS region

Figure 4 shows MOZAIC O_3 observations between the 340 and 350 K isentropic levels, for winter (DJF) and summer (JJA), MOCAGE-Climat T42 fields, and relative differences. The model tends to underestimate UTLS mixing ratios at mid and northern latitudes, and to overestimate them in the tropics; this behaviour is somewhat seasonally dependent. For instance, discrepancies are less important in autumn, when the planetary wave activity increases and transports ozone towards the polar lower stratosphere, but discrepancies have also an inter-annual variability, with a different behaviour in 2002 for instance (not shown). The fact that modeled O_3 is weaker than MOZAIC O_3 is in apparent contradiction with comparisons with TOMS observations (model columns larger than TOMS ones at northern latitudes see Sect. 3.7.1). However, Figs. 17 and 18 throw some light on this as they show that, at the same location, MOCAGE-Climat can both underestimate mixing ratios in the UTLS region and overestimate them at lower pressures that drive the total column value (see for example the profile at Resolute in July).

Two types of O_3 distributions can be distinguished, depending on the region of the world (see Fig. 5): at northern mid-latitudes, with sampling in the UTLS, MOCAGE-Climat and MOZAIC have similar shapes, with fewer occurrences of the smallest mixing ratios (0–20 ppbv) and a spread of large ones, but MOCAGE-Climat shifts the maxima towards larger mixing ratios and has fewer occurrences of very high mixing ratios typical of the stratosphere. At tropical latitudes, with narrow distributions centered around low mixing ratios, typical of the troposphere, the model reproduces the atmosphere well.

Our results are different from those of Law et al. (2000) who compared ozone from five tropospheric CTMs to MOZAIC observations. They found that models underestimated the tropospheric O_3 while they mainly overpredicted

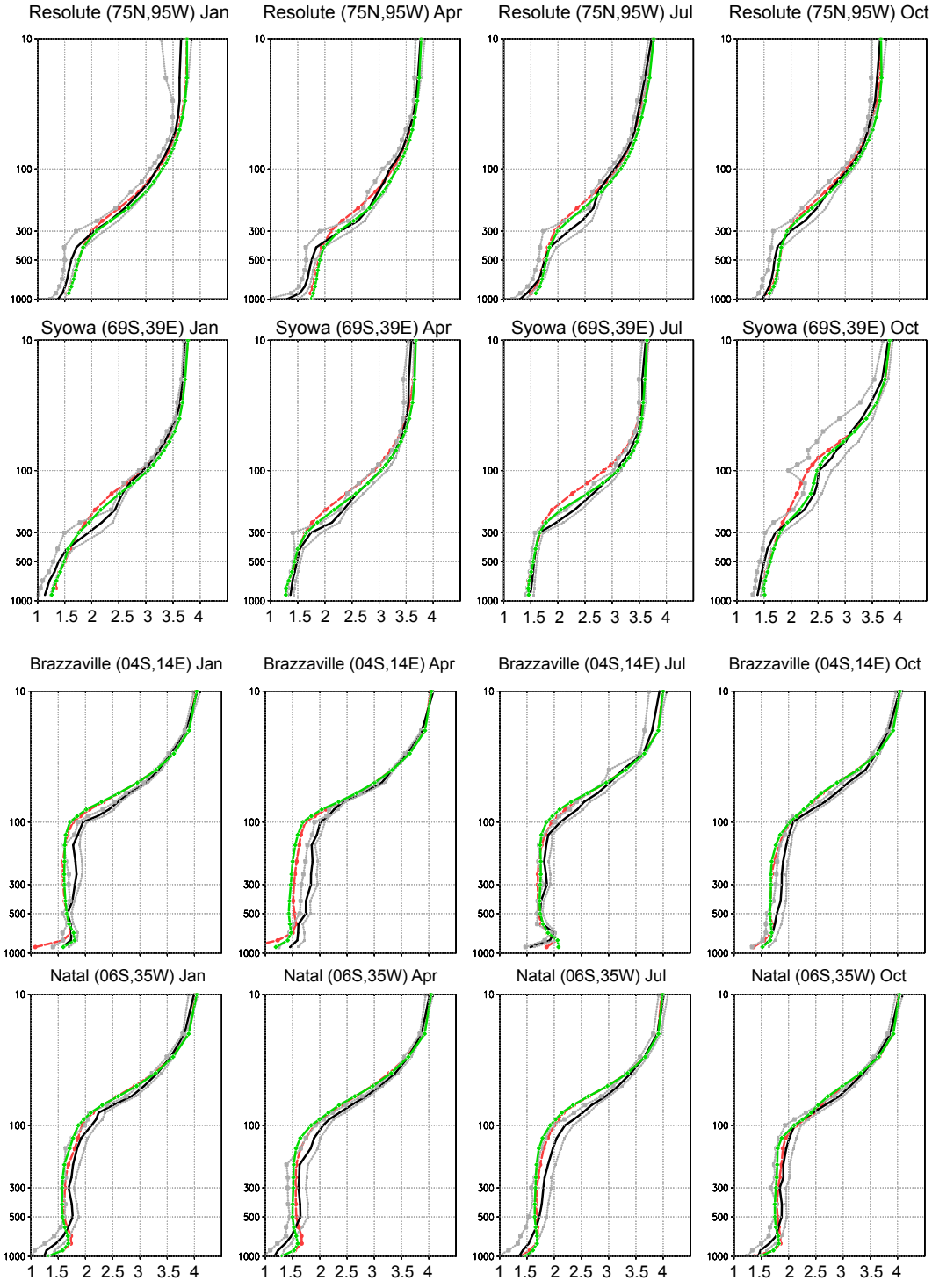

Fig. 17. MOCAGE-Climat vertical profiles of O_3 mixing ratios (ppbv) against Logan (1999a) observations, from 1000 to 10 hPa (black curve, ± 1 standard deviation as grey curves), at various sites in January (left column), April (middle left), July (middle right), and October (right). MOCAGE-Climat T21 simulations appear as red profiles, T42 simulations as green ones (both axes have a logarithmic scale).

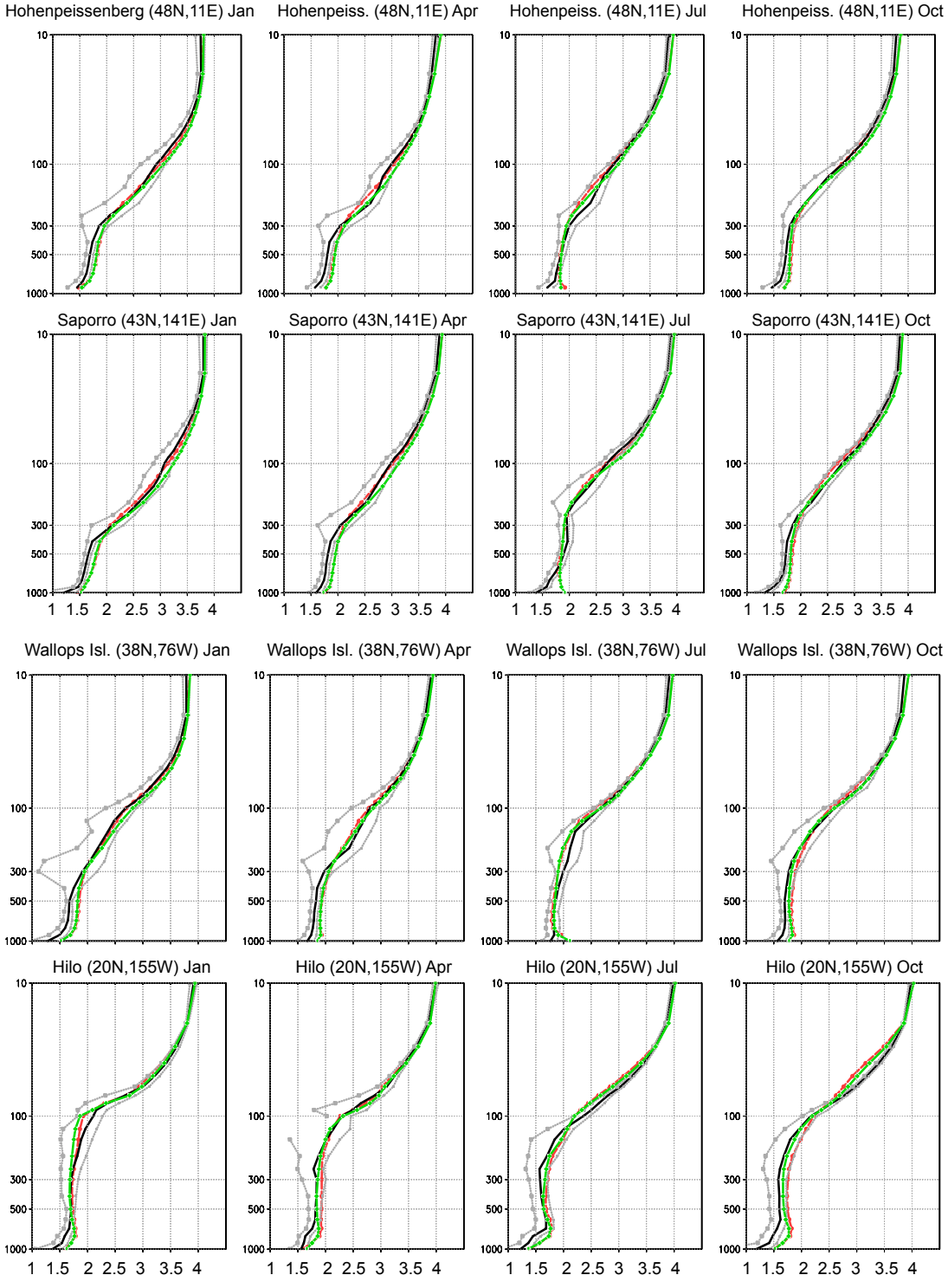

Fig. 18. As in Fig. 17.

the stratospheric O_3. They explained that the overprediction could be due, in addition to horizontal and vertical resolutions, to the stratospheric influx as the evaluated CTMs, mainly tropospheric, had a rather "poor" representation of the stratosphere. MOCAGE-Climat describes both layers, and tends to slightly underestimate stratospheric O_3, especially at high mixing ratios. This would seem to confirm the Law et al. (2000) argument.

3.7.4 Tropospheric ozone

Figures 17 and 18 show vertical profiles of O_3 mixing ratios, from 1000 to 10 hPa, at various sites of the Logan (1999a) climatology, in January, April, July and October; both MOCAGE-Climat T21 and T42 simulations appear together with observations and their standard deviation.

At a number of mid-latitudes stations in the Northern Hemisphere, such as Hohenpeissenberg or Sapporo, simulations show ozone concentrations to be higher than the observations up to the tropopause, except in July where agreement with observations is quite good. In July, however, simulated concentrations are larger in the boundary layer at a few sites, and this is in part related to the higher levels of ozone precursors emitted from the surface in 2000. For the Wallops Island site for instance, the period of observations spans the years 1980–1993. Wild (2007), who explored the variability in current CTMs when simulating the tropospheric ozone budget, demonstrated the importance of the emissions of the surface precursors. Seasonal variations in the boundary layer and the lower troposphere, reflecting variations in photochemistry and/or in the O_3 precursors linked for instance to the seasonal cycle of the biomass burning activity, are correctly simulated (see for example Wallops Island or Natal). At the tropical stations, the model tends to slightly overestimate mixing ratios in the lower part of the troposphere, and somewhat underestimate them in its upper part. This could reflect some weaknesses in the convection as well as in the deposition processes. O_3 in the upper-part of the tropical troposphere would also be greatly enhanced with the introduction in MOCAGE-Climat of a parameterization of NO_x emissions from lightning, as outlined in Labrador et al. (2005). The resolution of the tropopause is better at mid-latitudes than at high ones (e.g., Resolute and Syowa stations). At these high latitudes, the model overestimates the height of the tropopause, with a smoother vertical gradient; the agreement between model and observations in the UTLS region is better for tropical stations (see Natal and Hilo). Simulations at T42 lead to outputs that conform better with observations in the UTLS region.

A closer insight into the simulated seasonal cycle of ozone at selected stations is provided in Figs. 19 and 20 with mixing ratios at three pressure levels (800, 500, and 300 hPa). At 800 hPa the model simulates quite well the spring maximum that exists at most sites. Values at pristine air sites at high latitudes or at mid-latitudes (e.g., Lauder) are in the range of observations, i.e., lower than 60 ppbv the whole year. At tropical sites, the seasonal cycle is quite similar to observations with a clear maximum at some stations linked to the biomass burning activity (e.g., Brazzaville, Natal), somewhat too accentuated in the model. At 500 hPa, the seasonal cycle is correctly simulated at about half of the sites studied, with good simulations of the tropical sites (e.g., Natal, Samoa). For the other half of the sites, mixing ratios are within the ± 1 standard deviation range during half of the year, from May to October, while they are too high during the rest of the year. At 300 hPa, simulations are well within the range of observations, except for Brazzaville, with large standard deviations of observations at high latitudes (e.g., Alert, Syowa) reflecting stratospheric air intrusion. The coincidence between observations and simulations is particularly good at Lauder and Naha.

3.8 Summary statistics

We provide in this section a synthesized view of how the four simulations T21, T21BL1, T42 and T42BL1 compare with observations. This is shown in Fig. 21 as three Taylor plots (Taylor, 2001). The horizontal and vertical axes give the normalized standard deviation (model standard deviation/observation standard deviation), the curved axis gives the correlation coefficient, and the distance between the model and the observations (not plotted at 1 on the horizontal axis) is a measure of the centered root mean square error.

The first plot (see Fig. 21a) shows model outputs and observations in the stratosphere (100–1 hPa) against the Grooss and Russel (2005) and Randel et al. (1998) climatologies for all the chemical species previously analysed in the paper, i.e. N_2O, CH_4, NO_x, ClO, HNO_3, HCl, O_3. The points that represent the four simulations are almost coincident for O_3, HNO_3 and N_2O. Furthermore, the points for the simulations with and without the simplified boundary layer (T42 and T42BL1 for instance) are very close for all chemical species except for ClO. This is because we present daytime mixing ratios against the observations for the T21 simulation, that we recomputed in a second step as ClO observations appeared to be daytime observations. For the other three simulations we used for the Taylor diagram 6-hourly averages, hence the discrepancy between the ClO points. The T21 simulation is closer to observations than the T42 simulation for CH_4, NO_x and HCl. Overall, although there are minor differences between the four simulations, the T21 simulation is the one that provides the best comparisons to the Grooss and Russel (2005) and Randel et al. (1998) climatologies with correlation coefficients higher than 0.9 and variabilities very comparable to the variabilities of the observations. This could be due to the coherence between the horizontal resolutions of the observations and the model.

The second plot (see Fig. 21b) displays statistical information concerning the model and the MOZAIC observations in the UTLS (340–350 K layer), for O_3, CO and NO_y. Three simulations are shown (T21, T42 and T42BL1) as coinci-

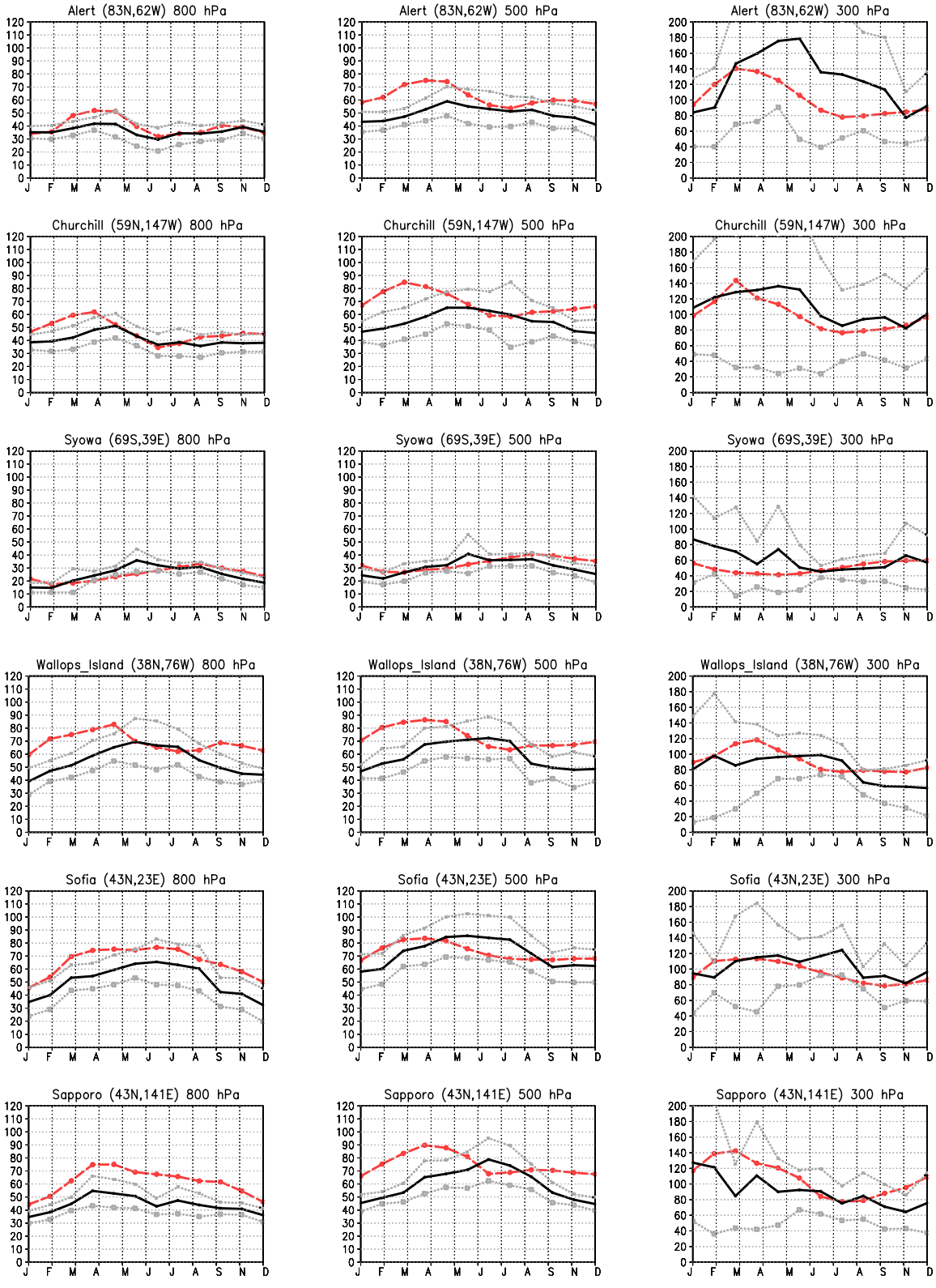

Fig. 19. MOCAGE-Climat monthly O_3 mixing ratios (ppbv) at three different pressure levels, 800 (left), 500 (middle), and 300 hPa (right), against Logan (1999a) observations (black curve, ± 1 standard deviation as grey curves). MOCAGE-Climat T21 simulations appear as the red curves.

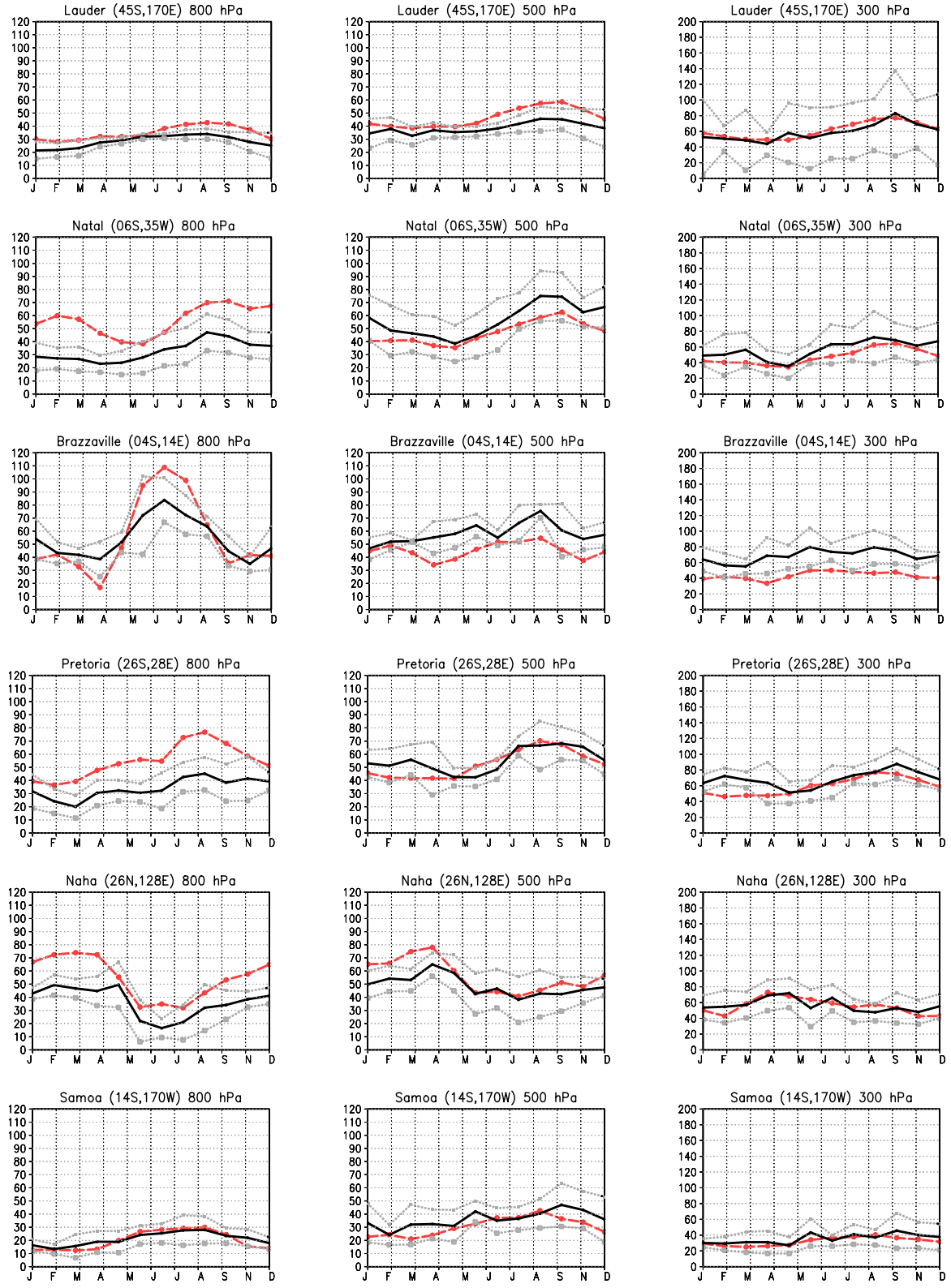

Fig. 20. As in Fig. 19.

Table 7. Biases between modeled and observed tropospheric O_3 (model-obs, ppbv).

	High lats 1000-800	High lats 800-400	Mid lats 1000-800	Mid lats 800-400	Tropics 1000-800	Tropics 800-400
T21	1.5	4.3	13.5	12.9	14.1	3.9
T21BL1	4.2	7.9	21.3	18.7	18.9	7.6
T42	7.5	6.9	14.7	12.0	15.8	0.6
T42BL1	9.6	9.9	18.6	16.6	19.8	4.3

dent outputs with aircraft observations. The correlation coefficient for NO_y is poor ($\sim$0.3) while those for O_3 and CO are near 0.8. For O_3, the variability of the T42 simulation is closer to the variability of the observations than that of the T21 simulation. This is not the case for CO. The T42 and T42BL1 simulations have very close points, and agree better with the observations than the T21 simulation.

The third plot (see Fig. 21c) presents information on ozone in the troposphere. O_3 modeled and measured mixing ratios over various latitude bands, i.e., latitudes higher than 60 S or 60 N (high latitudes), latitudes between 30 N and 30 S (tropics), and mid-latitudes, and for two pressure layers, 1000–800 hPa and 800–400 hPa, are shown. Clearly, simulations are further apart from observations in the tropical latitudes, with the lowest correlation coefficient for the 800–400 hPa layer. The closest group of points to observations is the high latitudes 800–400, then comes the mid-latitudes 800–400, with model variability very similar to the observed variability and a correlation coefficient close to 0.8. The T21 simulation produces slightly better statistical scores than the T42 simulation, except for the 1000–800 hPa layer in the tropics. The Taylor plot does not indicate differences in biases that we show in Table 7: again, BL1 simulations, both at T21 and T42 resolutions are further away from observations, with for instance a bias of 21.3 ppbv for the T21BL1 simulation at mid-latitudes between 1000 and 800 hPa versus 13.5 for the T21 simulation. Biases are the smallest for the T21 simulation, except for the T42 case in the tropics between 800–400 hPa where the small bias of 0.6 ppbv is a blend of a positive bias at the highest pressures of the layer considered and a negative bias at the lowest ones. Overall, these scores for O_3 in the troposphere are satisfactory given the effect of the horizontal resolution of models on ozone production efficiency. For instance, Liang and Jacobson (2000) and references therein, point out that integrated ozone production may be overpredicted by as much as 60% in coarse-model grid cells exposed to different air masses.

4 Sensitivity to surface processes

A number of recent studies have outlined the response of CTMs to surface emissions, running the models with various emission scenarios (Lamarque et al., 2005; Dentener et al., 2006; Stevenson et al., 2006; Shindell et al., 2006). We present in this section results related to the response in the sink component of the surface processes, that is the dry deposition process. Our objective is to complement with a climatological perspective the few results already published on the sensitivity of the boundary layer mixing ratios and of the deposition fluxes to the dry deposition velocity (Ganzeveld and Lelieveld, 1995; Ganzeveld et al., 1998). We performed an additional 6-year simulation (2000–2005) noted T21DvClim. T21DvClim is similar to the T21 simulation except that the deposition velocities are climatological monthly deposition velocities calculated from the on-line velocities of the T21 simulation. We computed hourly climatologies as the diurnal cycle of the deposition velocity of a number of species (e.g., HNO_3, O_3) is well defined (Michou et al., 2004). We outline in Sect. 4.1 results about mixing ratios over the whole atmosphere, and we describe in Sect. 4.2 how dry deposition fluxes have been impacted by this change in the deposition velocities.

4.1 Mixing ratios

We synthesized the main differences between the T21 and T21DvClim simulations with regard to mixing ratios as follows: we analysed absolute relative differences of zonal monthly averages, and for each model level we looked at the maximum of these relative differences. In the lines below, the maximum (respectively the mean) presented correspond to the maximum (respectively the mean) of these maximum values. The highest maximum relative differences are found for HNO_3, reaching 58%, with an average value of 17%; the largest differences appear in the troposphere: at altitudes below 200 hPa, maximum relative differences are higher than 20% but are close to zero above 100 hPa. In general, for all the species presented here, maximum relative differences are close to zero above 100 hPa. The next species in terms of large relative differences is NO_2, linked to HNO_3, up to 41%, and a mean of 10%; in the end, total NO_2 columns differ by about 1% on average over the whole globe and the year, and by a maximum of 35% (not shown). Then comes OH and O_3 with maxima of 25 and 21%, and means of 5 and 2% respectively. For O_3, the relative differences decrease rapidly

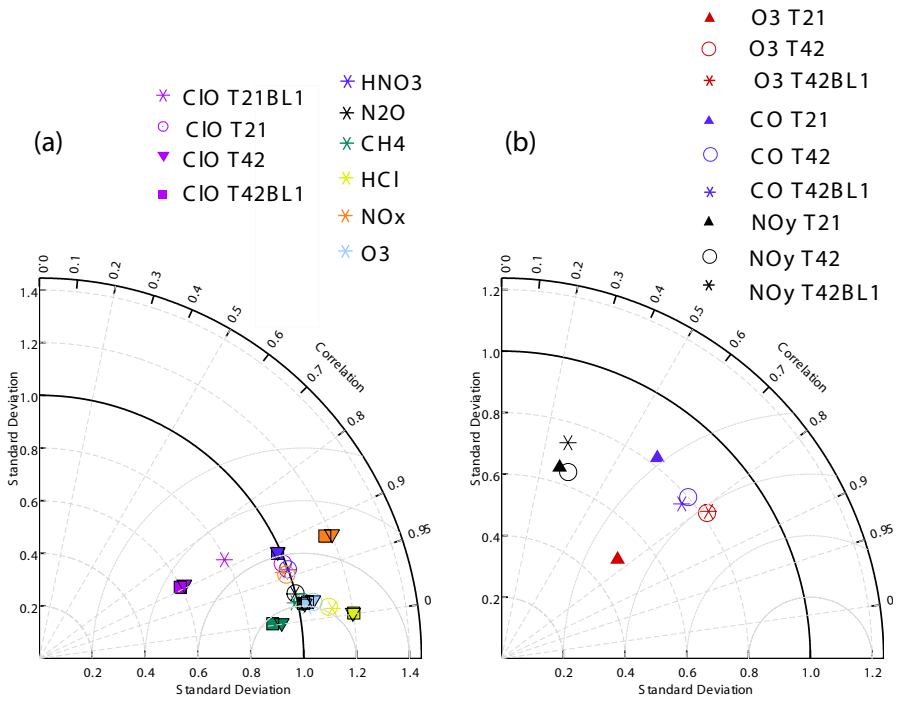

Fig. 21. Taylor type plot of modeled mixing ratios from the T21, T21BL1, T42 and T42BL1 simulations: **(a)** in the stratosphere 100–1 hPa against the Grooss and Russel (2005) and Randel et al. (1998) climatologies. **(b)** in the UTLS, 340–350 K layer against MOZAIC data. **(c)** in the troposphere against the Logan (1999a) climatology, over various latitude bands, latitudes higher than 60 S or 60 N (H), latitudes between 30 N and 30 S (T), and mid-latitudes (M), and for two pressure layers, 1000–800 hPa and 800–400 hPa.

from the surface up to about 800 hPa (lowest 10 levels of the model); the highest differences appear in May. Finally, all maximum relative differences are below 6% for CO throughout the whole atmosphere. As for ClO and HCl they have non significant relative differences in the troposphere due to their very small mixing ratios, and relative differences lower than 10% in the stratosphere. For N_2O, relative differences are almost nil throughout the atmosphere.

4.2 Dry deposition fluxes

We have computed deposition fluxes (moles m^{-2} s^{-1}) as the product of the gas concentration at the lowest level of the model (moles m^{-3}) and of its dry deposition velocity ($m\,s^{-1}$). Deposition fluxes may differ by region/model because of differences in the geography of the emissions, the strength and quality of the atmospheric transport, the chemical reactions involved from emission to deposition, and the processes covered to calculate the dry deposition velocity.

Our T21 O_3 deposition flux of 794 $Tg(O_3)$ yr^{-1} is lower than those simulated by a number of recent models: Stevenson et al. (2006) presented results from simulations performed by 26 chemistry models; the O_3 deposition flux of the ensemble mean for 2000 was of 1003 $Tg(O_3)$ yr^{-1}, with a standard deviation of 200 $Tg(O_3)$ yr^{-1}. Models included

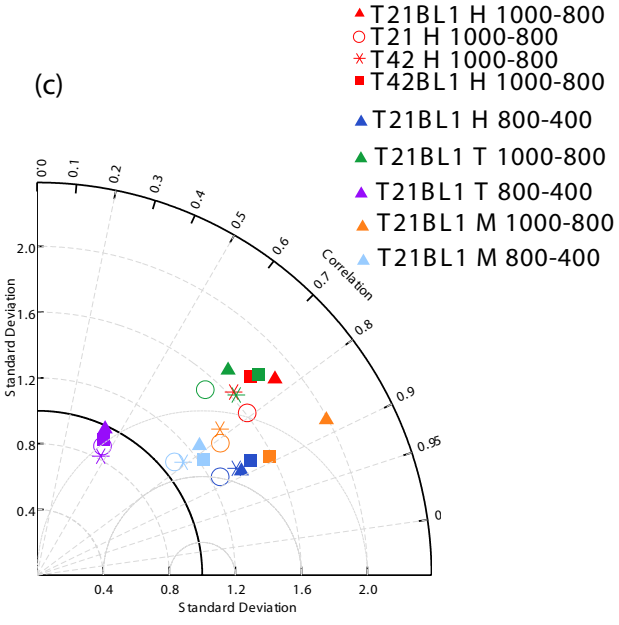

Fig. 21. Continued.

Table 8. Summary of results from the T21 and T21DvClim simulations related to dry deposition: annual dry deposition fluxes, and global annual mean mixing ratios at the surface, with standard deviation in parentheses.

	T21	T21DvClim
O_3 dep. flux ($Tg\,yr^{-1}$)	794	785
HNO_3 dep. flux ($Tg(N)\,yr^{-1}$)	13.9	11.1
NO_2 dep. flux ($Tg(N)\,yr^{-1}$)	5.6	5.5
NO dep. flux ($Tg(N)\,yr^{-1}$)	0.01	0.01
PAN dep. flux ($Tg(N)\,yr^{-1}$)	2.0	1.9
NO_{fl} dep. flux ($Tg(N)\,yr^{-1}$)	21.5	18.6
O_3 mix. ratio (ppbv)	24.8 (12.1)	24.1 (11.9)
HNO_3 mix. ratio (pptv)	140.3 (220.4)	108.9 (183.4)
NO_2 mix. ratio (ppbv)	0.8 (2.3)	0.8 (2.2)

deposition schemes of varying levels of sophistication, but all used resistance type formulations (Wesely, 1989) coupled to prescribed land cover distributions, as we do in MOCAGE-Climat. These ozone deposition fluxes are larger than those of the IPCC TAR (Prather et al., 2001), that reported a mean O_3 flux of $770\,Tg(O_3)\,yr^{-1}$. Stevenson et al. (2006) indicated that the reasons for this change were not immediately obvious, but probably partially related to the higher total NO_x emissions used compared to earlier studies; also isoprene emissions were somewhat higher; and NMHC schemes have developed in sophistication over the last five years. Our emissions of NO_x are lower than those of Stevenson et al. (2006), by about 9%; so are our emissions of isoprene (15% lower) and monoterpenes (60% lower). Wild (2007) indicate also that at coarse resolution the dry deposition flux is systematically underestimated, 5–8% at the 300–600 km grid scales investigated.

The ratio of Northern Hemisphere flux to Southern Hemisphere flux is of 2.2; both the hemispheric repartition of land and ocean, that induces higher deposition velocities in the Northern Hemisphere, and the hemispheric repartition of industrialized regions, that generate higher surface O_3 concentrations, contribute to this unequal partitioning of the fluxes. Deposition over oceans amounts to only 38% of the global deposition. Monthly fluxes are shown in Fig. 22 for the T21 simulation. The strong seasonal cycle over the continents of the temperate latitudes of the Northern Hemisphere, with larger deposition fluxes from May to September, is essentially driven by the deposition velocity (not shown here); in the tropical latitudes, a seasonal cycle exists with maxima from July through September south of the Equator, linked to higher O_3 surface concentration due to emissions from biomass burning; at high latitudes, a very small deposition velocity prevents deposition any time of the year.

In addition to studying the O_3 deposition flux, we have also analyzed the flux of nitrogen species, as all these species are closely linked to each other. After their emissions, NO and NO_2 undergo a series of chemical reactions and deposition, either dry deposition at the surface or wet removal by rain. MOCAGE-Climat has a reasonable description of the chemistry relevant to nitrogen species. Our nitrogen flux is the flux of the so-called NO_{fl} species, where NO_{fl}=$HNO_3 + NO_2 + NO + PAN$; the dry deposition flux from other nitrogen species can be neglected, because of very low mixing ratios or deposition velocities. The T21 run simulated a global mean NO_{fl} dry deposition flux of $21.5\,Tg(N)\,yr^{-1}$, that represents 52% of the nitrogen emitted. This ratio is in line with recent studies: Dentener et al. (2006), who reported results from 26 models, essentially focussed on wet nitrogen deposition, quoting that dry deposition was an equally important process to remove nitrogen species, but that use of the dry deposition measurements which are not global was beyond the scope of their analysis. The relative importance of dry deposition for removal of NO_y varied significantly among models, from 30 to 60%.

Lamarque et al. (2005) investigated nitrogen deposition using six CTMs. The total deposition over land ranged from 25 to $40\,Tg(N)\,yr^{-1}$ and represented about 70% of the total nitrogen emitted, the rest being oceanic deposition as models are at steady state or close to it. Our dry deposition over land is of 34% (coherent with the 70% just cited), while the amounts deposited over Asia $5.3\,Tg(N)\,yr^{-1}$, Europe (3.3), and North America (3.0) are very close to those of Lamarque et al. (2005) ($\sim$5, $\sim$3, and $\sim$3 respectively). In addition, our maximum deposition rates (not shown) are of 0.4–0.5 $g(N)\,m^{-2}\,yr^{-1}$ over part of Western Europe, of the Eastern USA and of China; these rates are consistent with the total nitrogen deposition rates of Lamarque et al. (2005). Rates over Africa also are similar, while those over South America are lower than the mean model in Lamarque et al. (2005); over the South American continent however deposition variability among models is the highest in Lamarque et al. (2005).

The largest part of our NO_{fl} dry deposition flux is due to the HNO_3 flux (65%); then comes the NO_2 flux (26%, see Table 8). The NO_2 dry deposition flux is still very controversial, in particular because of debate on the dry deposition velocity (Holland et al., 2004; Kirkman et al., 2002), but also on how to consider the rapid in-air reactions between NO, NO_2, and O_3 that may occur between the soil and the height at which the deposition velocity is computed. Wesely and Hicks (2000) noted that such a task represented a significant challenge to modelers, especially if the processes were to be described adequately in regional and large-scale models. Finally, Trebs et al. (2006) reported that NO_2 significantly accounted for N dry deposition over a tropical pasture in the Amazon Basin, based on measurements valid for the entire year.

With regard to the dry deposition fluxes, the T21DvClim and the T21 simulations produced very similar O_3 fluxes ($785\ Tg\,yr^{-1}$ versus 794), and likewise for NO_2

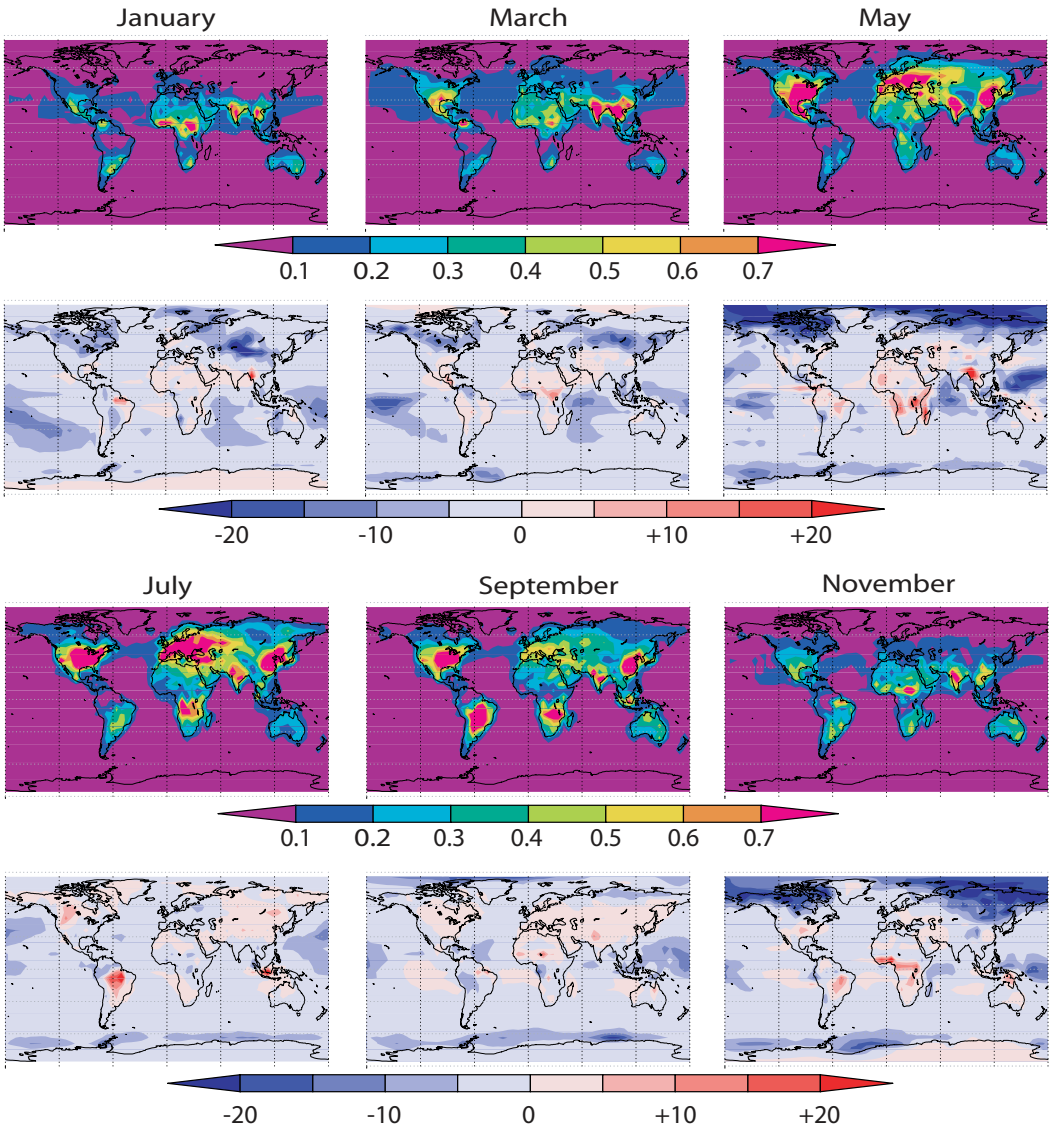

Fig. 22. MOCAGE-Climat T21 O_3 dry deposition fluxes ($g\,m^{-2}\,month^{-1}$), and relative differences ($100\times((T21DvClim-T21)/T21)$), in January (left, 2 upper panels), March (middle, 2 upper panels), May (right, 2 upper panels), July (left, 2 bottom panels), September (middle, 2 bottom panels), and November right, 3 bottom panels).

($5.5\ Tg(N)\,yr^{-1}$ versus 5.6) (see Table 8), with mixing ratios at the surface of the model highly correlated ($r>0.99$). Locally however these fluxes may differ by up to 20% (see Fig. 22). In the case of HNO_3, outputs from the two simulations differ more, with a global flux for T21DvClim about being 20% lower, and quasi-systematically lower mixing ratios at the surface (not shown). The variability of the HNO_3 deposition velocity is high as it is driven by the aerodynamic resistance and thus the stability of the atmosphere. It is not surprising that the use of climatological deposition velocities instead of deposition velocities calculated on-line has a great impact on HNO_3 amounts. Furthermore, as HNO_3 is at the end of the oxidation chain, changes in the budgets of various other species seem to have a cumulative effect for HNO_3, hence the large differences we see here between the T21 and T21DvClim simulations.

5 Conclusions

We have presented the global troposphere and stratosphere configuration of the Météo-France Chemistry and Transport Model MOCAGE-Climat. The model, which includes 82 chemical species and 242 thermal reactions, simulates the global 3-D distribution of ozone and its precursors, both in the troposphere and the stratosphere, up to the mid-mesosphere (∼70 km). The version of MOCAGE-Climat

discussed in this paper has been driven by the ECMWF operational analyses, on T21 and T42 horizontal grids and 60 hybrid vertical levels. At the surface, emissions and dry deposition are taken into account: these emissions consist of monthly or yearly inventories, representative of the year 2000, and include both anthropogenic and biogenic sources; dry deposition is calculated on-line using the 6-hourly meteorology of the ECMWF. The model can run with or without a procedure that considers the model's lowest levels as one layer for chemistry; this procedure significantly reduces computing cost.

Several 6-year simulations have been performed with the meteorology of the years 2000–2005, at two horizontal resolutions, with and without the reduced boundary layer, and with on-line or climatological deposition velocities. Model outputs have been compared thoroughly to observations, both from satellite and in-situ measurements at climatological timescales. This comparison exercise highlighted the strong non-linear linkages between the chemical species of MOCAGE-Climat.

A number of the discrepancies between the model and the observations are likely related to the meteorological forcing in the stratosphere. Indeed, age of air simulations confirmed that the Brewer-Dobson circulation of the ECMWF analyses is at least two times too fast, and that this discrepancy increases with the horizontal resolution. This results in too much ozone being accumulated in the lower to mid-stratosphere in our model as shown by the comparisons to the NIWA/TOMS total columns, to the UARS measurements, or to the ozone sondes. At the same time, ozone mixing ratios are too low in the tropical lower stratosphere. Experiments to simulate age of air driving the CTM with another meteorological model, i.e., the ARPEGE-Climat GCM, revealed that much older age of air could be obtained. This is promising for long-term chemistry-climate interactions as further steps will be to drive the full CTM with ARPEGE-Climat.

In the stratosphere, setting aside shortcomings linked to the meteorology, N_2O is in fair agreement with observations (UARS and ODIN satellites); CH_4 variability, both spatially and seasonally, is satisfactory, though modelled mixing ratios slightly underestimate observations; consequently H_2O mixing ratios are also too low throughout the stratosphere. HNO_3 is also quite accurately simulated, but sedimentation of nitric acid included in Polar Stratospheric Clouds appears too weak. Finally, the model evaluation revealed that the reservoir form HCl is somewhat too abundant, while NO_x is correctly simulated.

Ozone in the UTLS does not show any systematic bias; differences with observations, either MOZAIC or ozone sondes, vary depending on the season, but also on the latitude and on the year. These results confirm the conclusions of Law et al. (2000) that the stratosphere and the troposphere are together mandatory to simulate correctly ozone in the UTLS.

In the troposphere, better agreement is obtained at mid and high latitudes than in the tropics; at equatorial stations, the model underestimates observations over the entire free troposphere while mixing ratios are too high in the boundary layer. This reflects weaknesses both in the dry deposition over these regions, where very few measurements enable validation, and in the convective transport that does not seem strong enough. Though the model seems to capture some of the seasonal variability of the tropospheric ozone, agreement with observations is better in summer.

NO_2 total colums are in general overestimated, as revealed by comparisons to SCIAMACHY NO_2 columns. This overestimation is more important in the winter months over the Northern Hemisphere. Parallel to this positive bias and linked to it, HNO_3 is also overestimated in the first 3–4 km of the troposphere when compared with aircraft measurements, while it matches well with the observations above 4 km. This bias of HNO_3 may also reflect insufficient loss via the wet deposition process. Overall, as OH is biased high in the lower troposphere, this would tend to generate too much oxidation in the model. This in turn would lead to a positive bias in HNO_3, then in NO_x and finally in tropospheric O_3.

A general feature for CO is that the model underestimates observations in the Northern Hemisphere and overestimates them in the Southern Hemisphere. A similar underestimation exists in many current CTMs and seems to be related to the emissions of CO (Shindell et al., 2006).

Simulations with the simplification of the boundary layer lead to model outputs being less similar to observations from ozone sondes, not only at the lowest levels of the model, but also up to the mid-troposphere. The impact of the bulk boundary layer is negligible in the rest of the atmosphere, so it appears that this simplified boundary layer is an interesting option for long-term integrations of the model. Comparisons of the T21 and T42 resolution outputs lead to the conclusion that the T21 outputs are closer to observations in the stratosphere, and also, more surprisingly, in the troposphere. In the UTLS however the T42 simulation obtains better scores.

Dry deposition fluxes of O_3 and nitrogen species are within the range of values reported by recent intercomparison model exercises (Stevenson et al., 2006), though at the low end. The use of climatological deposition velocities versus on-line ones had the greatest impact on HNO_3 and NO_2 in the troposphere; O_3 was impacted up to 800 hPa. Deposition fluxes differed locally up to 20%. However, given the uncertainties not only on this deposition process but also on the model chemistry and dynamics, the climatological deposition velocity option appears reasonable for the study of chemistry and climate interactions. The benefit will be a reduction in computer time.

The future, besides the on-going evolution of the operational, air quality version of the CTM that has repercussions on all versions of the model, will be to make simulations over decades or centuries with MOCAGE-Climat coupled to the GCM ARPEGE-Climat. Ultimately, both models will be part of the global Earth modelling system of CNRM.

Appendix A

Observations used for the evaluation

A1 NIWA-TOMS

The assimilated NIWA data base combines satellite-based ozone measurements from four Total Ozone Mapping Spectrometer (TOMS) instruments, three different retrievals from the Global Ozone Monitoring Experiment (GOME) instruments, and data from four Solar Backscatter Ultra-Violet (SBUV) instruments. Comparisons with the global ground-based World Ozone and Ultraviolet Data Center (WOUDC) Dobson spectrophotometer network have been used to remove offsets and drifts between the different datasets to produce a global homogeneous total ozone column dataset that combines the advantages of good spatial coverage of satellite data with good long-term stability of ground-based measurements. Updated versions of the TOMS (version 8), GOME (version 3.1) and SBUV (version 8) retrieval software, together with assimilated total column ozone fields from Royal Netherlands Meteorological Institute (KNMI), have been used to compute this climatological dataset which comprises global monthly fields from 1978 to 2005 at 1.25° (longitude) by 1° (latitude) resolution. Trends in the satellite data, particularly Earth Probe TOMS data from 2002 onwards, have been corrected. For further details on the NIWA dataset see Bodeker et al. (2005).

Total ozone columns derived from the TOMS measurements (WMO, 1988) represent the primary source of information of the NIWA dataset. Since the first launch in 1978, the TOMS measures radiances of the solar UV radiation backscattered by the atmosphere, at six different wavelengths, and the ozone amount is determined by the ratio of measurements in different channels from the Beer-Lambert equation with a typical resolution of 60 to 38 km. A daily total ozone column dataset is generated, except over polar night regions due to the instrument characteristics. Accuracy is of about 1%, but decreases at large zenithal angles (McPeters et al., 1996). Because of the length of its measurement record, TOMS data are very useful for ozone model validation.

A2 HALOE-MLS-CLAES/UARS

We worked with two climatologies of a number of stratospheric compounds derived from measurements made onboard the Upper Atmosphere Research Satellite (UARS) on an asynchronous orbit. Both climatologies use the results of the version 19 retrieval software for the Halogen Occultation Experiment (HALOE) that utilises the solar occultation technique, making daily observations of up to 15 sunrise and 15 sunset profiles. HALOE has been validated against a variety of measurements; generally, the accuracy of the retrievals decreases near the tropopause (see Table 6 for typical values for the various trace gases).

The Grooss and Russel (2005) climatology has been built from the instrument data of HALOE that observed mixing ratios of important trace species in the stratosphere for more than ten years, starting in 1991. A zonal climatology has been compiled for O_3, H_2O, CH_4, NO_x, and HCl. In this article we used data on 5 degree latitude bins and 22 pressure levels from 316 to 0.1 hPa. Seasonal dependence is taken into account with monthly data derived from 1991–2002 observations. The most recent data since September 2002 have not been included in this climatology, since in 2002 a very unusual major warming occurred in Antarctica, and as observations have been less frequent after 2002.

The primary data analyzed in the Randel et al. (1998) climatology are HALOE vertical profile measurements covering the period 1991–1997. Data have been combined as monthly zonal averages, on 4 degree bins equivalent latitudes (i.e., the latitude of an equivalent potential vorticity distribution arranged symmetrically about the pole), and on 16 pressure levels spanning 100–0.32 hPa (approximately 16-56 km), with a vertical spacing of about 2.5 km. HALOE data have been complemented with Microwave Limb Sounder (MLS) (version 4) and Cryogenic Limb Array Etalon Spectrometer (CLAES) (final retrieval version) instrument data, both with measurements of additional chemical species and measurements in winter polar latitudes where HALOE observations are unavailable. The period of observations for CLAES is much shorter however, that is October 1991–May 1993. We analyse in this article simulations of HNO_3, N_2O and ClO against CLAES HNO_3, N_2O, and MLS ClO observations.

A3 SMR/ODIN

The Odin mini-satellite is a Swedish-led project funded jointly by Sweden, Canada, France, and Finland (Murtagh et al., 2002). It was launched in February 2001, and is still operational. Odin includes two instruments that measure various compounds: the Optical Spectrograph and Infrared Imager System (OSIRIS) and the Sub-Millimeter Radiometer (SMR) (Frisk et al., 2003). In this study we used retrievals of the 502.296-GHz N_2O line obtained from the SMR data (see a description of the retrieval method in (Rodgers, 2000)). Measurements have been analyzed using version V222 up to July 2005 (Urban et al., 2005) and version V225 after October 2005. N_2O can then be retrieved from about 100 hPa to pressures below 1 hPa with a vertical resolution of about 2–3 km. The total systematic error covers 3–35 ppbv for mixing ratios from 0 to ∼150 ppbv, respectively. Validation of the N_2O observations appears in Urban et al. (2005).

For the present study, we restricted our evaluation to N_2O data with a measurement response greater than 0.75, i.e., where a priori information is in minority. Measurements have been monthly averaged into 10° latitude boxes from August 2001 to Dec 2005 in the vertical domain 100–1 hPa.

A4 MOPITT/TERRA

The Measurements Of Pollution In The Troposphere (MOPITT) instrument, on-board the NASA satellite Terra, has been making nadir observations since March 2000. MOPITT views the Earth over all latitudes with a pixel size of 22 km by 22 km and a cross-track swath that gives a near-global distribution of CO every 3 days, providing the first continuous global measurements of CO in the troposphere (Drummond and Mand, 1996). MOPITT measures the infrared radiance upwelling from the Earth's surface and atmosphere; retrievals cannot therefore be performed over cloudy regions. CO mixing ratio profiles and total column amounts are retrieved, although there is considerable correlation between levels with about 1.5–2 independent pieces of information. Since the inversion of the measured radiances is an ill-posed problem, meaning there is not a unique solution, it is necessary to constrain the retrievals with *a priori* information. In polar regions, MOPITT CO retrievals are weighted by the a priori profile much more heavily than in other regions, and therefore contain less information. Similarly, night-time MOPITT retrievals often contain less information than daytime retrievals, especially over land. A summary of the retrieval technique appears in Deeter et al. (2003). Generally the accuracy is better than 10%; validation results are provided in Emmons et al. (2004, 2007).

In this study we used level 3 version 3 monthly profiles available from the ftp site ftp://l0dps01u.ecs.nasa.gov/MOPITT/MOP03M.003/, which consist of averages gridded on a global $1^\circ \times 1^\circ$ grid. Mixing ratios on 7 vertical levels (surface, 850, 700, 500, 350, 250, and 150 hPa) are provided together with the averaging kernels.

A5 SCIAMACHY/ENVISAT

SCIAMACHY (SCanning Imaging Absorption spectroMeter for Atmospheric CartograpHY) is an instrument on-board ESA's environmental satellite Envisat launched in March 2002, having an equator crossing time at 10.00 a.m. on descending mode. SCIAMACHY observes earthshine radiance in limb and nadir viewing geometry, and solar and lunar light transmitted through the atmosphere in occultation viewing geometry. Vertical profiles and columns of a variety of atmospheric constituents are inferred, but we considered here NO_2 columns only. The typical size of the nadir ground-pixel for NO_2 is 30 km×60 km, and SCIMACHY provides a global coverage at the equator within 6 days. A complete description of SCIAMACHY and its mission can be found in Bovensmann et al. (1999) and references therein. Piters et al. (2006) present an overview of SCIAMACHY validation. For the NO_2 columns, the largest uncertainties are due to clouds, but other large errors come from surface albedo, and a priori profile shape. Generally, the accuracy is better than 10^{15} molec cm^{-2}, but the discrepancy with other measurements can be as high as 3.5 10^{15} molec cm^{-2} at polluted sites of the Northern Hemisphere. Several comparisons of the NO_2 columns with ground-based and other satellite observations have recently been published (Schaub et al., 2007; Blond et al., 2007; Boersma et al., 2007[1]).

We obtained the data from the Tropospheric Emission Monitoring Internet Service (TEMIS) web site http://www.temis.nl/airpollution/no2col/data/. They consist of global, monthly, total and tropospheric columns at $0.25^\circ \times 0.25^\circ$ horizontal resolution. We chose to evaluate our model results against SCIAMACHY retrievals rather than GOME ones, as the GOME data were available until June 2003 only. The slant columns from SCIAMACHY observations are derived by the Belgian Institute for Space Aeronomy (see Eskes and Boersma, 2003, for details on the method). The retrieval technique of TEMIS includes a data assimilation technique to estimate the stratospheric part of the NO_2 column (KNMI, TM4 model), which is an essential step in determining quantitatively accurate tropospheric NO_2 and total columns (see Boersma et al., 2004, for details).

A6 MOZAIC

The European Measurement of OZone and water vapor by AIrbus in-service airCraft program (MOZAIC) aims to document the global distribution of some chemical species in the troposphere and the lower stratosphere using instruments on-board regular long-range aircraft (Marenco et al., 1998). This project results from the collaboration of the aeronautics industry, airline companies, and research laboratories for the development and operation of specific instruments, the distribution of observations, and their use for the validation of models (Law et al., 1998, 2000). Five long-range aircraft were equipped for the regular measurements of meteorological and chemical parameters during whole flights. Flight parameters (time, geographical coordinates, pressure, and aircraft speed) are measured every 4 s, together with thermodynamical (temperature, wind speed) and chemical (O_3, H_2O, CO, and NO_y) parameters in the vicinity of the aircraft. During phase I of MOZAIC (from 1993 to 1996), O_3 and H_2O were the only chemical compounds measured. New instruments were developed during phase II (from 1997 to 1999) for sampling CO (Nédélec et al., 2003) and NO_y (Volz-Thomas et al., 2005), while O_3 and H_2O measurements were on-going. Since the installation of these new instruments (phase III), CO and NO_y measurements complement O_3 and H_2O observations. Almost 20 000 flights have been documented between the beginning of MOZAIC in 1994 and May 2006. The spatial coverage of the MOZAIC measurements is interesting, as aircraft fly over most of the Northern Hemisphere. However, the main air corridors, between Europe and North America, represent almost half of the sampled flights;

[1] Boersma, K. F., Jacob, D. J., Eskes, H. J., Pinder, R., Wang, J., van der A. R. J.: Intercomparison of SCIAMACHY and OMI tropospheric NO_2 columns: observing the diurnal evolution of chemistry and emissions from space, J. Geophys. Res., submitted, 2007.

some flights cross the Equator. About 90% of the MOZAIC measurements are made during the cruise, between 9 and 12 km. The remaining measurements are performed during ascent and descent phases, providing information on the vertical structure of the tropospheric chemistry.

We chose to use data from the MOZAIC database (http://mozaic.aero.obs-mip.fr/web/) evaluated in the literature that are averaged data every 1 minute and/or every 150 m along the vertical axis for the period extending from 1 January 2000 to 30 April 2004. For NO_y measurements, only the reliable data have been retained excluding values below the detection limit (Volz-Thomas et al., 2005). No comparison was conducted for water vapour measurements because MOCAGE-Climat H_2O mixing ratios in the UTLS are those of the ECMWF analyses already evaluated in Oikonomou and O'Neill (2006). We averaged data in 3D boxes, $2.8° \times 2.8°$ along the horizontal, and in the vertical the layer between the 340 and 350 K isentropic levels, where most of the observations are performed. We further made averages over 3-month periods to study the seasonal variability; monthly periods included too few data. In addition to this climatological analysis, we computed histogram distributions that take into account all the 1 minute data available in six regions of the world, to distinguish among mid and tropical latitudes, oceans and continents. These regions cover North America (130–90 W , 30–70 N), South America (80–40 W, 45 S–10 N), the northern Atlantic ocean (60–15 W, 10–60 N), Europe (10 W–30 E, 30–70 N), Africa (15 W–45 E, 35 S–30 N), and Siberia/Asia (45–155 E, 10–60 N).

A7 Other non-satellite observations

We used part of the climatology of Logan (1999a) which includes observations from a number of ozonesonde stations, mainly from the WOUDC. We analyzed data from 23 stations that we retained, which represent about two thirds of the stations in the Logan (1999a) dataset, namely those that included observations after 1980, and with a climatology for all the months of the year. Only five of these stations are located in the 30 S–30 N band; the others are situated at higher latitudes, in polluted as well as pristine areas. The monthly profiles include data on 22 pressure levels, both in the troposphere and in the stratosphere, from the surface up to 10 hPa (10 levels up to 200 hPa).

We also made comparisons with the three-dimensional climatology distribution of tropospheric OH by Spivakovsky et al. (2000). Although advances have been made in measuring concentrations of OH, one has to rely on models to provide an integrated measure of the oxidative capacity of the atmosphere because of the extreme variability of OH in time and space. The monthly distribution of Spivakovsky et al. (2000) has been computed using observations of a number of precursors for OH, including for instance O_3, H_2O, and various nitrogen species, over the period 1978–1996. The distribution of OH was then derived as a function of these precursors, temperature and cloud cover on a $8°$ lat$\times 10°$ lon grid, from the surface up to 100 hPa in the tropics (200 elsewhere).

Finally, we completed our reference set with the data compiled by Emmons et al. (2000) that consist of tropospheric measurements of ozone and its precursors from a number of aircraft campaigns. Although these are not climatologies in the sense of a long term average, they provide a unique picture of the global distribution of these species. We used averaged profiles over a number of regions of the world with a 1 km vertical resolution.

Acknowledgements. This work was partially funded by EC within the QUANTIFY Integrated Project under contract no. 003893 (GOCE). The authors acknowledge the EU MOZAIC project (EVK2-1999-00141) for data collection and analysis at CNRS, Forschungszentrum Jülich, University of Cambridge, and Météo-France. We also acknowledge MOZAIC support from EADS Airbus and the airlines Air France, Deutsche Lufthansa, Sabena, and Austrian Airlines who carry the MOZAIC instruments free of charge and perform maintenance. We would like to thanks the EU funded project SCOUT-O3 and the SPARC/CCM-Val project for their help and making available their data. We want to particularly mention G. E. Bodeker (NIWA), J.-U. Grooss (ICG), W. J. Randel (NCAR), and C. M. Spivakovsky (U. of Harvard) for their help with the data. Finally, we want to thank two anonymous reviewers for their very fruitful comments.

Edited by: M. Dameris

References

Andres, R. J. and Kasgnoc A. D.: A time-averaged inventory of subaerial volcanic sulfur emissions, J. Geophys. Res., 103, 25 251–25 261, 1998.

Bechtold, P., Bazile, E., Guichard, F., Mascart, P., and Richard, E.: A mass flux convection scheme for regional and global models, Q. J. Roy. Meteor. Soc., 127, 869–886, 2001.

Blond, N., Boersma, K. F., Eskes, H. J., van der A, R. J., Van Roozendael, M., De Smedt, I., Bergametti, G., and Vautard, R.: Intercomparison of SCIAMACHY nitrogen dioxide observations, in-situ measurements, and air quality modeling results over Western Europe, J. Geophys. Res., 112, D10311, doi:10.1029/2006JD007277, 2007.

Bodeker, G. E., Shiona, H., and Eskes, H.: Antarctic ozone depletion indicators, Atmos. Chem. Phys., 5, 3811–3845, 2005, http://www.atmos-chem-phys.net/5/3811/2005/.

Boering, K. A., Wofsy, S. C., Daube, B. C., Schneider, H. R., Loewenstein, M., Podolske, J. R., and Conway, T. J.: Stratospheric mean ages and transport rates from observations of carbon dioxide and nitrous oxide, Science, 274, 1340–1343, 1996.

Boersma, K. F., Eskes, H. J., and Brinksma, E. J.: Error analysis for tropospheric NO_2 retrieval from space, J. Geophys. Res., 109, D04311, doi:10.1029/2003JD003962, 2004.

Bousserez, N., Attié, J.-L., Peuch, V.-H., Michou, M., Pfister, G., Edwards, D., Emmons, L., Mari, C., Barret, B., Arnold, S. R., Heckel, A., Richter, A., Shlager, H., Lewis, A., Avery, M., Sachse, G., Browell, E. V., and Hair, J. W.: Evaluation of the MOCAGE chemistry transport model during the

ICARTT/ITOP experiment, J. Geophys. Res., 112, D10S42, doi:10.1029/2006JD007595, 2007.

Bouwman, A. F., Van der Hoek, K. W., and Olivier, J. G. J.: Uncertainties in the global source distribution of nitrous oxide, J. Geophys. Res., 100, 2785–2800, 1995.

Bovensmann, H., Burrows, J. P., Buchwitz, M., Frerick, J., Noel, S., Rozanov, V. V., Chance, K. V., and Goede, A. P. H.: SCIAMACHY: Mission objectives and measurement modes, J. Atmos. Sci., 56, 127–150, 1999.

Brasseur, G. P. and Solomon, S.: Aeoronomy of the middle atmosphere, D. Reidel Publishing Company, 452 pp., 1986.

Brasseur, G. P., Hauglustaine, D. A., Walters, S., Rasch, P. J., Müller, J.-F., Granier, C., and Tie, X. X.: MOZART, a global chemical transport model for ozone and related chemical tracers. 1. Model description, J. Geophys. Res., 103, 28 265–28 289, 1998.

Bregman, A., Meijer, E., and Scheele, R.: Key aspects of stratospheric tracer modeling using assimilated winds, Atmos. Chem. Phys., 6, 4529–4543, 2006, http://www.atmos-chem-phys.net/6/4529/2006/.

Brewer, A. W.: Evidence for a world circulation provided by the measurements of helium and water vapour distribution in the stratosphere, Q. J. Roy. Meteor. Soc., 75, 351–363, 1949.

Cariolle, D. and Déqué, M.: Southern hemisphere medium-scale waves and total ozone disturbances in a spectral general circulation model, J. Geophys. Res., 91, 10 825–10 846, 1986.

Cariolle, D., Lasserre-Bigorry, A., Royer, J.-F., and Geleyn, J.-F.: A general circulation model simulation of the springtime Antarctic ozone decrease and its impact on mid-latitudes, J. Geophys. Res., 95, 1883–1898, 1990.

Cariolle, D. and Teyssèdre, H.: A revised linear ozone photochemistry parameterization for use in transport and general circulation models: multi-annual simulations Atmos. Chem. Phys., 7, 2183–2196, 2007, http://www.atmos-chem-phys.net/7/2183/2007/.

Cathala, M.-L., Pailleux, J., and Peuch, V.-H.: Improving global chemical simulations of the upper troposphere-lower stratosphere with sequential assimilation of MOZAIC data, Tellus, 55B, 1–10, 2003.

Carslaw, K. S., Luo, B., Peter, T., and Clegg, S. L.: Vapour pressures of H_2SO_4/HNO_3/HBr/H_2O solutions to low stratospheric temperatures, Geophys. Res. Lett., 22, 247–250, 1995.

Chapman, S.: A Theory of Upper-Atmospheric Ozone, Memoirs of the Royal Meteorological Society, 3, 103–25, 1930.

Chipperfield, M. P., Cariolle, D., and Simon, P.: A 3D transport model study of chlorine activation during EASOE, Geophys. Res. Lett., 21, 1467–1470, 1994.

Chipperfield M. P.: New version of the TOMCAT/SLIMCAT offline chemical transport model: Intercomparison of stratospheric tracer experiments, Q. J. Roy. Meteor. Soc. , 132, 1179-1203, 2006.

Clark H. L., Cathala, M.-L., Teyssèdre, H., Cammas, J.-P., and Peuch, V.-H.: Cross-tropopause fluxes of ozone using assimilation of MOZAIC measurements in a global CTM, Tellus, 59B, 39–49, 2007.

Crassier, V., Suhre, K., Tulet, P., and Rosset, R.: Development of a reduced chemical scheme for use in mesoscale meteorological models, Atmos. Environ., 34, 2633–2644, 2000.

Crutzen, P. J.: The influence of nitrogen oxide on the atmospheric ozone content, Q. J. Roy. Meteor. Soc., 96, 320–325, 1970.

Deeter, M. N., Emmons, L. K., Francis, G. L., et al.: Operational carbon monoxide retrieval algorithm and selected results for the MOPITT instrument, J. Geophys. Res., 108(D14), 4399, doi:10.1029/2002JD003186, 2003.

Dentener, F., Stevenson, D., Cofala, J., Mechler, R., Amann, M., Bergamaschi, P., Raes, F., and Derwent, R.: The impact of air pollutant and methane emission controls on tropospheric ozone and radiative forcing: CTM calculations for the period 1990 2030, Atmos. Chem. Phys., 4, 8471–8538, 2004, http://www.atmos-chem-phys.net/4/8471/2004/.

Dentener, F., Drevet, J., Lamarque, J.-F., Bey, I., Eickhout, B., Fiore, A. M., Hauglustaine, D., Horowitz, L. W., Krol, M., Kulshrestha, U. C., Lawrence, M., Galy-Lacaux, C., Rast, S., Shindell, D., Stevenson, D., Van Noije, T., Atherton, C., Bell, N., Bergman, D., Butler, T., Cofala, J., Collins, B., Doherty, R., Ellingsen, K., Galloway, J., Gauss, M., Montanaro, V., Muller, J.-F., Pitari, G., Rodriguez, J., Sanderson, M., Solmon, F., Strahan, S., Schultz, M., Sudo, K., Szopa, S., and Wild, O.: Nitrogen and sulfur deposition on regional and global scales: A multimodel evaluation, Global Biogeochem. Cy., 20, GB4003, doi:10.1029/2005GB002672, 2006.

Déqué, M., Dreveton, C., Braun, A., and Cariolle, D.: The ARPEGE-IFS atmosphere model: a contribution to the French community climate modelling, Clim. Dynam., 10, 249–266, 1994.

Drummond, J. R. and Mand, G. S.: The Measurements of pollution in the troposphere (MOPITT) instrument: overall performance and calibration requirements, J. Atmos. Oceanic Technol., 13, 314–320, 1996.

Dufour, A., Amodei, M., Ancellet, G., and Peuch, V.-H.: Observed and modelled "chemical weather" during ESCOMPTE, Atmos. Res., 74, 161–189, 2004.

Drobinski, P., Saïd, F., Ancellet, G., Arteta, J., Augustin, P., Bastin, S., Brut, A., Caccia, J.-L., Campistron, B., Cautenet, S., Colette, A., Cros, B., Corsmeier, U., Coll, I., Dabas, A., Delbarre, H., Dufour, A., Durand, P., Guénard, V., Hasel, M., Kalthoff, N., Kottmeier, C., Lemonsu, A., Lohou, F., Masson, V., Menut, L., Moppert, C., Peuch, V.-H., Puygrenier, V., and Reitebuch, O.: Regional transport and dilution during high pollution episodes in southeastern France : summary of findings from the ESCOMPTE experiment, J. Geophys. Res., 112, D13105, doi:10.1029/2006JD007494, 2007.

Edwards, D. P., Pétron, G., Novelli, P. C., Emmons, L. K., Gille, J. C., and Drummond, J. R.: Southern Hemisphere carbon monoxide interannual variability observed by Terra/Measurement of Pollution in the Troposphere (MOPITT), J. Geophys. Res., 111, D16303, doi:10.1029/2006JD007079, 2006.

Egorova T., Rozanov, E., Zubov, V., Manzini, E., Schmutz, W., and Peter, T.: Chemistry-climate model SOCOL: a validation of the present-day climatology, Atmos. Chem. Phys., 5, 1557–1576, 2005, http://www.atmos-chem-phys.net/5/1557/2005/.

El Amraoui, L., Peuch, V.-H., Ricaud, P., Massart, S., Urban, J., Semane, N., Teyssèdre, H., Cariolle, D., and Karcher, F.: Ozone loss in the 2002/2003 Arctic vortex deduced from the assimilation of Odin/SMR O_3 and N_2O measurements: H_2O as dynamical tracer, Q. J. Roy. Meteor. Soc., in press, 2007.

Emmons, L. K., Hauglustaine, D. A., Muller, J.-F., Carroll, M.

A., Brasseur, G. P., Brunner, D., Staehelin, J., Thouret, V., and Marenco, A.: Data composites of airborne observations of tropospheric ozone and its precursors, J. Geophys. Res., 105, 20 497–20 538, 2000.

Emmons, L. K., Deeter, M. N., Gille, J. C., Edwards, D. P., Attié, J.-L., Warner, J., Ziskin, D., Francis, G., Khattatov, B., Yudin, V., Lamarque, J.-F., Ho, S.-P., Mao, D., Chen, J. S., Drummond, J., Novelli, P., Sachse, G., Coffey, M. T., Hannigan, J. W., Gerbig, C., Kawakami, S., Kondo, Y., Takegawa, N., Schlager, H., Baehr, J., and Ziereis, H.: Validation of Measurements of Pollution in the Troposphere (MOPITT) CO retrievals with aircraft in situ profiles, J. Geophys. Res., 109, D03309, doi:10.1029/2003JD004101, 2004.

Emmons, L. K., Pfister, G. G., Edwards, D. P., Gille, J. C., Sachse, G., Blake, D., Wofsy, S., Gerbig, C., Matross, D., and Nédélec, P.: Measurements of Pollution in the Troposphere (MOPITT) validation exercises during summer 2004 field campaigns over North America: J. Geophys. Res., 112, D12S02, doi:10.1029/2006JD007833, 2007.

Eskes, H. J. and Boersma, K. F.: Averaging kernels for DOAS total-column satellite retrievals, Atmos. Chem. Phys., 3, 1285–1291, 2003,
http://www.atmos-chem-phys.net/3/1285/2003/.

Farman, J. C., Gardiner, B. G., and Shanklin, J. D.: Large losses of total ozone in Antarctica reveal seasonal ClO_x/NO_x interaction, Nature, 315, 207–210, 1985.

Feng, W., Chipperfield, M. P., Dorf, M., Pfeilsticker, K., and Ricaud, P.: Mid-latitude ozone changes: studies with a 3-D CTM forced by ERA-40 analyses, Atmos. Chem. Phys., 7, 2357–2369, 2007,
http://www.atmos-chem-phys.net/7/2357/2007/.

Frisk, U., Hagström, M., Ala-Laurinaho, J., et al.: The Odin satellite I: Radiometer design and test, Astron. Astrophys., 402(3), L27–L34, doi:10.1051/0004-6361:20030335, 2003.

Fung, I., John, J., Lerner, J., Matthews, E., Prather, M., Steele, L. P., and Fraser, P. J.: Three-dimensional model synthesis of the global methane cycle, J. Geophys. Res., 96, 13 033–13 065, 1991.

Ganzeveld, L. and Lelieveld, J.: Dry deposition parameterization in a chemistry general circulation model and its influence on the distribution of reactive trace gases, J. Geophys. Res., 100, 20 999–21 012, 1995.

Ganzeveld, L., Lelieveld, J., and Roelofs, G.-J.: A dry deposition parameterization for sulfur oxides in a chemistry and general circulation model, J. Geophys. Res., 103, 5679–5694, 1998.

Geer, A. J., Lahoz, W. A., Bekki, S., Bormann, N., Errera, Q., Eskes, H. J., Fonteyn, D., Jackson, D. R., Juckes, M. N., Massart, S., Peuch, V.-H., Rharmili, S., and Segers, A.: The ASSET intercomparison of ozone analyses: method and first results, Atmos. Chem. Phys., 6, 5445–5474, 2006,
http://www.atmos-chem-phys.net/6/5445/2006/.

Giorgi, F. and Chamedeis, W. L.: Rainout lifetimes of highly soluble aerosols and gases as inferred from simulations with a general circulation model, J. Geophys. Res., 91, 14 367–14 376, 1986.

Guenther, A., Hewitt, C. N., Erickson, D., Fall, R., Geron, C., Graedel, T., Harley, P., Klinger, L., Lerdau, M., McKay, W. A., Pierce, T., Scholes, B., Steinbrecher, R., Tallamraju, R., Taylor, J, and Zimmerman, P.: A global model of natural volatile compound emissions, J. Geophys. Res., 100, 8873–8892, 1995.

Grooss, J.-U. and Russell III, J. M.: Technical note: A stratospheric climatology for O_3, H_2O, CH_4, NO_x, HCl and HF derived from HALOE measurements, Atmos. Chem. Phys., 5, 2797–2807, 2005,
http://www.atmos-chem-phys.net/5/2797/2005/.

Hadjinicolaou, P., Pyle, J. A., and Harris, N. R. P.: The recent turnaround in stratospheric ozone over northern middle latitudes: A dynamical modelling perspective, Geophys. Res. Lett., 32, L12821, doi:10.1029/2005GL022476, 2005.

Hall, T. M. and Waugh, D. W.: Timescales for the stratospheric circulation derived from tracers, J. Geophys. Res., 102, 8991–9001, 1997.

Harnisch, J., Borchers, R., Fabian, P., and Maiss, M.: Tropospheric trends for CF_4 and C_2F_6 since 1982 derived from SF_6 dated stratospheric air, Geophys. Res. Lett., 23, 1099–1102, 1996.

Hauchecorne, A., Bertaux, J.-L., Dalaudier, F., Cot, C., Lebrun, J.-C., Bekki, S., Marchand, M., Kyrola, E., Tamminen, J., Sofieva, V., Fussen, D., Vanhellemont, F., Fanton d'Andon, O., Barrot, G., Mangin, A., Théodore, B., Guirlet, M., Snoeij, P., Koopman, R., Saavedra de Miguel, L., Fraisse, R., and Renard, J.-B.: First simultaneous global measurements of nighttime stratospheric NO_2 and NO_3 observed by Global Ozone Monitoring by Occultation of Stars (GOMOS)/Envisat in 2003, J. Geophys. Res., 110, D18301, doi:10.1029/2004JD005711, 2005

Hauglustaine, D. A., Hourdin, F., Jourdain, L., Filiberti, M.-A., Walters, S., Lamarque, J.-F., and Holland, E. A.: Interactive chemistry in the Laboratoire de Météorologie Dynamique general circulation model: Description and background tropospheric chemistry evaluation, J. Geophys. Res., 109, D04314, doi:10.1029/2003JD003957, 2004.

Holland, E. A., Braswell, B. H., Sulzman, J., and Lamarque, J.-F.: Nitrogen deposition onto the United States and western Europe: a synthesis of observations and models, Ecol. Appl., 15, 38–57, 2005.

Honoré, C., Rouil, L., Vautard, R., Beekmann, M., Bessagnet, B., Dufour, A., Elichegaray, C., Flaud J-M., Malherbe, L., Meleux, F., Menut, L., Martin, D., Peuch, A., Peuch, V.-H., and Poisson, N.: Predictability of regional air quality in Europe: the assessment of three years of operational forecasts and analyses over France, J. Geophys. Res., in press, doi:2007JD008761R, 2007.

Horowitz, L. W., Walters, S., Mauzerall D. L., et al.: A global simulation of tropospheric ozone and related tracers: description and evaluation of MOZART, version 2, J. Geophys. Res., 108, 4784, doi:10.1029/2002JD002853, 2003.

Houghton, J. T., Ding, Y., Griggs, D. J., Noguer, M., van der Linden, P. J., and Xiaosu, D.: Climate Change 2001: The Scientific Basis, contribution of Working Group I to the Third Assessment Report of the Intergovernmental Panel on Climate Change (IPCC) Cambridge University Press (Eds.), UK, 2001.

Intergovernmental Panel on Climate Change, Climate change 1994: radiative forcing of climate change and an evaluation of the IPCC IS92 emissions scenarios, Cambridge University Press (Eds.), UK, 1995.

Jöckel, P., Tost, H., Pozzer, A., Brühl, C., Buchholz, J., Ganzeveld, L., Hoor, P., Kerkweg, A., Lawrence, M. G., Sander, R., Steil, B., Stiller, G., Tanarhte, M., Taraborrelli, D., van Aardenne, J., and Lelieveld, J.: The atmospheric chemistry general circulation model ECHAM5/MESSy1: consistent simulation of ozone from the surface to the mesosphere, Atmos. Chem. Phys., 6, 5067–

5104, 2006,
http://www.atmos-chem-phys.net/6/5067/2006/.

Josse, B., Simon, P., and Peuch, V.-H.: Rn−222 global simulations with the multiscale CTM MOCAGE, Tellus, 56B, 339–356, 2004.

Kirkman, G. A., Gut, A., Ammann, C., Gatti, L. V., Cordova, A. M., Moura, M. A. L., Andreae, M. O., and Meixner, F. X.: Surface exchange of nitric oxide, nitrogen dioxide, and ozone at a cattle pasture in Rondonia, Brazil, J. Geophys. Res., 107, 8083, doi:10.1029/2001JD000523, 2002.

Labrador L. J., von Kuhlmann, R., and Lawrence, M. G.: The effects of lightning-produced NOx and its vertical distribution on atmospheric chemistry: sensitivity simulations with MATCH-MPIC, Atmos. Chem. Phys., 5, 1815–1834, 2005,
http://www.atmos-chem-phys.net/5/1815/2005/.

Lamarque, J.-F., Kiehl, J. T., Brasseur, G. P., Butler, T., Cameron-Smith, P., Collins, W. D., Collins, W. J., Granier, C., Hauglustaine, D., Hess, P. G., Holland, E. A., Horowitz, L., Lawrence, M. G., McKenna, D., Merilees, P., Prather, M. J., Rasch, P. J., Rotman, D., Shindell, D., and Thornton, P.: Assessing future nitrogen deposition and carbon cycle feedback using a multimodel approach: Analysis of nitrogen deposition, J. Geophys. Res., 110, D19303, doi:10.1029/2005JD005825, 2005.

Law, K. S., Plantevin, P.-H., Shallcross, D. E., Rogers, H. L., Grouhel, C., Thouret, V., Marenco, A., and Pyle, J. A.: Evaluation of modelled O_3 using MOZAIC data, J. Geophys. Res., 103, 25 721–25 740, 1998.

Law, K. S., Plantevin, P.-H., Thouret, V., Marenco, A., Asman, W. A. H., Lawrence, M., Crutzen, P. J., Müller, J.-F., Hauglustaine, D. A., and Kanakidou, M.: Comparison between global chemistry transport model results and Measurement of Ozone and Water Vapor by Airbus In-Service Aircraft (MOZAIC) data, J. Geophys. Res., 105, 1503–1526, 2000.

Lefèvre, F., Brasseur, G. P., Folkins, I., Smith, A. K., and Simon, P.: Chemistry of the 1991–1992 stratospheric winter: three-dimensional model simulations, J. Geophys. Res., 99, 8183–8195, 1994.

Li, Q., Jiang, J. H., Wu, D. L., Read, W. G., Livesey, N. J., Waters, J. W., Zhang, Y., Wang, B., Filipiak, M. J., Davis, C. P., Turquety, S., Wu, S., Park, R. J., Yantosca, R. M., and Jacob, D. J.: Convective outflow of South Asian pollution: A global CTM simulation compared with EOS MLS observations, Geophys. Res. Lett., 32, L14826, doi:10.1029/2005GL022762, 2006.

Liang, J. and Jacobson, M. Z.: Effects of subgrid segregation on ozone production efficiency in a chemical model, Atmos. Environ., 34, 2975–2982, 2000.

Liu, H., Jacob, D. J., Bey, I., and Yantosca, R. M.: Constraints from ^{210}Pb and ^{7}Be on wet deposition and transport in a global three-dimensional chemical-transport model driven by assimilated meteorological fields, J. Geophys. Res., 106, 12 109–12 128, 2001.

Logan, J. A.: An analysis of ozonesonde data for the troposphere: Recommendations for testing 3-D models, and development of a gridded climatology for tropospheric ozone, J. Geophys. Res., 104, 16 115–16 149, 1999a.

Logan, J. A.: An analysis of ozonesonde data for the lower stratosphere: Recommendations for testing models, J. Geophys. Res., 104, 16 151–16 170, 1999b.

Louis, J.-F.: A parametric model of vertical eddy-fluxes in the atmosphere, Bound. Lay. Meteor., 17, 187–202, 1979.

McLinden, C., Olsen, S. C., Hannegan, B., Wild, O., Prather, M. J., and Sundet, J.: Stratospheric ozone in 3-D models: A simple chemistry and the cross-tropopause flux, J. Geophys. Res., 105, 14 653–14 665, 2000.

Madronich, S. and Flocke, S.: The role of solar radiation in atmospheric chemistry, in: Handbook of Environmental Chemistry, edited by: Boule, P., Springer-Verlag, New York, 1–26, 1998.

Marenco, A., Thouret, V., Nédélec, P., Smit, H., Helten, M., Kley, D., Karcher, F., Simon, P., Law, K., Pyle, J., Poschmann, G., Von Wrede, R., Hume, C., and Cook, T.: Measurement of ozone and vapor by Airbus in-service aircraft: The MOZAIC airborne program, An overview, J. Geophys. Res., 103, 631–642, 1998.

McPeters, R. D. and Labow, G. J.: An assessment of the accuracy of 14.5 years of Nimbus 7 TOMS Version 7 ozone data by comparison with the Dobson network, Geophys. Res. Lett., 23, 3695–3698, 1996.

Mari, C., Jacob, D. J., and Bechtold, P.: Transport and scavenging of soluble gases in a deep convective cloud, J. Geophys. Res., 105, 22 255–22 267, 2000.

Matthews, E. and Fung, I.: Methane emissions from natural wetlands: Global distribution, area, and environmental characteristics of sources, Global Biogeochem. Cy., 1, 61–86, 1987.

Michou, M. and Peuch, V.-H.: Surface exchanges in the MOCAGE multiscale Chemistry and Transport Model, J. Water Sci., 15, 173–203, 2002.

Michou, M., Laville, P., Serça, D., Fotiadi, A., and Peuch, V.-H.: Measured and modeled dry deposition velocities over the ESCOMPTE area, Atmos. Res., 74, 89–116, 2004.

Monge-Sanz, B. M., Chipperfield, M. P., Simmons, A. J., and Uppala, S. M.: Mean age of air and transport in a CTM: Comparison of different ECMWF analyses, Geophys. Res. Lett., 34, L04801, doi:10.1029/2006GL028515, 2007.

Murtagh, D., Frisk, U., Merino, F., et al.: An overview of the Odin atmospheric mission, Can. J. Phys., 80, 309–319, 2002.

Nédélec, P., Cammas, J.-P., Thouret, V., Athier, G., Cousin, J.-M., Legrand, C., Abonnel, C., Lecoeur, F., Cayez, G., and Marizy, C.: An Improved Infra-Red Carbon Monoxide Analyser for Routine Measurements aboard Commercial Airbus Aircraft : Technical Validation and First Scientific Results of the MOZAIC III Program, Atmos. Chem. Phys., 3, 1551–1564, 2003,
http://www.atmos-chem-phys.net/3/1551/2003/.

Nho-Kim, E.-Y., Michou, M., and Peuch, V.-H.: Parameterization of size dependent particle dry deposition velocities for global modeling, Atmos. Environ., 38, 1933–1942, 2004.

Noilhan, J. and Mahfouf, J.-F.: The ISBA land surface parameterisation, Glob. Plan. Change, 13, 145–159, 1996.

Norton, W., Bregman, A., Chipperfield, M. P., et al.: TOwards the Prediction of stratospheric Ozone (TOPOZ-2), Final report, European Commission, ENV4-CT97-0542, 2000.

Oikonomou, E. K., and O'Neill, A.: Evaluation of ozone and water vapor fields from the ECMWF reanalysis ERA-40 during 1991-1999 in comparison with UARS satellite and MOZAIC aircraft observations, J. Geophys. Res., 111, D14109, doi:10.1029/2004JD005341, 2006.

Olivier, J. G. J., Bouwman, A. F., Van der Maas, C. W. M., Berdowski, J. J. M., Veldt, C., Bloos, J. P. J., Visschedijk, A. J. H., Zandveld, P. Y. J., and Haverlag, J. L.: Description of EDGAR Version 2.0: A set of global emission inventories of greenhouse gases and ozone-depleting substances for all an-

thropogenic and most natural sources on a per country basis and on 1°×1° grid, RIVM Rep 771060002/TNO MEP report nr. R96/119, RIVM, Bilthoven, The Netherlands, 1996.

Park, J. H., Ko, M. K. W., Jackman, C. H., Plumb, R. A., Kaye, J. A., and Sage, K. H. (Eds.): Models and measurements intercomparison II, NASA/T-1999 209554, Natl. Aeronaut. And Space admin., Washington, D.C., 1999.

Piters, A. J. M., Bramstedt, K., Lambert, J.-C., and Kirchhoff, B.: Overview of SCIAMACHY validation: 2002–2004, Atmos. Chem. Phys., 6, 127–148, 2006, http://www.atmos-chem-phys.net/6/127/2006/.

Pradier, S., Attié, J.-L., Chong, M., Escobar, J., Peuch, V.-H., Lamarque, J.-F., Khattatov, B., and Edwards, D.: Evaluation of 2001 springtime CO transport over West Africa using MOPITT CO measurements assimilated in a global chemistry transport model, Tellus, 58B, 3, 163–176, 2006.

Prather, M. and Ehhalt, D.: Atmospheric chemistry and greenhouse gases, in Climate Change 2001: The Scientific Basis. Contribution of Working Group I to the Third Assessment Report of the Intergovernmental Panel on Climate Change, edited by: Houghton, J. T., Ding, Y., Griggs, D. J., et al., Cambridge Univ. Press, New York, 239–287, 2001.

Prinn, R. G., Weiss, R. F., Fraser, P. J., Simmonds,P. G., Cunnold, D. M., Alyea, F. N., O'Doherty, S., Salameh, P., Miller, B. R., Huang, J., Wang, R. H. J., Hartley, D. E., Harth, C., Steele, L. P., Sturrock, G., Midgley, P. M., and McCulloch, A.: A history of chemically and radiatively important gases in air deduced from ALE/GAGE/AGAGE, J. Geophys. Res., 105, 17 751–17 792, 2000.

Ramaswamy, V., Boucher, O., Haigh, J., Hauglustaine, D., Haywood, J., Myhre, G., Nakajima, T., Shi, G. Y., and Solomon, S.: Radiative forcing of climate change, in Climate Change 2001: The Scientific Basis, Contribution of Working Group I to the Third Assessment Report of the Intergovernmental Panel on Climate Change, edited by Houghton, J. T., Ding, Y., Griggs, D. J., et al., Cambridge Univ. Press, New York, 349–416, 2001.

Randeniya, L. K., Vohralik, P. F., and Plumb, I. C.: Stratospheric ozone depletion at Northern mid latitudes in the 21^{st} century: the importance of future concentrations of greenhouse gases nitrous oxide and methane, Geophys. Res. Lett., 29(4) 1051, doi:10.1029/2001GL014295, 2002.

Randel, W. J., Wu, F., Russell III, J. M., Roche, A., and Waters, J. W.: Seasonal cycles and QBO variations in stratospheric CH4 and H2O observed in UARS HALOE data J. Atmos. Sci., 55, 163–185, 1998.

Ren, X., Brune W., Mao J., et al.: HO_x observation and model comparison during INTEX-NA 2004, J. Geophys. Res., in press., 2007.

Ricaud, P., Barret, B., Attié, J.-L., Le Flochmoën, E., Motte, E., Teyssèdre, H., Peuch, V.-H., Livesey, N., Lambert, A., and Pommereau, J.-P.: Impact of land convection on troposphere-stratosphere exchange in the tropics, Atmos. Chem. Phys., 7, 5639–5657, 2007, http://www.atmos-chem-phys.net/7/5639/2007/.

Rodgers, C. D.: Inverse methods for atmospheric sounding: theory and practice, World Sci., River Edge, N. J., 1st ed., 256 pp., 2000.

Russell, J. M., Gordley, L. L., Park, J. H., Drayson, S. R., Tuck, A. F., Harries, J. E., Ciccerone, R. J., Crutzen, P. J., and Frederick, J. E.: The Halogen Occultation Experiment, J. Geophys. Res., 98, 10 777–10 798, 1993.

Savage, N. H., Law, K. S., Pyle, J. A., Richter, A., Nub, H., and Burrows, J. P.: Using GOME NO2 satellite data to examine regional differences in TOMCAT model performance, Atmos. Chem. Phys., 4, 1895–1912, 2004, http://www.atmos-chem-phys.net/4/1895/2004/.

Schaub, D., Boersma, K. F., Keller, J., Folini, D., Brunner, D., Buchmann, B., Berresheim, H., and Staehelin, J.: SCIAMACHY tropospheric NO_2 over the Alpine region and importance of pixel surface pressure for the column retrieval, Atmos. Chem. Phys. Discuss., 7, 429–468, 2007, http://www.atmos-chem-phys-discuss.net/7/429/2007/.

Scheele, M. P., Siegmund, P.C., and van Velthoven, P. F. J.: Stratospheric age of air computed with trajectories based on various 3D-Var and 4D-Var data sets, Atmos. Chem. Phys., 5, 1–7, 2005, http://www.atmos-chem-phys.net/5/1/2005/.

Simpson, I. J., Blake, D. R., Rowland, F. S., and Chen, T.-Y.: Implications of the recent fluctuations in the growth rate of tropospheric methane, Geophys. Res. Lett., 29(10), doi:10.1029/2001GL014521, 2002.

Spivakovsky, C. M., Logan, J. A., Montzka, S. A., Balkanski, Y. J., Foreman-Fowler, M., Jones, D. B. A., Horowitz, L. W., Fusco, A. C., Brenninkmeijer, C. A. M., Prather, M. J., Wofsy, S. C., and McElroy, M. B.: Three-dimensional climatological distribution of tropospheric OH: Update and evaluation, J. Geophys. Res., 105, 8931–8980, 2000.

Shindell, D. T., Faluvegi, G., Stevenson, D. S., Krol, M. C., Emmons, L. K., Lamarque, J.-F., Pétron, G., Dentener, F. J., Ellingsen, K., Schultz, M. G., Wild, O., Amann, M., Atherton, C. S., Bergmann, D. J., Bey, I., Butler, T., Cofala, J., Collins, W. J., Derwent, R. G., Doherty, R. M., Drevet, J., Eskes, H. J., Fiore, A. M., Gauss, M., Hauglustaine, D. A., Horowitz, L. W., Isaksen, I. S. A., Lawrence, M. G., Montanaro, V., Müller, J.-F., Pitari, G., Prather, M. J., Pyle, J. A., Rast, S., Rodriguez, J. M., Sanderson, M. G., Savage, N. H., Strahan, S. E., Sudo, K., Szopa, S., Unger, N., van Noije, T. P. C., and Zeng, G.: Multimodel simulations of carbon monoxide: Comparison with observations and projected near-future changes, J. Geophys. Res., 111, D19306, doi:10.1029/2006JD007100, 2006.

Stevenson, D. S., Dentener, F. J., Schultz, M. G., Ellingsen, K., van Noije, T. P. C., Wild, O., Zeng, G., Amann, M., Atherton, C. S., Bell, N., Bergmann, D. J., Bey, I., Butler, T., Cofala, J., Collins, W. J., Derwent, R. G., Doherty, R. M., Drevet, J., Eskes, H. J., Fiore, A. M., Gauss, M., Hauglustaine, D. A., Horowitz, L. W., Isaksen, I. S. A., Krol, M. C., Lamarque, J.-F., Lawrence, M. G., Montanaro, V., Müller, J.-F., Pitari, G., Prather, M. J., Pyle, J. A., Rast, S., Rodriguez, J. M., Sanderson, M. G., Savage, N. H., Shindell, D. T., Strahan, S. E., Sudo, K., and Szopa, S.: Multimodel ensemble simulations of present-day and near-future tropospheric ozone, J. Geophys. Res., 111, D08301, doi:10.1029/2005JD006338, 2006.

Stockwell, W. R., Kirchner, F., Khun, M., and Seefeld, S.: A new mechanism for regional atmospheric chemistry modelling, J. Geophys. Res., 102, 25 847–25 879, 1997.

Strahan, S. E. and Polansky, B. C.: Meteorological implementation issues in chemistry and transport models, Atmos. Chem. Phys., 6, 2895–2910, 2006, http://www.atmos-chem-phys.net/6/2895/2006/.

Taylor, K. E.: Summarizing multiple aspects of model performance

in a single diagram, J. Geophys. Res., 106, 7183–7192, 2001.

Trebs, I., Lara, L. L., Zeri, L. M. M., Gatti, L. V., Artaxo, P., Dlugi, R., Slanina, J., Andreae, M. O., and Meixner, F. X.: Dry and wet deposition of inorganic nitrogen compounds to a tropical pasture site (Rondonia, Brazil), Atmos. Chem. Phys., 6, 447–469, 2006, http://www.atmos-chem-phys.net/6/447/2006/.

Urban, J., Lautié, N., Le Flochmoën, E., Jimenez, C., Eriksson, P., de la Noë, J., Dupuy, E., El Amraoui, L., Frisk, U., Jegou, F., Murtagh, D., Olberg, M., Ricaud, P., Camy-Peyret, C., Payan, S., Dufour, G., Huret, N., Pirre, M., Robinson, A. D., Harris, N. R. D., Bremer, H., Kleinbohl, A., Kullmann, K., Kunzi, K., Kuttipurath, J., Ejiri, M., Nakajima, H., Sasano, Y., Sugita, T., Yokota, T., Piccolo, C., Raspollini, P., and Ridolfi, M.: Odin/SMR Limb Observations of Stratospheric Trace Gases: Validation of N_2O, J. Geophys. Res., 110, D09301, doi:10.1029/2004JD005394, 2005.

van der Werf, G. R., Randerson, J. T., Collatz, G. J., and Giglio, L.: Carbon emissions from fires in tropical and subtropical ecosystems, Global Change Biol., 9, 547–562, 2003.

van Noije, T. P. C., Eskes, H. J., van Weele, M., and van Velthoven, P. F. J.: Implications of the enhanced Brewer-Dobson circulation in European Centre for Medium-Range Weather Forecasts reanalysis ERA-40 for the stratosphere-troposphere exchange of ozone in global chemistry transport models, J. Geophys. Res., 109(D19), D19308, doi:10.1029/2004JD004586, 2004.

van Noije, T. P. C., Eskes, H. J., Dentener, F. J., Stevenson, D. S., Ellingsen, K., Schultz, M. G., Wild, O., Amann, M., Atherton, C. S., Bergmann, D. J., Bey, I., Boersma, K. F., Butler, T., Cofala, J., Drevet, J., Fiore, A. M., Gauss, M., Hauglustaine, D. A., Horowitz, L. W., Isaksen, I. S. A., Krol, M. C., Lamarque, J.-F., Lawrence,M. G., Martin, V., Montanaro, V., Müller, J.-F., Pitari, G., Prather, M. J., Pyle, J. A., Richter, A., Rodriguez, J. M., Savage, N. H., Strahan, S. E., Sudo, K., Szopa, S., and van Roozendael, M.: Multi-model ensemble simulations of tropospheric NO2 compared with GOME retrievals for the year 2000, Atmos. Chem. Phys., 6, 2943–2979, 2006, http://www.atmos-chem-phys.net/6/2943/2006/.

Volz-Thomas, A., Berg, M., Heil, T., Houben, N., Lerner, A., Petrick, W., Raak, D., and Pätz, H.-W.: Measurements of total odd nitrogen (NO_y) aboard MOZAIC in-service aircraft: instrument design, operation and performance, Atmos. Chem. Phys., 5, 583–595, 2005, http://www.atmos-chem-phys.net/5/583/2005/.

Wesely, M. L.: Parameterization of surface resistances to gaseous dry deposition in regional-scale numerical models, Atmos. Environ., 23, 1293–1304, 1989.

Wesely, M. L. and Hicks, B. B.: A review of the current status of knowledge on dry deposition, Atmos. Environ., 34, 2261–2282, 2000.

Wild, O.: Modelling the global tropospheric ozone budget: exploring the variability in current models, Atmos. Chem. Phys., 7, 2643–2660, 2007, http://www.atmos-chem-phys.net/7/2643/2007/.

Williamson, D. L. and Rash, P. J.: Two-dimensional semi-lagrangian transport with shape-preserving interpolation, Mon. Weather Rev., 117, 102–129, 1989.

World Health Organization: Health aspects of air pollution with particulate matter, ozone, and nitrogen dioxide, Rep. EUR/03/5042688, Bonn, 2003.

World Meteorological Organisation: Report of the international ozone trends panel-1988, WMO report, 18, 1988.

World Meteorological Organisation: Scientific assessment of ozone depletion-1998, WMO report, 44, 1998.

World Meteorological Organisation: Scientific assessment of ozone depletion-2002, WMO report, 47, 2002.